Detection of Single Enzyme Molecules and Catalytic Nucleic Acids using Microfluidics and Selection of Aptamers using Capillary Electrophoresis-SELEX

A THESIS SUBMITTED TO THE FACULTY OF

UNIVERSITY OF MINNESOTA

BY

Jing Yang

IN PARTIAL FULFILLMENT OF THE REQUIREMENTS

FOR THE DEGREE OF

DOCTOR OF PHILOSOPHY

Michael T. Bowser, Advisor

February 2014

Acknowledgements

I would like to thank Prof. Zheng Hu and Dr. Fan Zhang at Nanjing University for giving me the chance to be exposed to cutting-edge scientific research in chemistry and mentoring me during my undergraduate research.

Thank you to my PhD research advisor Prof. Mike Bowser for all his help and guidance for my research and thesis. I'm grateful for his help to fund me through PhD studies and support me to present my work to scientific community at the 29th MicroScale Bioseparations Symposium. I especially appreciate his dedication to create and inspire innovative ideas. Most importantly, I would like to thank him for always encouraging me to try and be confident whenever I was in difficulty.

Thank you to the whole Bowser group people for the help during my PhD study and research, especially Meng Jing for training me on CE-SELEX, Yixiao Sheng and Ryan Turgeon for training me microfluidic fabrication, Rachel Harstad for helping me with cell culturing, Thane Taylor for helping me with qPCR and confocal fluorescence microscope, and Eric Castro for helping me setting up the droplet assay, as well as all the helpful discussions with all of them.

Finally, I would like to thank my family for all the support. Thank you to my husband Chunxi Luo for helping me through the difficult times of my life and always stay by my side. Thank you to my parents for always supporting me and all my decisions. Without their unconditional love and care, I wouldn't have achieved what I have today.

Dedication

To my parents,

who always supported my education.

Abstract

Aptamers are single stranded DNA or RNA molecules that can bind targets with high affinity and specificity. They are selected in vitro from a large library of synthetic oligos via Systematic Evolution of Ligand by Exponential enrichment (SELEX) process. Conventional SELEX techniques using affinity chromatography and nitrocellulose filtration have identified aptamers for a wide range of targets. Although proven successful, the conventional SELEX is also time-consuming and labor-intensive. Capillary electrophoresis-SELEX (CE-SELEX) has later been introduced for aptamer selection, which greatly reduces the selection time and the number of cycles needed and minimizes the non-specific interactions and steric hindrance.

CE-SELEX has been previously performed mainly against large protein targets. A small molecule target N-methyl mesoporphyrin (NMM) is now proved to be suitable for CE-SELEX. Aptamers with high nM to low μM affinity are selected by CE-SELEX and two out eight randomly picked sequences are also capable of catalyzing the corresponding metal insertion reaction. It greatly expands the capability of CE-SELEX and indicates that any target that can generate enough change in hydrodynamic size of the oligos upon binding can be used in CE-SELEX. Not only have we explored the low size limitation of targets for CE-SELEX, but also we have applied CE-SELEX against a fully intact membrane target - transferrin receptor (TfR) which is difficult for conventional SELEX. Aptamers with a few tens of nM K_d have been selected after four rounds of CE-SELEX. These aptamers binding receptors involved in receptor-mediated endocytosis process could be potentially engineered for transporting therapeutic cargos for treating intracellular targets.

Besides aptamer selection using CE-SELEX, binding interactions between DNA/RNA analogs and important cardiac muscle proteins have also been studied. Using affinity CE and fluorescence polarization measurements, various DNA/RNA analogs, such as oligos of different lengths, L-DNA, O-methyl RNA, and Ca^{2+} pump Sarco(endo)plasmic reticulum Ca^{2+}-ATPase (SERCA) and regulatory protein phospholamban (PLN), and contractile proteins such as troponin and myosin have been employed in the study. This sequence-independent binding affinity indicates possible direct nucleic acid regulation effect on protein functions and shows their potential as drug candidates for PLN super-inhibition caused heart failure.

Finally, other than binding affinities, catalytic activities of nucleic acid oligos have also been assessed. A novel platform allowing multiple turnover reactions of catalytic sequences has been designed and fabricated in PDMS. Single enzyme molecules have been detected successfully and their kinetics have been studied using the microwell array device as a proof-of-concept. Unfortunately, when applying DNA/RNA libraries, we can't detect any catalytic sequences, indicating either the abundance or catalytic activity is too low to be detected.

Table of Contents

List of Tables

List of Figures

List of Abbreviations

RNA	*Ribonucleic Acid*
ssDNA	*Single Stranded Deoxyribonucleic Acid*
dsDNA	*Double Stranded Deoxyribonucleic Acid*
LNA	*Locked Nucleic Acid*
PEG	*Polyethylene Glycol*
HDV	*Hepatitis Delta Virus*
VS	*Varkud Satellite*
RNase P	*Ribonuclease P*
SELEX	*Systematic Evolution of Ligand by Exponential enrichment*
PCR	*Polymer Chain Reaction*
CE	*Capillary Electrophoresis*
EOF	*Electroosmotic Flow*
LIF	*Laser Induced Fluorescence*
APCE	*Affinity Probe Capillary Electrophoresis*
LC	*Liquid Chromatography*
CEC	*Capillary Electrochromatography*
MALDI-MS	*Matrix-Assisted Laser Desorption Ionization-Mass Spectrometry*
CMACS	*Continuous-flow Magnetic Activated Chip-based Separation*
MMS	*Micromagnetic Separation*
μFFE	*Micro-Free Flow Electrophoresis*
TSA	*Transition State Analog*
ACE	*Affinity Capillary Electrophoresis*
FP	*Fluorescence Polarization*
KCE	*Kinetic Capillary Electrophoresis*
NECEEM	*Non-Equilibrium Capillary Electrophoresis of Equilibrium Mixture*
EMSA	*Electrophoretic Mobility Shift Assay*
HPLC	*High Performance Liquid Chromatography*
FRET	*Fluorescence Resonance Energy Transfer*
MAB	*Molecular Aptamer Beacon*
SPR	*Surface Plasmon Resonance*
CD	*Circular Dichroism*
ITC	*Isothermal Titration Calorimetry*
VEGF	*Vascular Endothelial Growth Factor*
IgE	*Immunoglobulin E*
NPY	*Neuropeptide Y*
HIV-RT	*Human Immunodeficiency Virus-Reverse Transcriptase*
LDH-1	*Lactate Dehydrogenase*
NADH	*Nicotinamide Adenine Dinucleotide reduced form*
NAD	*Nicotinamide Adenine Dinucleotide*
ELISA	*Enzyme Linked Immunosorbent Assay*
CCD	*Charge Coupled Device*
CAD	*Computer Aided Design*
PDMS	*Polydimethylsiloxane*
PC	*Polycarbonate*
PMMA	*Polymethylmethacrylate*
PE	*Polyethylene*
PP	*Polypropylene*
PS	*Polystyrene*

FDG	*Fluorescein-di-β-D-Galactopyranoside*
FMG	*Fluorescein-mono-β-D-Galactopyranoside*
NMM	*N-Methyl Mesoporphyrin*
MP	*Mesoporphyrin*
siRNA	*Small Interfering RNA*
TfR	*Transferrin Receptor*
$C_{12}E_8$	*Octaethylene Glycol Monododecyl Ether*
PLN	*Phospholamban*
SERCA	*Sarco(endo)plasmic Reticulum* Ca^{2+}*-ATPase*
SR	*Sarcoplasmic Reticulum*
PMCAs	*Plasma Membrane* Ca^{2+} *ATPases*
NCXs	Na^{+}/Ca^{2+} *Exchangers*
cAMP	*cyclic Adenosine Monophosphate*
PKA	*Protein Kinase A*
TnC	*Troponin C*
TnI	*Troponin I*
TnT	*Troponin T*
RME	*Receptor-Mediated Endocytosis*
CCV	*Clathrin-Coated Vesicle*
CME	*Clathrin-Mediated Endocytosis*
CvME	*Caveolin-Mediated Endocytosis*
GSL	*Glycosphingolipid*
GPI	*Glycosylphosphatidylinositol*
FADS	*Fluorescence-Activated Droplet Sorting*

Preface

Chapters 1 and 3 were reproduced in part with permission from:

1. Yang, J.; Bowser, M. T. "Capillary Electrophoresis-SELEX Selection of Catalytic DNA Aptamers for a Small-Molecule Porphyrin Target" *Anal. Chem.* **2013**, 85, 1525-1530.

Chapter 1: Introduction

1.1 Functional Nucleic Acids

All life in today's world is almost exclusively based on the nucleic acids genomes and protein based enzymes. It has been traditionally believed that the chemical uniformity of nucleic acids would make them function only for genetic information storage and transfer. However, in vitro selection has discovered a number of nucleic acid sequences for binding and catalysis [1], which demonstrates the great structural and functional versatility of nucleic acids. Although a nucleic acid molecule is comprised of only four chemically similar subunits, RNA and single stranded DNA (ssDNA) can fold into various complex secondary and tertiary structures (Figure 1.1) and form binding sites and catalytic centers much like proteins. RNA and ssDNA capable of binding targets are named aptamers meaning fit. Sequences that are able to catalyze reactions are named ribozymes for catalytic RNA or deoxyribozymes for catalytic DNA.

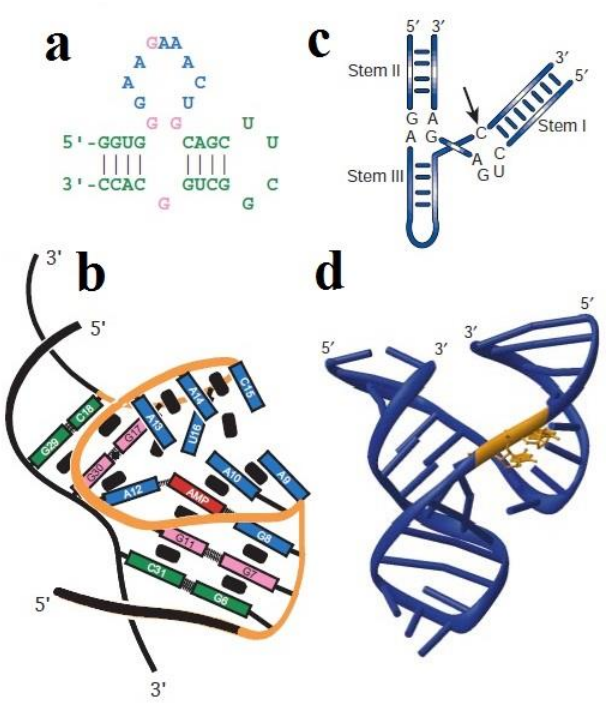

Figure 1.1. (a) Secondary and (b) tertiary structures of an ATP aptamer [2]. (c) Secondary and (d) tertiary structures of a Hammerhead ribozyme [3].

1.1.1 Aptamers

Aptamers are in vitro selected short single stranded DNA (ssDNA) or RNA molecules that can bind certain targets with high affinity and specificity. The in vitro selection process requires the sequences to have two constant primer binding regions for polymerase chain reaction (PCR) amplification of bound sequences. A central random region of 30-80 bases is also required

for various folding of the ssDNA or RNA structures. A ssDNA or RNA library containing a large number of random sequences would have a lot of unique folded structures, such as stem, loop, bulge, and G-quadraplex structures. Through in vitro selection, sequences with the right folding and shape that fit the binding sites of the target can be selected and amplified from the other non-binding sequences. A number of aptamers have been selected for various target molecules including proteins [4-6], peptides [7, 8], small molecules [9], metal ions [10, 11], and even organelles [12] and entire cells [13].

In addition to aptamers with natural RNA or ssDNA sequences, a number of modifications have been introduced to enhance the stability and bioavailability of aptamers. RNA generally has lower in vivo stability than ssDNA due to the presence of the 2'-OH group on the ribose moity. Therefore, it has been substituted by a number of modifications including 2'-fluoro, amino and O-methyl groups to increase the biostability [14-16]. Both ends (5' and 3') of RNA aptamers are vulnerable sites for exoribonuclease degradation. Circular RNA aptamers that join both ends of the linear form can be used to increase the resistance to nuclease degradation [17]. The 3' or 5' capping modification can also improve the stability of aptamers against exonuclease degradation [18]. Locked nucleic acid (LNA) provides a more rigid structure and the reduced conformational flexibility renders a high aptamer stability against degradation [19]. Spiegelmers are the mirror images (L- form) of natural D-aptamers [20, 21]. They are intrinsically resistant to enzymatic degradation due to the fact that they are not recognized by natural enzymes built from L-amino acids. Spiegelmers are developed through mirror-image SELEX in which natural D-oligonucleotides are selected against unnatural peptide targets with D-amino acids building blocks. Then the corresponding L- form of the selected D-aptamers would bind the natural L-peptide targets according to the principle of chirality. This technique eliminates the necessity of tedious post-SELEX modification for the selected aptamers. Moreover, in order to lower renal clearance rate of the relatively small aptamers, polyethylene glycol (PEG) moity has been added to aptamers to increase the effective molecular size and prevent them from cleared via kidney too fast [22, 23].

Compared to their protein counterparts - antibodies, aptamers possess many advantages [24]. Aptamers can be selected in vitro and cost-effectively synthesized once their sequence is determined while the generation of antibodies requires animal immunization. They can work under non-physiological conditions that may be fatal for antibodies. They can be easily modified by a variety of functional groups and attached to solid phase substrates using various chemistries. They have long shelf life and can be denatured and renatured easily. They are typically smaller

than antibodies. And most importantly, aptamers can be selected for virtually any kind of targets, but antibodies can only be raised against targets that generate immune response.

1.1.2 Catalytic Nucleic Acids

The first discovery of RNA with enzyme-like properties was in 1982 when a pre-rRNA from Tetrahymena was found to undergo autocatalytic rearrangements [25]. In later years, a couple of natural occurring catalytic RNA molecules have been discovered, such as hammerhead, hairpin, hepatitis delta virus (HDV), varkud satellite (VS), group I intron, group Ⅱ intron and ribonuclease P (RNase P) [3]. They play important roles in RNA cleavages and ligations. This has led people to think of the prebiotic world hypothesis which was brought into notice by Gilbert in 1986 [26]. In this hypothesis, it is assumed that unlike the current world which uses proteins for enzymatic reactions and nucleic acids for genetic information storage and transfer, there was a stage in early life which uses only one molecular species-the nucleic acid that serves to carry both genetic information and enzymatic activities. Such a prebiotic stage requires nucleic acids to have great diversity and potential in catalyzing chemical reactions. Great efforts have been put into the discovery of new nucleic acid catalysts. Using in vitro selection and transition state analog methods, people have selected a broad range of artificial ribozymes and also deoxyribozymes with various activities, such as RNA/DNA cleavage [27-29] and ligation [30, 31], biphenol isomerization [32, 33], Diels-Alder reaction [34, 35], porphyrin metalation [36-38], ester hydrolysis [39], aminoacylation [40-42], peptide bond formation [43-45], N-glycosidic bond formation [46] and hydrolysis [47], N-alkylation [48], S-alkylation [49], Michael addition [50], aldol condensation [51] and Claisen condensation [52]. This not only leads support to the prebiotic world hypothesis, but also indicates the great potential of nucleic acids to be used as novel biocatalysts in biotechnology and organic synthesis.

Ribozymes and deoxyribozymes take a number of approaches to carry out catalysis quite resembling protein enzymes. 1) General acid-base catalysis. Deprotonation of 2' hydroxyl group makes RNA a strong nucleophile. The oxyanion in the phosphate can be protonated and become a good leaving group. 2) Conformational effects. Just as a protein must fold into its active conformation, nucleic acid catalysts must also fold into a proper conformation to orientate the substrates and employ proximity effect. 3) Transition state stabilization. They can lower the activation energy of a chemical reaction by binding more tightly to the transition state than the ground state. 4) Electrostatic effect. Metal ions, nucleobases and phosphate groups apply electrostatic effects to assist catalysis. 5) Cofactors. Metal ions and amino acids can be introduced as cofactors to further enhance their catalytic potentials [53]. 6) Modified nucleobases. Nonnatural DNA/RNA bases can be incorporated to provide more functional groups [54].

1.1.3 Applications of Functional Nucleic Acids

Due to the excellent recognition and binding ability, aptamers have become important tools in analytical chemistry. They have been used as affinity probes in capillary electrophoresis (APCE) for the detection and quantification of proteins and determination of binding parameters [55-57]. Detection of small molecule targets [58] and enantiomers [59] has also been accomplished in APCE. The use of laser-induced fluorescence (LIF) gives high sensitivity for detection. In addition, ultrasensitive detection of trace amounts of proteins has been realized by PCR amplifying the aptamer probes recognizing the protein targets [60]. In this affinity-PCR technique, the signal can be amplified to improve sensitivity by several orders of magnitude (180 molecules). They can be immobilized onto the chromatography column and used as affinity stationary phases for liquid chromatography (LC) or capillary electrochromatography (CEC). Separation of different analytes [61-63], purification [64] and quantification [65] of the targets have been achieved using aptamer based affinity chromatography. Stereo-specific aptamers have been used for chiral separations as well [66, 67]. In addition, aptamers used in affinity Matrix-assisted Laser Desorption Ionization-Mass Spectrometry (MALDI-MS) have been described [68, 69].

Aptamers also have great potentials in clinical applications. Similar to DNA microarrays for genomic sample screening, aptamer microarray can be used for identification and quantification of protein samples for proteomics. Ellington group has demonstrated the use of aptamer microarrays for high throughput, parallel and rapid detection of multiple proteins using fluorescence scanning [70]. Photo-aptamers selected that can covalently bond target proteins under UV radiation allow stringent wash and further advance the sensitivity and selectivity of this technique [71]. Besides diagnostics, aptamers developed against disease-related targets to block specific sites and inhibit functions can become therapeutic agents. Aptamers targeting the vascular endothelial growth factor (VEGF) have been developed into drugs for treating age-related macular degeneration [72]. A number of other aptamer based drugs are currently in clinical trials [73].

Similar to aptamers, catalytic nucleic acids can also be combined with other signal transduction elements to assemble analytical sensors [74]. Ribozymes catalyzing in *trans* RNA cleavage reactions such as hammerhead ribozymes can potentially bind and cleave target mRNA in a catalytic manner and suppress target gene expression. Apparently, they can also act effectively using antisense-based suppression approaches as well. Theoretically, these ribozymes can be designed to cleave any RNA species (*e.g.* viral genome) and the specificity is determined by altering the substrate recognition regions. Therefore, they have been used in preclinical and

clinical studies as therapeutic solutions for treating cancers and HIV or viral infections [75-77]. Ribozymes and deoxyribozymes can be used as potential biocatalysts for organic synthesis [78, 79]. This is especially advantageous over traditional small-molecule catalysts when high selectivity is desired.

1.2 SELEX

1.2.1 History of SELEX

In 1990, Tuerk and Gold isolated high affinity nucleic acids ligands against bacteriophage T4 DNA polymerase from a randomized RNA pool using a process referred to as Systematic Evolution of Ligands by EXponential Enrichment (SELEX) [80]. They introduced completely random sequences for the eight loop bases of the wild-type 18 bases long hairpin mRNA encoding the target protein to construct the starting RNA library. These sequences were subjected to selection for binding to the polymerase target on nitrocellulose filters. The selected RNA sequences are reverse transcribed and amplified to double stranded DNA (dsDNA) and then transcribed to generate a new pool of RNA with enriched binding affinity for the next round of selection. Sequences with binding affinity similar to the wide-type hairpin have been evolved after four rounds of SELEX selection. Among the two predominant consensus sequences found, one is the wide-type sequence and the other one is a sequence with four different loop bases. They bind the polymerase with similar low K_d of 5 nM which is 100 times lower than the non-specific RNA binding.

Meanwhile, Ellington and Szostak used a similar in vitro selection method independently to select RNA sequences with high affinity for six small organic dyes [81]. Instead of nitrocellulose filter partitioning, the RNA pool was subjected to affinity chromatography separation. Dye molecules were cross-linked to agarose beads in the column and binding sequences were also retained in the column upon binding the dyes and eluted later for collection. After four to five cycles, the abundance of bound sequences was enriched from less than 0.1% for the starting library to over 50%. Unlike the Gold's work using a library containing partial randomized bases (65,536 variants), Szostak used a completely random synthesized pool with a larger number of sequences (10^{13} copies). Furthermore, the staring pool of the Gold's study was randomized based on a known target binding sequence, while the library used in Szostak's study had no apparent affinity for the targets. However, in their study, there was no competition for binding as the ligand was in access.

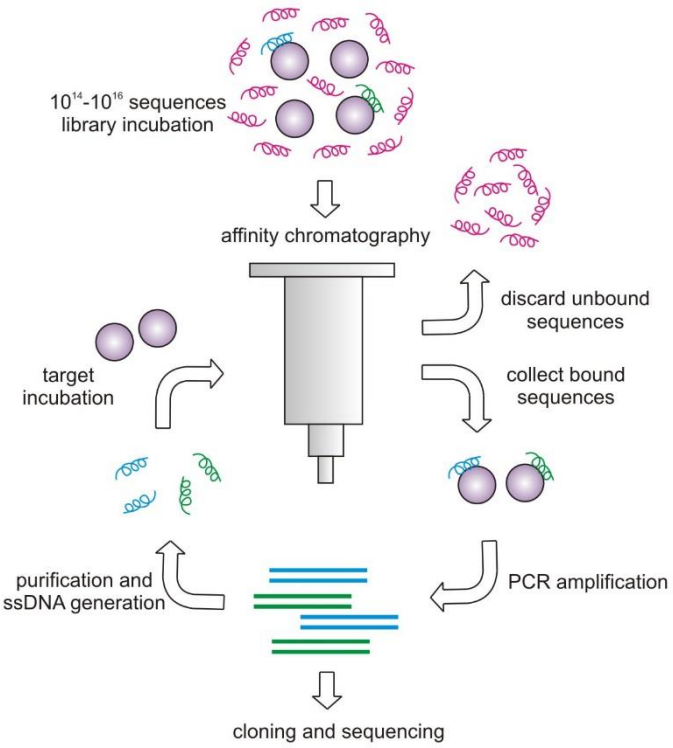

Figure 1.2. Schematic illustration of SELEX process

The nitrocellulose filtration and affinity column methods have soon become standard SELEX procedures for selection of aptamers against many different target molecules over the past two decades. The nitrocellulose filter retains most of the proteins and thus can be used for selection against protein targets; while target molecules can also be immobilized to the affinity column by either covalent bonding or affinity tags and used for aptamer selection.

1.2.2 Recent Progress in SELEX Methods

Ever since the first introduce of SELEX, a number of new partitioning techniques have been employed in SELEX for more efficient and convenient selection, such as centrifugation, magnetic separation, surface plasmon resonance, flow cytometry, gel mobility shift, capillary electrophoresis and microfluidic devices.

Centrifugation is a way to separate particles from liquid solution using gravity. When used in SELEX separation, the bound fraction is precipitated upon changing buffer composition or by immunoprecipitation and unbound sequences are removed with the supernatant. Rhie and

Tahiri-Alaoui have used centrifugation to co-precipitate the prion protein from Scrapie-associated Fibrils (SAF) with bound RNA sequences [82]. Similarly, using a 5-20% sucrose gradient centrifugation, RNA variants binding bacteriophage Φ29 prohead were evolved [83]. Homann has selected RNA aptamers against African trypanosomes using centrifugation as well [84].

Magnetic beads can be easily handled and thus enable fast, efficient and even automated separation by use of a magnet to trap the bound sequences. Strehlitz has developed a technique named FLuMag-SELEX in which fluorescent labeled DNA library and target coated magnetic beads are used for aptamer selection [85, 86]. Compared to the non-magnetic beads that require centrifugation separation, magnetic separation is a more efficient technology. A semi-automated SELEX using magnetic beads has also been developed [87]. A robotic workstation with magnetic rods were employed to implement the collection of aptamer bound magnetic beads, wash and resuspension of bound sequences. Cox and Ellington further developed an automated platform for selection of RNA against an oligonucleotide by using complete robotic liquid and mechanical manipulations and a magnetic bead separator equipment [88].

Surface plasmon resonance (SPR) has been broadly used to study biomolecular interactions to obtain both thermodynamic and kinetic information of binding events [89-91]. It takes use of evanescent wave on the boundary of metal film and the liquid sample. The change of the reflection angle is determined by the local reflection index which is changed upon the adsorption or binding of ligand to the surface-coated targets. Misono and Kumar [92] have used SPR for simultaneous selection and affinity characterization of aptamers binding influenza virus hemagglutinin (HA). High affinity RNA aptamers have been selected after five cycles and conserved regions of the aptamers have been identified. In their study, the RNA library was injected onto a CM4 chip with immobilized target protein HA. Binding sequences were then dissociated and fraction collected upon washing the flow cell for reverse transcription, PCR amplification and next round of selection. The binding affinity of each round pool showed increased response on SPR with increasing rounds. In this way, binding ability of the sequences can be estimated even before they were selected. Similarly, aptamers binding HIV-1 gp120 SU glycoprotein have also been successfully selected using SPR and they have been proven to neutralize the HIV-1 infectivity by over 1,000-fold [93].

Flow cytometry is a powerful and high speed technique to gain physical and chemical information of cells. When coupled with cell sorting instrumentations, it allows rapid cell/bead sorting and ligand identification from a large combinatorial library. Yang and Gorenstein [94] have done preliminary two-color flow cytometric aptamer selection against NF-κB p50 and p65

proteins. They constructed one-bead one-sequence oligonucleoside phosphorodithioate (ODN) library and the bead library was then incubated with protein targets for binding. A primary antibody binding the protein targets and a secondary labeled antibody binding the primary antibody were used to identify the beads with the binding sequences. Beads with high fluorescence intensity can be easily detected by flow cytometry and sorted into microcentrifuge tubes for PCR and sequencing. Blank and Schluesener [95] have used flow cytometry to monitor the progress of selection against YPEN-1 rat endothelial cells. The starting library contained ~10^{15} of DNA sequences with 60 random bases flanked by two 18-nt primer regions. Binding sequences were partitioned from unbound sequences using centrifugation. Starting from the second round, FITC label was added to the DNA via incorporating FITC labeled primer in PCR. This fluorescent label allowed the monitoring of the selection using flow cytometry. The selected pools showed progressive increase in fluorescence intensity of the bound cells.

Gel electrophoresis separates compounds based on how fast they move towards the poles under electric field. The speed or electrophoretic mobility of individual molecule is determined by their sizes and charges. The highly negatively charged nucleic acids move towards the anode when applying separation voltage. The binding sequences form complex with protein targets and thus slow down the moving speed of these binding sequences resulting in up shift of bands from the unbound sequences. Afterwards, the binding sequences can be recovered from the gel band by crush-and-soak method and then amplified for next round of selection. A RNA pool was selected for their affinity for ScVL viral particles and investigated for their packaging and replication activities [96]. The binding mixture was separated by agarose gel electrophoresis and the shifted band was excised and extracted for binding sequences. DNA sequences binding bacterial protein Integration Host Factor (IHF) were separated by nondenaturing polyacrylamide gel electrophoresis and the gel fragment was visualized under UV with ethidium bromide staining [97].

Compared to gel electrophoresis, capillary electrophoresis has much higher resolution and thus is a more efficient separation technique. The electrophoretic mobility of nucleic acids changes greatly upon binding large protein targets. In CE-SELEX, equilibrium mixture of targets and nucleic acids were loaded onto a capillary. Upon applying high voltage, binding complex was separated from unbound sequences and migrated into the collection vial for amplification and next cycle. This technique also allows the binding and separation to take place in homogenous solution environment and minimizes non-specific interaction [98]. DNA aptamers have been selected against human IgE [99], Neuropeptide Y [100] and HIV-RT [101] using CE-SELEX within only

2-4 rounds due to the high resolution of CE separation. However, the low loading capacity of the capillary may potentially limit the total pool size for selection.

Microfluidics technology is gaining great attentions in aptamer selection as well as applications as it provides a miniaturized environment for high speed processing, low sample consumption and potential for automation. Using target coated magnetic beads, the Soh group has developed a microfluidic device named continuous-flow magnetic activated chip-based separation (CMACS) for SELEX selection of aptamers [102]. An external magnet was used to magnetize the Ni strips embedded in the microfluidic channels. Magnetic beads with coated target proteins and bound DNA aptamers traveled from the edge sample stream to the center of the buffer stream by both the hydrodynamic force and magnetophoretic forces imposed and were collected into the center product outlet. The same group later developed an improved microfluidic device: micromagnetic separation (MMS) chip which utilized arrayed nickel strips in grids in the wide separation chamber to generate magnetic force and grasp the aptamer-bound beads [103, 104]. Other than magnetic manipulation, an electrophoresis based separation technique, micro Free Flow Electrophoresis (μFFE) that combines the continuous sample injection and free solution separation in electrophoresis was also used for SELEX. High affinity DNA aptamers against IgE have been isolated after only 1 cycle using μFFE-SELEX [105]. In μFFE, the analyte stream is introduced into the separation chamber longitudinally and deflected laterally by applying a separation voltage perpendicular to the flow direction of the analyte stream. In this way, continuous sample injection, separation and collection can be achieved. Another advantage of using microfluidics in SELEX is that different steps in SELEX can be carried out using different microfluidic parts and these parts can be put together to assemble an integrated and automated selection platform [106]. Microfluidic separation and on-chip PCR amplification have been coupled together to make integrated device for SELEX selection of aptamers [107].

Other than different partitioning methods used in SELEX, photoSELEX has been emerged as an innovative method to select aptamers with extreme high affinity and specificity. Jensen has used photoreactive chromophore 5-iodouracil in the RNA pool for isolation of aptamers against HIV Rev by nitrocellulose filter partitioning and denaturing gel partitioning [108]. The isolated aptamers not only bind but also cross-link the protein target with long wavelength UV laser light treatment. UV radiation of 5-IU produces uracil-5-yl radical which reacts with aromatic amino acids and cysteine. DNA library with 5-bromo-2'-deoxyuradine (BrdU) was used for photoSELEX as well [109]. This modified base specifically cross-links aromatic and sulfur-baring amino acids after absorbing UV light radiation only in close proximity. The covalent

bonded binding complex allows the use of harsh washing condition and only aptamers binding the protein target tight enough and in close proximity can be selected.

1.2.3 Selection of Catalytic Sequences

Highly selective catalytic antibodies can be selected from a large library in the immune system by the transition state analog (TSA) method [110]. The same strategy has been used to isolate ribozymes with catalytic activities. The method starts with the proper design of the transition state analog for the reaction of interest. Then a random pool of RNA molecules is screened for their affinity to the analog. Prudent *et al.* used the TSA method to isolate ribozymes catalyzing the isomerization of a bridged biphenyl [32]. In 1996, Conn *et al.* found another ribozyme capable of catalyzing porphyrin metalation using the TSA approach [36].

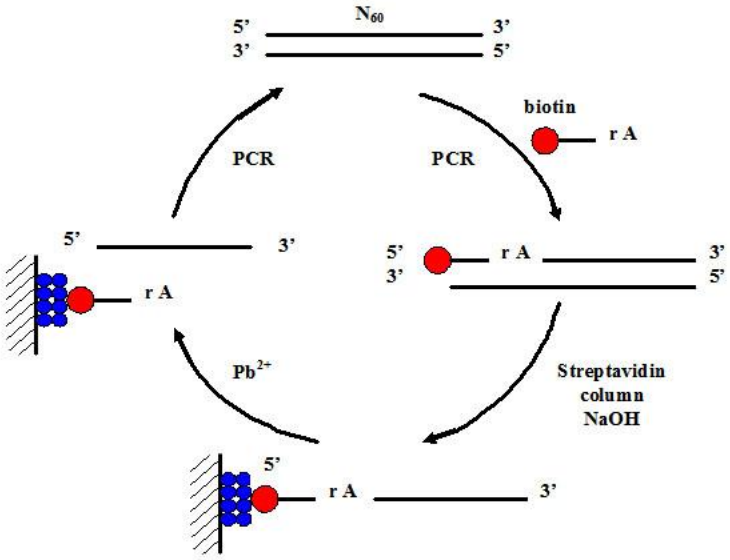

Figure 1.3. Schematic illustration of the in vitro selection of a RNA cleaving deoxyribozyme [111]. The catalytic sequences can cut themselves from the column and collected for PCR amplification and further rounds of selection and enrichment.

Another more popular approach is the direct in vitro selection method in which catalytic sequences can be separated from the other inactive sequences due to some kind of self-modification of the active sequences as a result of the catalytic reaction. Bartel and Szostak used the direct selection strategy to isolate ribozymes catalyzing RNA ligation from a random pool of RNA molecules [30]. A RNA pool is transcribed from a ligated DNA containing 220 random bases,

with all molecules beginning with a 5'-triphosphate group. Incubation of the RNA pool and the tagged substrate RNA leads to the ligation of catalytic sequences to the tagged substrates. The ligated active sequences can be retained by the oligonucleotide affinity column complimentary to the tagged sequence while the inactive sequences are washed away. The retained sequences are amplified for the next round of selection by selective polymerase chain reaction (PCR) amplification using a primer complementary to the tagged sequences. The in vitro selection has also been used for the discovery of a deoxyribozyme that cleaves RNA in the presence of Pb^{2+} by Breaker and Joyce [111].

1.3 CE-SELEX

1.3.1 Capillary Electrophoresis

Electrophoresis and chromatography are two main techniques commonly used in analytical separation. Chromatography is based on the partitioning of compounds between two different phases; while electrophoresis describes the movement of charged particles under uniform electric field. Capillary electrophoresis (CE) taking use of a narrow fused silica capillary (20-150μm ID, 350-400μm OD) as the separation channel is now the modern type of electrophoresis for analytical separation [112]. Compared to the traditional electrophoresis, the small diameter and the large surface area of capillary greatly reduce the Joule heating by fast dissipating heat. This allows the use of high voltage or electric field which improves the separation efficiency. A typical CE separation takes only seconds to a few minutes. The capillary can be filled with many separation media allowing multiple modes of CE separation to be carried out. Arrayed capillary electrophoresis further facilitates high-throughput analysis.

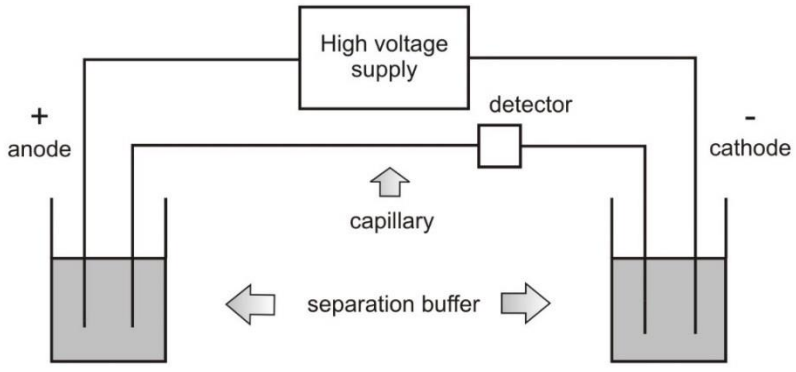

Figure 1.4. Schematic illustration of capillary electrophoresis system

When migrating under electric field, charged particles experience two main forces, electric force (F_E=qE) and friction force (F_f=$6\pi\eta rv$). The electric force and the friction force reach balance within a short time and the particles start to travel at constant velocities.

$$6\pi\eta r\mu_{em}E = qE \quad 1.1$$

$$\mu_{em} = \frac{q}{6\pi\eta r} = \frac{ze}{6\pi\eta r} = \frac{2\varepsilon\zeta}{3\eta} \quad 1.2$$

Here electrophoretic mobility (μ_{em}) is defined as the velocity under unit electric field. q is the charge of the particle, r is the hydrodynamic radius of the particle, η is the viscosity of the solution, ε is the dielectric constant of the solution, ζ is the electrokinetic potential or zeta potential of the infinitely diluted particle. So the electrophoretic mobility is an intrinsic property of the charge particle and it is determined by the particle's charge to size ratio (q/r). Therefore, CE separation is based on the difference in electrophoretic mobility.

Due to the dissociation of silanol groups (-Si-O$^-$) in aqueous solutions, the capillary wall has fixed negative charges. These charges attract positively charged ions and result in a higher concentration of positive charges in relative to the bulk solution. These positive charges form the electric double layer. The Charges in the stern layer adsorb tightly with the surface and cannot move; while the diffusional layer or part of it can move at the slippery plane under electric field. They also exert forces on the solvent molecules nearby and drag the whole bulk solution to move to the same direction. This phenomenon is named electroosmotic flow (EOF). Therefore, the apparent velocity of the analyte is the sum of the velocity of the analyte itself and that of EOF.

$$\mu_{total} = \mu_{analyte} + \mu_{EOF} \quad 1.3$$

$$\mu_{EOF} = \frac{\varepsilon\zeta_{EOF}}{\eta} \quad 1.4$$

The electrophoretic mobility of EOF is determined by the zeta potential of the capillary wall and is much greater than that of the analytes ($\mu_{EOF} > 10\mu_{analyte}$) [113]. Therefore, all analytes are carried along with the bulk solution to the negatively charged cathode in the order of positive, neutral and negative charges. In this way, ionic analytes can be separated according to their

charge to mass ratio or electrophoretic mobility. Neutral analytes are not charged and thus migrate as a single peak. So the separation of neutral analytes requires additional mechanisms such as micellar electrokinetic chromatography (MEKC) that uses micelles as pseudo-stationary phase [114, 115].

The peak broadening effect of any analytical separation techniques comes from the following processes: separation, injection and detection.

$$\sigma^2 = \sigma_{sep}^2 + \sigma_{inj}^2 + \sigma_{det}^2 \qquad 1.5$$

$$\sigma^2 = \sigma_{DL}^2 + \sigma_{DR}^2 + \sigma_P^2 + \sigma_T^2 + \sigma_E^2 + \sigma_{inj}^2 + \sigma_{det}^2 \qquad 1.6$$

The subscript *sep, inj, det, DL, DR, P, T, E* are referred to peak broadening effects from separation, injection, detection, longitudinal diffusion, radial diffusion or eddy diffusion, phase transfer, joule heating and electric field respectively. σ_T^2 and σ_E^2 are characteristic of CE separation. σ_{inj}^2 and σ_{det}^2 are general terms. Phase transfer in CE is also minimal as it does not involve partitioning between two phases. So ideally in CE, longitudinal diffusion is the only peak broadening effect ($\sigma^2 \approx \sigma_{DL}^2$). Similar to chromatography, the separation efficiency of CE is characterized by theoretical plate number *N* or plate height *H*.

$$N = \frac{L_{eff}}{H} = \frac{L_{eff}^2}{\sigma_{DL}^2} = \frac{L_{eff}^2}{2Dt_R} = \frac{\mu V L_{eff}}{2DL} \qquad 1.7$$

Apparently, higher voltage (*V*), less diffusion (*D*) and greater mobility (μ) generate narrower peaks and higher column efficiency. However, high column efficiency does not necessary lead to good separation. Another parameter resolution (R_s) describing the degree of separation is also important. Resolution characterizes how two adjacent peaks are separated from each other. Under ideal conditions,

$$R_s = \frac{2(t_2 - t_1)}{w_1 + w_2} = \frac{1}{2}\sqrt{N}\left(\frac{\mu_1 - \mu_2}{\mu_1 + \mu_2}\right) = \frac{\mu_1 - \mu_2}{4\sqrt{2}}\sqrt{\frac{VL_{eff}}{LD(\mu_1 + \mu_2)/2}} = \frac{\Delta\mu}{4\sqrt{2}}\sqrt{\frac{VL_{eff}}{LD\bar{\mu}}} \qquad 1.8$$

Therefore, the resolution also depends on the difference of electrophoretic mobility ($\Delta\mu$).

1.3.2 Capillary Electrophoresis-SELEX

Capillary electrophoresis has been extensively used to study aptamer-protein bindings previously and has been proven to be capable of separating the aptamers bound to the protein target from the free unbound aptamers with high resolutions [55-57]. This naturally leads people to explore the possibility of applying CE for SELEX selection of aptamers. The first couple of CE-SELEX selections were successfully performed against protein targets [99, 101, 116, 117]. Not limited to large protein targets, CE-SELEX selection has been performed against a smaller peptide target - neuropeptide Y (NPY) [100]. It consists of only 36 amino acids and has a molecular weight of 4272 g/mol which is even smaller than the ssDNA itself (25 kDa). Aptamers with 300 nM K_d have been successfully selected using CE-SELEX after only 4 rounds of selection. Recently, CE-SELEX selection against an even smaller compound – N-methyl mesoporphyrin (NMM, MW = 588 g/mol) has been demonstrated [38]. These studies have greatly expanded the scope of CE-SELEX applications.

In CE-SELEX, the ssDNA/RNA sequences are firstly heated and then cooled down to room temperature to allow them to fold into the most stable secondary and tertiary structures. Target molecules are added then with these sequences and incubated in free solution to achieve binding equilibrium. The concentration of target molecules is kept low to promote competition for sequences to bind. A few nanoliter of the equilibrium mixture is injected onto a separation capillary. The bound sequences are separated from the unbound sequence using free solution zone capillary electrophoresis under either equilibrium or non-equilibrium conditions.

In free solution zone capillary electrophoresis separation, nucleic acid molecules carrying high density of negative charges have the highest electrophoretic mobility against the EOF and thus migrate off the capillary last. Targets usually carry less negative charges and migrate off the capillary before the DNA peak. Therefore, the binding complex has an intermediate mobility and comes off the capillary after the target peak but before the free DNA peak. The libraries are usually labeled with fluorescent dyes to facilitate detection with laser induced fluorescence (LIF) due to the ease of labeling chemistry for nucleic acids than proteins. Therefore, only the large excess of free DNA peak is observed and a blind collection of all components before the free unbound DNA peak is adopted for fraction collection.

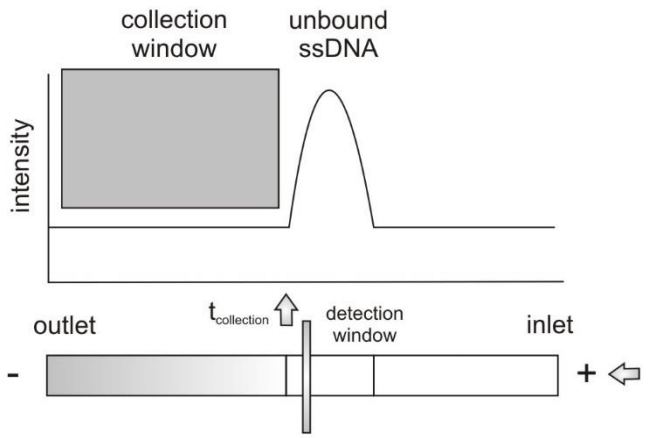

Figure 1.5. Schematic illustration of the fraction collection in CE-SELEX. The binding complex migrates off the capillary before the free unbound ssDNA peak and is collected until the leading edge of the unbound peak reaches the buffer vial ($t_{collect}$).

The collected bound sequence are then PCR amplified, purified and made single stranded again for the next round of selection. These steps repeat until there is no further improvement in binding affinity or sequence heterogeneity. Then the selected pools are made double stranded by PCR and ligated onto cloning vectors. The vectors containing selected sequences are transfected to *Escherichia coli* and individual colonies are raised. The plasmids are extracted and sequenced to obtain the specific sequence information for individual clones.

Compared to conventional SELEX, aptamers are evolved after only 1-4 rounds using CE-SELEX selection rather than 8-12 rounds for conventional SELEX. This greatly attributes to the high resolution of CE separation of bound and unbound sequences. Moreover, the free solution environment in CE-SELEX eliminates the necessity for negative selections against solid support and linker molecules for immobilizing target compounds and the nitrocellulose filter surface, which further simplifies and accelerates the process. In a direct comparison of CE-SELEX with conventional SELEX for selection against ricin toxin [118], after 9 rounds of selection, only 9.8% of the pool binds the target for the microtiter plate method and 38.5% of the pool binds for affinity chromatography SELEX. On the contrary, 87.2% binding abundance was achieved using CE-SELEX after only 4 rounds of selection.

1.3.3 Characterization of binding parameters

The dissociation constants (K_d) of selected sequences need to be assessed after each round of CE-SELEX to monitor the progress of the selection and evaluate the selected aptamers. Assuming a 1:1 binding ratio, the concentrations of the aptamer (A), the target (T) and the aptamer-target complex (C) are described in the following equations:

$$A + T \rightleftharpoons C \tag{1.9}$$

$$K_d = \frac{[A][T]}{[C]} \tag{1.10}$$

$$f_b = \frac{[C]}{[A] + [C]} = \frac{[T]}{K_d + [T]} \tag{1.11}$$

f_b here represents the bound fraction of the aptamers and K_d is the dissociation constant of the binding system. In two-ligand binding system, the concentration of one ligand is held constant (e.g. aptamer) and titrated with increasing concentration of another ligand. The bound fraction of the constant ligand can be measured by a number of analytical techniques and fitted with the concentration of the other ligand (e.g. protein) added to yield the K_d values. The total protein concentration $[T]_t$ is usually used as the free protein concentration $[T]$ for the above equation. This requires the total aptamer concentration used to be lower than or equivalent to K_d so that the $[T]_t \approx [T]$.

Like other SELEX selection methods, the separation technique itself can be used to measure the K_d values. The dissociation rate of the aptamer-protein complex is often slower than the CE separation time ($k_{off} << 1/t_C$) and thus the equilibrium composition of the complex is properly reserved after nonequilibrium separation. CE separation of the binding samples gives rise to two distinct peaks representing the binding complex and the free ligand (e.g. aptamer) respectively. As the protein concentration increases, the complex peak increases and the free aptamer peak decreases in both height and area, indicating an increase in the bound fraction. To couple with the CE-LIF detection, the aptamer is fluorescently labeled and the bound fraction can be calculated from the decrease in the free aptamer peak[98] or the increase in the complex peak[57] quantitatively ($f_b = 1 - \frac{I}{I_0}$ when I and I_0 are the unbound aptamer peak in the presence and absence of targets, or $f_b = \frac{I}{I_0}$ when I and I_0 are complex peak at partial and fully bound. Due to

the loss of complex caused by wall-adsorption and dissociation, the free aptamer peak is more often used as an indicative of the bound fraction.

If complex dissociation is significant during separation (k_{off} ~ or >> $1/t_C$), kinetic parameters (rate constants k_{on} and k_{off}) can also be obtained in addition to the binding equilibrium constant (K_d or K_a) using so-called nonequilibrium capillary electrophoresis of equilibrium mixture (NECEEM) developed by the Krylov group [119-121]. Since the run buffer does not contain either free aptamers or proteins under nonequilibrium condition, the complex dissociates as it migrates out of the equilibrium sample zone. The amount of aptamer dissociated from the complex decreases exponentially and forms an exponential decay curve following the free aptamer peak. This part can be fitted by a single-exponential curve to generate the dissociation rate constant k_{off} assuming the quantum yield of the dye in the free aptamer and the complex is the same.

$$I_t = I_{t_A} \exp(k_{off} \frac{t_C}{t_A - t_C}(t - t_A)) \qquad 1.12$$

t_C, t_A and t are the migration time for the complex peak, free aptamer peak and any time point on the exponential decay part. I_t and I_{tA} are the intensity at time t on the exponential decay and the intensity of the free aptamer peak at t_A.

The binding constant (K_a) can be calculated using the peak areas of the complex, the exponential decay part and the free aptamer. Since $K_d = \frac{1}{K_a} = \frac{k_{off}}{k_{on}}$, the complete kinetic parameter profile can be revealed.

$$K_a = \frac{1 + (A_C + A_{exp})/A_A}{[T]_t\left(1 + A_A/(A_C + A_{exp})\right) - [A]_t} \qquad 1.13$$

$$k_{on} = k_{off} K_a \qquad 1.14$$

A_C, A_{exp} and A_A represent the peak area of the complex peak, the exponential decay and the free aptamer peak respectively. $[T]_t$ and $[A]_t$ are the total concentration of the target and the aptamer respectively. k_{on} can be derived from k_{off} and K_a.

The same group has developed another two kinetic CE (KCE) techniques named sweeping CE[122] and plug-plug kinetic CE (ppKCE) [123, 124] for binding kinetic measurement. The SweepCE prefills the capillary with the low mobility ligand (e.g. aptamer) and applies electrophoresis from solution containing the high mobility ligand (e.g. protein). The high mobility ligand continuously binds the low mobility ligand and forms complex with higher mobility than the aptamer. Therefore, the aptamers are swept out of the capillary and the binding rate constant k_{on} can be calculated using a mathematical model for the sweeping region. In the ppKCE method, the sample plug of the low mobility ligand are injected before the plug of the high mobility ligand onto the capillary. Upon applying separation voltage, the faster moving ligand passes through the slow moving ligand zone resulting in the formation of the complex. Continuing electrophoresis starts to separate the two ligand zones and dissociate the complex. Therefore, it better represents the kinetic processes of binding and dissociation (k_{on} and k_{off}); while the NECEEM describes the equilibrium status and then the dissociation process (K_d or K_a and k_{off}).

As opposed to fluorescence detection, label-free detection based on UV [124] and mass spectrometry [125] has been employed to eliminate the inconvenience of fluorescent labeling of aptamers. Moreover, with temperature control in CE, other thermodynamic parameters (ΔH and ΔS) of binding reactions can be revealed, as well as the dependence of kinetic parameters and equilibrium constant on temperature [126].

Besides capillary electrophoresis, similar approaches are taken to separate the complex and the free ligands using other separation techniques, such as dialysis [127], ultrafiltration [128], HPLC [129] and gel electrophoresis (electrophoresis mobility shift assay (EMSA)) [130]. The complex or free ligands are quantified and fitted to the binding isotherms to give the K_d values. Rather than separation based techniques, direct measurement of the binding mixtures is preferred as it better represents the equilibrium composition and avoids concerns regarding complex dissociation during separation. It also eliminates the time needed to separate binding mixtures and thus is much less time-consuming. In addition, binding measurements characterizing different properties of the analytes can be used as orthogonal techniques to confirm binding.

If the fluorescence of the labeled aptamer changes upon binding the target [131-133] or the target itself is fluorescent and the intensity changes upon binding the aptamer [38, 134], both enhancement and quenching in the fluorescence intensity of the binding mixture can be used to estimate the binding affinity. The microenvironment of the dye can be significantly different when forming the apamer-target complex from in the free unbound status. For example, Li used an aptamer molecular beacon labeled with fluorophore and quencher on either end of the aptamer

for the K_d measurement of thrombin-aptamer binding [132]. When in the absence of the target thrombin, the dual labeled aptamer takes random scrambled conformation and leaves the fluorophore and quencher separated, giving rise to fluorescence signal. With the addition of the thrombin, it binds the aptamer in a way that brings the fluorophore and quencher together and the fluorescence signal is quenched due to proximity. The opposite detection scheme has also been reported in which the quenched fluorescence signal is restored upon binding the thrombin [133]. In addition, fluorescence resonance energy transfer (FRET) has also been employed for binding measurement as it provides a lower background noise and less false positive signal compared to molecular apamer beacon (MAB) [135].

Another property of fluorescence, polarization, is also often impacted by binding interactions. For measuring fluorescence polarization (FP) or anisotropy, a polarized light is used to excite the fluorophore. The intensity of the emission fluorescence that are parallel and perpendicular to the excitation light are measured. The polarization (*P*) and anisotropy (*A*) are defined as below and they are basically mathematically interchangeable [136].

$$P = \frac{I_{\parallel} - I_{\perp}}{I_{\parallel} + I_{\perp}} \qquad 1.15$$

$$A = \frac{I_{\parallel} - I_{\perp}}{I_{\parallel} + 2I_{\perp}} \qquad 1.16$$

$I_{\parallel}$ and $I_{\perp}$ represent the emission fluorescence intensity that's parallel and perpendicular to the excitation light respectively. The measured polarization is determined by the following factors[136]:

$$\frac{1}{P} - \frac{1}{3} = \left(\frac{1}{P_0} - \frac{1}{3}\right)\left(1 + \frac{RT}{\eta V}\tau\right) \qquad 1.17$$

P is the measured polarization and P_0 is the limit polarization when there is no rotation. *R* is the universal gas constant, *T* is the absolute temperature, η is the viscosity of the sample, *V* is the molar volume and τ is the fluorescence life time of the dye. Target binding or complex formation causes the hydrodynamic volume *V* of the labeled ligand to increase and the polarization to increase as well. Actually $3\eta V/RT$ is the Debye rotational relaxation time and larger complex usually has a longer rotational time because of the larger volume. Therefore, the

measured polarization or anisotropy can be used to calculate the bound fraction and the dissociation constant [137, 138].

It is not uncommon when there are both fluorescence intensity and polarization changes. In such cases, the bound fraction calculated from fluorescent polarization measurement should be corrected for the fluorescence enhancement or quenching effect. For example, in the presence of fluorescence enhancement effect, the measured emission fluorescence comes more from the bound fraction and thus it contributes more to the polarization values. In other words, the measured polarization is proportional to the fluorescence intensity from the bound species. Therefore, the measured polarization value would be greater than in absence of that effect. This effect needs to be corrected using the following equations [139]:

$$Q_m = \frac{I_m - I_0}{I_0} \qquad 1.18$$

$$F_b = \frac{P - P_f}{P_b - P_f} \qquad 1.19$$

$$f_b = \frac{F_b}{1 + Q_m(1 - F_b)} \qquad 1.20$$

where Q_m is the fluorescence enhancement or quenching factor, I_m and I_0 are the fluorescence intensity of the fully bound and the free aptamer. F_b is the raw bound fraction calculated directly from the measured polarization (P), the polarization at fully bound (P_b) and polarization of free aptamer (P_f). It has to be corrected by the Q_m factor to generate the real bound fraction f_b.

The fluorescent labeling of aptamers can sometimes affect their proper foldings and structures or change the binding affinity. Therefore, label-free techniques have been applied as alternatives. Surface plasmon resonance (SPR) measures the reflection angle of the evanescent light at the interface of the metal film and the liquid sample [89-91]. Although it does not require fluorescent labeling, the aptamers still need to be immobilized onto the metal film. The angle shifted reflects the refraction index changes near the surface which is caused by the aptamers binding the target. The whole procedure includes baseline, association, dissociation, regeneration

and back to baseline. Therefore, it provides real-time monitor of the binding interaction and thus reveals the kinetic information [89, 91].

Rather than the heterogeneous SPR, UV-vis adsorption provides a homogeneous measurement of the binding mixture. Binding affinity can be estimated from intensity changes of either aptamer or target peaks and the peak shift upon binding [140, 141]. Circular dichroism (CD) is another UV-vis adsorption based technique that measures the differential adsorption of left and right circularly polarized light. Aptamer and protein are optical active or chiral molecules and thus showed signals in CD spectrum. Besides the basic primary structural information, the conformational chirality generates additional information in CD spectrum, yielding secondary and tertiary structure-specific spectrum. Therefore, the CD spectrum of aptamer before and after binding protein can be used to characterize binding affinity and further yield information on how the conformation changes [141, 142].

Isothermal titration calorimetry (ITC) is another free solution technique that measures the heat released or absorbed for the binding reaction. One ligand is titrated with a series of addition of the other ligand in the sample cell and the electric power needed to keep the temperature as the same as another identical reference cell is measured. It not only generates dissociation constant K_d values [143], but also thermodynamic parameters (ΔG, ΔH and ΔS) [144] and even kinetic information [145]. In this technique, the concentration of the ligand in the sample cell is kept in the range of $10 < c < 100$ ($c = n[ligand]/K_d$, n is the binding stoichiometry) to get a good measurement of the binding isotherm [146]. If the c is too small, the binding curve becomes too flat; while if the c is too large, it becomes too steep. For example, if the ligand concentration is too low, the heat released may not generate a sufficient signal for measurement. But on the contrary, if the ligand concentration is high enough to generate sufficient heat, it may be too high so that the binding isotherm becomes too steep. Therefore, ITC is not suitable for really tight binding (~pM K_d) and it also requires a lot more sample consumption.

1.4 Single Enzyme Molecule Detection

The lowest theoretical limit of detection one can reach is single molecule. The ability to detect single molecules removes averaging effect of ensemble bulk and reveals the small differences among individuals. This becomes important especially when dealing with biological macromolecules, such as proteins. In order to achieve detection at single molecule level, one approach is to interrogate the target molecules in extremely small volume. Both optical and

electric signals can be measured. Nanopores formed in lipid bilayers or synthetic membranes have been used to detect single molecules by monitoring the ionic current during their passage through the nanopores [147]. When individual fluorescent molecules are probed in ultra-small interrogation volumes illuminated by a laser beam, high signal can be achieved to realize single fluorophore detection [148]. This technology has now been used for single molecule sandwich immunoassays known as Singulex [149].

Another approach to increase the limit of detection is to amplify the signal generated by the target molecules. Enzyme molecules have been employed to amplify signal by converting multiple fluogenic substrates into fluorescent products [150]. In this way, detection of target molecules are achieved by detecting signal from the amplified fluorophores. Rather than indirect detection of the molecule of interest, another similar approach is to amplify the target molecule itself. An example is to take use of the nature of nucleic acids molecules that they can be amplified by PCR for detection of single DNA molecules [151]. And lastly, the signal from each fluorophore is intrinsically amplified by cycling the photons through excitation-emission process.

Since enzymes have the ability to amplify signaling molecules, they can be detected at very low concentrations. If enzyme molecules are further confined or trapped in ultra-small volumes, it adds extra sensitivity to the detection and eventually single enzyme molecules can be detected in various analytical instrument settings. The same concept can be extended to any species that can catalyze the production of suitable fluorophores.

1.4.1 Capillary Electrophoresis Assays

When a diluted enzyme solution is loaded into the capillary with the corresponding fluogenic substrate, individual enzyme molecules are capable of catalyzing the substrate molecules around it and generating fluorescent products. The number of peaks indicates the number of enzymes present in the entire capillary. The variation of the peak areas shows the differences in the activities among the enzyme molecules. Xue and Yeung have used this approach to study the differences in the chemical reactivity of individual lactate dehydrogenase (LDH-1) [152]. The enzymes were identified by detecting the fluorescent product NADH converted from nicotinamide adenine dinucleotide (NAD^+). They have attributed the heterogeneity of enzyme activities to different protein conformations. Craig and Dovichi have also used capillary electrophoresis to study alkaline phosphatase and focus more on enzyme kinetics [153, 154]. Reaction rates and activation energies were measured in their papers and the heterogeneity was attributed to the different post-translational modification of the primary structures. The same group has later

studied β-galactosidase and also found microheterogeneity among individual enzyme molecules [155].

In this type of assay, the small channel of capillary serves as reaction vessel for individual enzymatic reactions to take place and the high sensitivity of laser-induced fluorescence enables the detection of fluorescent products produced by single enzyme. Due to the small inner diameter of the capillary channel, amplified products are still highly localized with the template molecules to realize the detection of single enzyme molecules. The signal amplification and fluorescent labeling steps can be integrated simultaneously on-line in the capillary. Although single molecule detection limit has been achieved in this technique, there are still some drawbacks. The generated products can still diffuse longitudinal to cause broadened bands and reduced concentrations. In addition, the number of molecules that can be loaded and thus monitored within the confined capillary is limited.

1.4.2 Microwell Array Assays

The array format of the microwells provides high-throughput and allows the observation of large number of individual enzyme molecules simultaneously. Physical confinement of isolated microwells can further limit the diffusion of generated fluorescent products and accumulate enough high concentrations of detectable products within a short period of time. Tan and Yeung have utilized femtoliter-sized microwells to monitor single LDH-1 and Os (VIII) metal ion catalysis [156]. The microwells were made of either pores in polycarbonate membranes or silica vials fabricated using photolithography. The single enzyme molecules trapped in individual microwells were detected by imaging the array device using a laser-based optical microscope and a charge-coupled device (CCD) detection system. They have observed heterogeneous catalytic activities for the enzyme molecules but more similar activities for metal ion catalysis, indicating that the added structural degrees of freedom of protein enzymes affect their activities. This type of devices also allows for real-time monitoring of single molecules' enzymatic activities.

Similar device has been fabricated using soft-lithography on poly-dimethylsiloxane (PDMS) as well for single β-galactosidase studies [157]. Molecule heterogeneity has been identified and the distribution of single enzyme molecules in microwells was found to follow Poisson's law. Walt and co-workers have developed the microwell array assay using fiber-optics. The microarray of femtoliter-sized reaction chambers is created at the distal end of a glass fiber optic bundle by preferentially etching the core material relative to the cladding. After filled with the enzyme and substrate mixture, the microwells are sealed against silicon gasket [150] or immiscible

oil phase [158]. In this way, enzyme concentrations can be measured by counting individual enzyme molecules as digital signals [150]. Later, kinetic mechanisms [159, 160] and inhibition effects [161] of single enzymes have been studied using the same device. Walt has also further developed the microwell array into more versatile applications, such as digital ELISA [162], multiplexed ELISA [163-165], and single oligo sequence detection [166, 167].

1.4.3 Water-in-Oil Emulsion Assays

Isolated reaction chambers can also be created by enclosing aqueous solution in an immiscible oil phase as water-in-oil droplets. Batman has created 0.1-40 μm droplets by spraying an aqueous solution containing the enzyme and the fluogenic substrate in silicon oil [168]. Single enzyme molecules trapped in 14-15 μm droplets can be detected after 15hrs incubation at 37 ℃.

One difficulty using the above mentioned techniques is the retrieval or recovery of the positive molecules after identifying them. Similar difficulty is encountered for adding, mixing, splitting of the reaction content once the molecules are isolated in individual reaction chambers and the incubation period starts. Micromanipulation of these isolated single molecules is important when further application and treatment after screening are desired. Great efforts have been put into the single molecule manipulations [169], such as valves in PDMS devices [170] and microdroplet manipulation. Specifically for droplet-based micromanipulation, Noji group has developed a directly accessible femtoliter-sized droplet array on a hydrophilic-in-hydrophobic patterned surface [171]. The droplet array is formed by covering the patterned surface with aqueous solution first and then with oil. Droplets of aqueous solution retains on the patterned surface and isolated by the oil phase. Since no solid walls are present, these droplets can be accessed from outside using micropipette.

In addition to the droplet array formed on a surface, serial droplet array generated in narrow channels has also been developed as individual reaction chambers. Ismagilov group has utilized a PDMS device with a T-junction to generate monodispersed droplets in microfluidic channels [172]. The dynamic of the droplet formation and the break-up of the two threads is dominated by the pressure drop across the droplet as it forms [173]. The size of the droplets is determined by the width of the channel and the volumetric flow rates of two immiscible fluids. These microdroplets can then be further sorted and collected in microfluidic devices using dielectrophoretic actuation according to their fluorescence generated by enzyme activity [174]. Compared to the surface array format, this serial array requires the droplets to pass through the

detection zone individually and results in longer assay time. However, the automated droplet detection and sorting devices enable the convenient and fast recovery of the positive droplets.

1.5 Microfluidics

Given the extremely small interrogation volume required by the detection of single enzyme molecules, micro- or nano- fabricated devices are essential for the ultra-sensitive measurement. Microfluidic devices usually have lateral feature dimensions on the order of 10-100 μm. Simple two-dimentional devices usually contain only channel systems and more complicated three-dimentional systems even incorporate micropumps, valves and detectors on a single chip, which allows the manipulation of gases and liquids in a highly integrated and miniaturized microchip rather than labor intensive bench-top work. When compared with traditional macroscopic analysis systems, microfluidic systems possess many advantages. They require much smaller quantities of samples and reagents, which means decreased cost and minimal amount of waste. They provide faster, more automated and portable platforms for performing analyses and reactions. They can also be designed to achieve a high degree of multiplexing and high-throughput format. However, smaller features also make it more susceptible to blockage by particles and more non-specific adsorption to the surface.

1.5.1 Materials and Fabrication

Owing to highly developed techniques of microelectronics and micromachining, traditional microfluidic devices are usually fabricated on silicon and glass wafers. The features can be designed by the computer-aided design (CAD) program, and a chrome mask is used to transfer the designed features to the wafers. Using standard photolithography and subsequent wet etching of the wafers, microchannels can be fabricated on silicon and glass wafers. Another piece of wafer is then used to seal the device and form closed channels. However, silicon is not the ideal material for microfluidic applications. It is electrically semiconducting and thus proves to be problematic for use in analytical separations which usually apply high voltage to transport liquids. It is also optically opaque, which makes optical detection difficult. Glass is a transparent insulator and thus a preferred substrate material. The silanol groups (-Si-OH) can support electroosmotic flow (EOF) in electrophoresis separations. However, both materials are relatively expensive and require complicated fabrication procedures and clean room environment. The highest aspect ratio that can be achieved is limited by the wet etching method and dry etching technique of silicon is

expensive. Their surfaces are charged and the adsorption of biomolecules through electrostatic interactions or hydrogen bonding is problematic for bioanalysis.

Polymer microfluidic devices are less expensive and easy to fabricate using mass replication technologies. They can be fabricated with high aspect ratio and the surface can be modified to meet various application requirements. The most commonly used polymer materials in microfluidics include poly (dimethylsiloxane) (PDMS), polycarbonate (PC), polymethylmethacrylate (PMMA), polyethylene (PE), polypropylene (PP) and polystyrene (PS) [175]. The most widely used replication method includes master fabrication and replication process. The master can be fabricated by micromachining [176], electroplating [175], silicon micromaching [177], solid object printing [178], and rapid prototyping method [179]. The master then serve as a mold for the polymer replica by hot embossing [180], injection molding [177] and casting [179, 181, 182].

1.5.2 PDMS Microchips

Among all the polymer materials used in microfluidics, poly(dimethylsiloxane) (PDMS) is one of the most rapidly developing materials [183]. It is an elastomeric polymer which contains weakly cross-linked polymer chains and can be stretched when applying an external force and return to its original state when the force is removed [184]. As a result, it can be peeled off a mold without damaging the channels or the master. It is transparent and has a UV cutoff at 240nm [185], which allows the optical detection at a wide range of wavelengths. It can be readily sealed with other materials such as glass, polystyrene and PMMA. It is an electrical and thermal insulator, nontoxic, chemically inert, impermeable to water, commercially available and inexpensive. However, it is not solvent resistant. It is hydrophobic and does not support EOF. And it may introduce non-specific adsorption to the surface and easily trap air due to its permeability to gases.

The Whitesides group has pioneered in a rapid prototyping method to fabricate microfluidic systems in PDMS, which used a photoresist master for replica molding and thus cut the cost drastically.[179] It has proven to be efficient, rapid and cheap and has become a dominate technique in PDMS microfluidic fabrication. The master fabrication for rapid prototyping starts with the design of the features using a CAD program. The features are then printed to high-resolution transparencies or chrome masks. The masks are used to transfer the design to photoresist spin-coated substrate wafers in contact photolithography. Following the development of the photoresist, masters composed of a relief of photoresist on the wafers are created. The PDMS prepolymer is supplied in two parts: a base and a curing agent. The vinyl groups (-C=C-) contained in the base can react with the silicon hydride groups (-Si-H) present in the curing agent

and form a cross-linked elastomeric solid [185]. Once the photoresist master is ready, the PDMS prepolymer mixture is casted against it. The liquid PDMS prepolymer conforms to the shape of the master and replicates the features of the master with high fidelity (10nm). It is then cured at an elevated temperature. After the PDMS becomes solid, it is peeled off the master without damaging the master itself due to its elasticity and low surface free energy. This process can be repeated many times as long as the master remains intact. The photoresist patterns can last a very long time and the damage of the master usually comes from the breakage of fragile wafers or the poor adhesion of photoresist to the wafers.

The cured PDMS can be sealed to a flat surface to form closed channels both reversibly and irreversibly. When a PDMS surface is brought into contact with another flat surface, it conforms to the surface via Van der Waals force and closes the channels. The reversible sealing is watertight, fast but does not withstand high pressure (< 5 psi) [186]. It is easy to break the reversible sealing simply by peeling PDMS off the surface and reseal them many times. Irreversible sealing requires air plasma treatment of both surfaces [187]. PDMS has repeating units of -O-Si-$(CH_3)_2$- and the methyl groups (-Si-CH_3) can be oxidized by the plasma to form silanol groups (-Si-OH) [187, 188]. The oxidized PDMS surface is then quickly brought into contact with another surface containing appropriate groups (-OH, -COOH, ketone for 1 min) [185, 186] to form -Si-O-Si- bonds and seal the two surfaces irreversibly. Irreversible sealing is much more robust and withstands pressures of 30-50 psi [186]. PDMS can be sealed to a number of different materials, such as PDMS itself, glass, silicon, quartz, silicon nitride, polyethylene, polystyrene and glassy carbon [179].

The native PDMS surface is uncharged and hydrophobic due to the silane groups (-O-Si-$(CH_3)_2$). Therefore, it is difficult to fill the channels with aqueous solution and easy to generate bubbles. And the surface is subject to adsorption of hydrophobic species. Various surface modification methods have been developed to make PDMS microchips available for more applications, such as oxygen plasma treatment to alter the hydrophobic PDMS surface to hydrophilic [179, 189], dynamic surfactant coating [190] and covalent modification by catalyzed polymerization [191]. In addition, phospholipid bilayers [192] and proteins [193] have been used to immobilize biomolecules to PDMS microchip surfaces.

PDMS microfluidic devices have been widely used in bioanalytical researches. Native [181] and modified [179] PDMS channels have both been used to do separate DNA fragments, amino acids and peptides. Array format of assays can be carried out in PDMS microchips to achieve high-throughput analyses [194]. Chemical reactions [194], PCR [195] and immunoassays [196] can also be performed in PDMS devices.

1.6 Scope of Thesis

Ever since the first introduce of CE-SELEX, it has become a widely used and efficient tool for aptamer selection. However, most of the selections were performed against large protein targets. Mendonsa *et al.* has demonstrated a CE-SELEX selection against a smaller NPY peptide target. We are trying to explore the applications of CE-SELEX for even smaller targets and other difficult targets for conventional SELEX. Chapter 3 describes CE-SELEX selection against a small organic compound, indicating an even lower size limitation for the targets. Chapter 4 describes CE-SELEX selection against a fully intact membrane target, which is difficult to study using conventional SELEX. Furthermore, binding of aptamers and important protein biomarkers in cardiac muscle cells has been investigated using ACE and FP to study the therapeutic potentials of nucleic acids for treating heart diseases and the regulation mechanisms , which is discussed in Chapter 5. Besides aptamers, nucleic acids with catalytic activities are also of our interest. We are working on new strategies for catalytic nucleic acids detection and selection. Chapter 2 of the thesis describes a proof-of-concept experiment for the novel detection of catalytic nucleic acids using a single enzyme detection platform.

Chapter 2: Assessing the Abundance of Catalytic Nucleic Acids using Single Enzymatic Molecule Detection in a Microwell Array Device

2.1 Introduction

Despite comprising of only four chemically similar subunits, single stranded DNA (ssDNA) and RNA molecules can fold into various complex tertiary structures to bind different targets and even catalyze specific reactions [1]. Catalytic sequences have been successfully isolated by selecting for affinity towards a transition state analog of the reaction [32, 36, 110]. However, this selection strategy is based on a binding event rather than a direct catalytic reaction. Therefore, this indirect selection strategy only reflects the rate enhancement through stabilization of the transition state but ignores other possible catalytic mechanisms, which may limit the discovery of true catalysts. In addition, the method depends greatly on the correct choice of the transition state analog and thus it requires prior understanding of the mechanism. Moreover, the synthesis of the analog can be difficult. In vitro selection methods that separate sequences upon attaching to or cleaving from solid support by catalytic activities has become a more popular technique for catalysts selection [30, 111]. It discriminates catalytic sequences according to their ability to carry out real reactions. However, this method involves the self-modification of the catalytic sequence itself and thus can only be carried out in single turnover conditions. This contradicts the definition of catalysts which carry out multiple turnover reaction without being consumed or permanently modified. Therefore, it has only generated sequences with moderate rate acceleration, preventing the discovery of highly active catalysts. This method is also tedious, time consuming and expensive with no promise of successfully finding a new catalyst. Therefore, an ideal strategy would be to discriminate sequences according to their catalytic activities acting on free substrates with multiple turnovers.

Besides the selection of catalytic nucleic acids, there are still a lot of fundamental questions about the catalytic ability of nucleic acids that needs to be addressed, such as the scope of reactions that can be catalyzed by nucleic acids, the abundance of catalytic sequences in a random library for any given reaction, and how fast they can proceed. Current emphases are mostly put on the selection of active sequences from large pools and no previous work has been done to assess the frequency of active sequences. However, it would be interesting to study the catalytic abundance and efficiency of random libraries. This would help us to obtain pre-knowledge of the catalytic ability of nucleic acids before real selection of catalytic sequences and also conveniently test the prebiotic hypothesis. Such assessment would require discrimination of single catalytic sequences from large inactive ones. Considering the similarity of protein enzymes and ribozymes/deoxyribozymes, it would be an advantage to take use of single enzyme detection systems to study individual catalytic nucleic acid sequences. Various devices have been used to

achieve detection and characterization of enzymes at single molecule level by detecting fluorescent products generated in limited spaces as a result of enzymatic reactions [152, 154, 160, 171]. Similar strategy can be used to detect rare catalytic sequences in a large random library.

In this manuscript, we described an easy and convenient detection scheme that can be used to study catalytic nucleic acids. It can directly detect the catalytic products by isolated nucleic acid sequences acting on separate substrates with multiple turnovers. The method was firstly validated by the detection of single enzyme molecules as a model and then used to study the abundance, catalytic efficiency and functional range of nucleic acids. Large random libraries consisting of different RNA or ssDNA sequences have been incubated with fluogenic substrates in thousands of microwells fabricated in PDMS. The detection of catalytic sequences can be achieved by detecting fluorescent products generated by the active sequences.

2.2 Experimental Section

Chemicals and reagents

β-galactosidase (aqueous glycerol suspension) from *Escherichia coli* was purchased from Sigma-Aldrich (Saint Louis, MO). It was diluted to 4.22 μM in phosphate buffer containing 100 mM NaH_2PO_4 (Mallinckrodt, Paris, KY) and 1 mM $MgCl_2$ (Mallinckrodt) with a pH adjusted to 7.5, aliquoted and stored at -80 ℃. Fluorogenic substrate fluorescein-di-β-D-galactopyranoside (FDG) was obtained from Invitrogen (Grand Island, NY). AttoPhos substrate was purchased from Promega (Madison, WI). All samples and buffers used in nucleic acid experiments were prepared using nuclease-free water (Integrated DNA Technology Inc., Coralville, IA). The DNA library of 80 bases long, the RNA library of 50 bases long, and the RNaseAlert substrate were also purchased from Integrated DNA Technology Inc. (Coralville, IA). Both the DNA and the RNA libraries consist of completely random sequences, which allows the assessment of the catalytic abundance in completely random libraries.

Fabrication of the microwell array device

The microwell array device was fabricated on poly(dimethylsiloxane) (PDMS) using the rapid prototyping method [179]. A SU-8 photoresist SU-8 2010 (MicroChem Corp, Newton, MA) was spin-coated on a 4 inch Si wafer using the spinner CEE2 (Brewer Scientific, CA). After the soft bake, the photoresist was exposed to a UV light under the designed chrome mask using a contact aligner system MA-6 (Karl Suss, CA). Following the hard bake, the unexposed area was

removed by the developer propylene glycol monomethyl ether acetate (Sigma-Aldrich) while the exposed area remained on the Si wafer. The PDMS prepolymer (Sylgard 184, Dow Corning, MI) was then casted against the fabricated SU-8 master after it was treated in a fluorinated silane fume (tridecafluoro-1, 2, 2-tetrahydrooctyl)-1-trichlorosilane (United Chemical Technologies Inc, Bristol, PA). Following the baking at 60 ℃ in an oven, the PDMS layer hardened and was then peeled off the master and cut into desired size with the microwell array in the center of the chip. Each piece of the cut chips had a total of 40,000 microwells and the wells were grouped into 8 mm by 8 mm square. Each well was 10 μm in diameter and depth and they were 30 μm apart from each other.

Imaging of the device

The PDMS device was placed on a glass slide. A drop of fluorescein solution was pipetted onto the PDMS chip and another glass slide was pressed against the PDMS and squeezed the solution into the microwells. A SMZ 1500 stereomicroscope (Nikon Corp., Tokyo, Japan) mounted with an X-Cite 120PC metal halide lamp (EXFO Photonic Solutions Inc., Mississauga, Canada) and a QuantEM 512SC CCD camera (Photometrics, Tucson, AZ) were used to image the microchip. The microscope was equipped with an Endow GFP band-pass emission filter cube (Nikon Corp.) containing two band-pass filters (450-490 nm and 500-550 nm) and a dichroic mirror (495 nm cut-off). The entire instrument setup was enclosed in black fabric (Thorlabs, Newton, NJ). Image acquisition and data processing were accomplished by Micromanager software with Image J.

Single enzyme detection

The stock β-galactosidase was further diluted to a concentration so that on average there was less than one enzyme molecule in each well. The fluogenic substrate FDG was kept at 100 μM. The reaction buffer was 100 mM NaH_2PO_4, 1 mM $MgCl_2$ and 10 mg/mL bovine serum albumin (BSA). The BSA was added into the buffer to prevent enzyme adsorption to the PDMS wall and the resulting deactivation. After the FDG and the β-galactosidase were mixed in a vial, a drop of the mixture was immediately pipetted onto the microchip and the reaction mixture was sealed into the microwells by a glass slide. The microscope focused on 0.8 × 0.8 mm area (zoom 8×) of the micowell array and images of the focused area on the microchip were taken every 20 minutes during the incubation at room temperature.

Catalytic nucleic acid detection

Two different nucleic acid libraries were used to determine the abundance and the catalytic diversity and efficiency of completely random libraries. One was an 80 nt long single stranded DNA (ssDNA) library and the other was a 50 nt long RNA library. Three different substrates: FDG, AttoPhos and RNaseAlert substrate were tested to study the possible catalytic activity of the random libraries. 100-500 μM library was mixed with the fluogenic substrate and the mixture was pipette onto the microwell array chip. The reaction mixture was then incubated in each microwell for 2 hours at room temperature and images were taken every 20 minutes. The reaction buffer was 50 mM Tris, 100 mM NaCl, 100 mM KCl, 50 mM $MgCl_2$ and 0.05% Tween 20 at pH 7.0.

2.3 Results and Discussions

Imaging of the detection system

Figure 2.1a showed the image of the microwell array device enclosing 1 μM fluorescein under 8× zoom. These microwells were 10 μm in diameter and depth, and 40 μm apart from each other. They were grouped into 8 × 8 mm squares with 40,000 microwells and the solution was successfully filled into the PDMS wells upon squeezing by the glass slide. The distance between every adjacent two microwells was three times larger than the wells' diameter to leave enough contact area between the PDMS and glass to ensure good sealing. Different concentrations of fluorescein solution was enclosed in the microwells and the intensity of the microwells was found to be proportional to the concentration (Figure 2.1b). The standard deviation of different wells' intensities was less than 10% indicating a uniform filling of solutions using this method. The limit of detection calculated for fluorescein was 0.1 μM.

In order to further test the integrity of the sealing, an argon ion laser expanded into a ~150 μm wide line was employed to photobleach the center columns' microwells in the array for 5 minutes. Images of the photobleached area were taken periodically over 1 hour (Figure 2.1c and d). Clearly there was no cross-talk or diffusion of the fluorescein into the photobleached area from adjacent microwells for at least 1 hour, which proved the good sealing of the microwells.

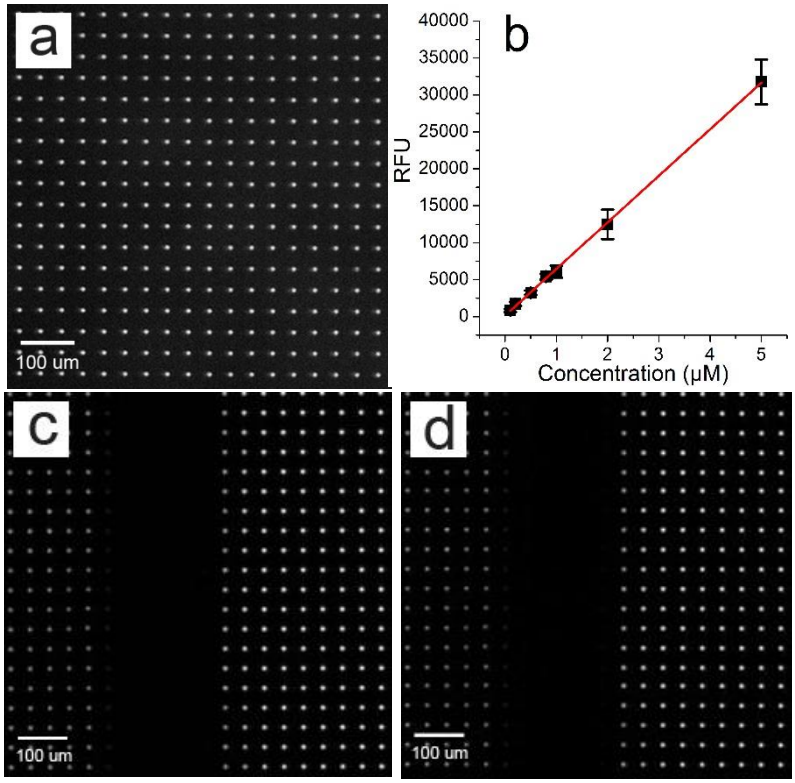

Figure 2.1. Microwells are 10 μm in diameter and depth and 40 μm apart from each other, with a volume of 785fL. (a) Microwell array enclosing 1 μM fluorescein. (b) Fluorecence intensity of microwells at different fluorescein concentration. (c) Image taken immediately after laser photobleaching. (d) Image taken 1 hour after photobleaching.

Single enzyme detection

β-galactosidase is a 465 kDa enzyme that catalyzes the hydrolysis of *β*-galactosides. Non-fluorescent substrate fluorescein-di-*β*-D-galactopyranoside (FDG) can go through a two-step hydrolysis catalyzed by *β*-galactosidase to form highly fluorescent products fluorescein-mono-*β*-D-galactopyranoside (FMG) and fluorescein. In the experiment, single enzyme molecules were incubated in individual microwells with excess substrates. Due to the small volume of the microwells, only 473 turnovers were enough to produce detectable amount of fluorescent products which can further be localized in the confined space in the microwells and the detection can be made in a relatively short period of time. Nonspecific adsorption to the highly hydrophobic PDMS surface can be a big problem for proteins especially for detection at single molecule level. A number of methods were used to prevent nonspecific adsorption of proteins to

PDMS [197-200]. Here, a concentrated BSA solution (10 mg/mL) was added to the reaction buffer to block the large surface area of the PDMS wall in the small microwells with such high surface to volume ratio to prevent enzyme adsorption and deactivation.

When 1.05 pM β-galactosidase was applied into the 785 fL microwells, on average there was 1 enzyme molecule in every 2 microwells. But statistically the enzyme molecules' distribution would result in a few microwells with more than 1 molecule and therefore more empty wells. After 1 hour's incubation at room temperature, 481 microwells were imaged and 134 of them (27.9%) became fluorescent while the others remained dark (Figure 2.2a and b). The distribution of enzyme molecules in the microwells should follow a Poisson distribution considering the limited number of enzyme molecules compared to the wells:

$$P\ (n, \lambda) = \frac{\lambda^k e^{-\lambda}}{n!} \qquad 2.1$$

where the λ is the average number of enzymes in each microwell (0.5 in this case) and *n* is the actual number of enzymes in these wells. So theoretically the percent of the total fluorescent wells should be 39.3%. This is close to the experimental result which is 27.9%. From the histogram, we noticed that the fluorescence intensity of the microwells covered a broad range but could be grouped into four distinct distributions. The four peaks were evenly spaced in the order of increasing fluorescence intensity and represented the microwells with zero, one, two and three enzymes respectively. More specifically, the percentage of peak area for 0, 1, 2 and 3 enzyme molecules were 71.2%, 24.6%, 3.5% and 0.7%. Those were in good agreement with the percentages predicted by Poisson's law which were 60.7%, 30.3%, 7.6% and 1.3%. Images of the microwell array and the histograms of the fluorescence of the wells using different enzyme concentrations were summarized in Figure 2.2. They showed similar distinct peaks and obeyed the Poisson's distribution. Furthermore, the broad distribution of the intensity under a single peak indicated the high heterogeneity of the activity of different enzyme molecules and the bulk activity is the average of all the individual enzyme molecules.

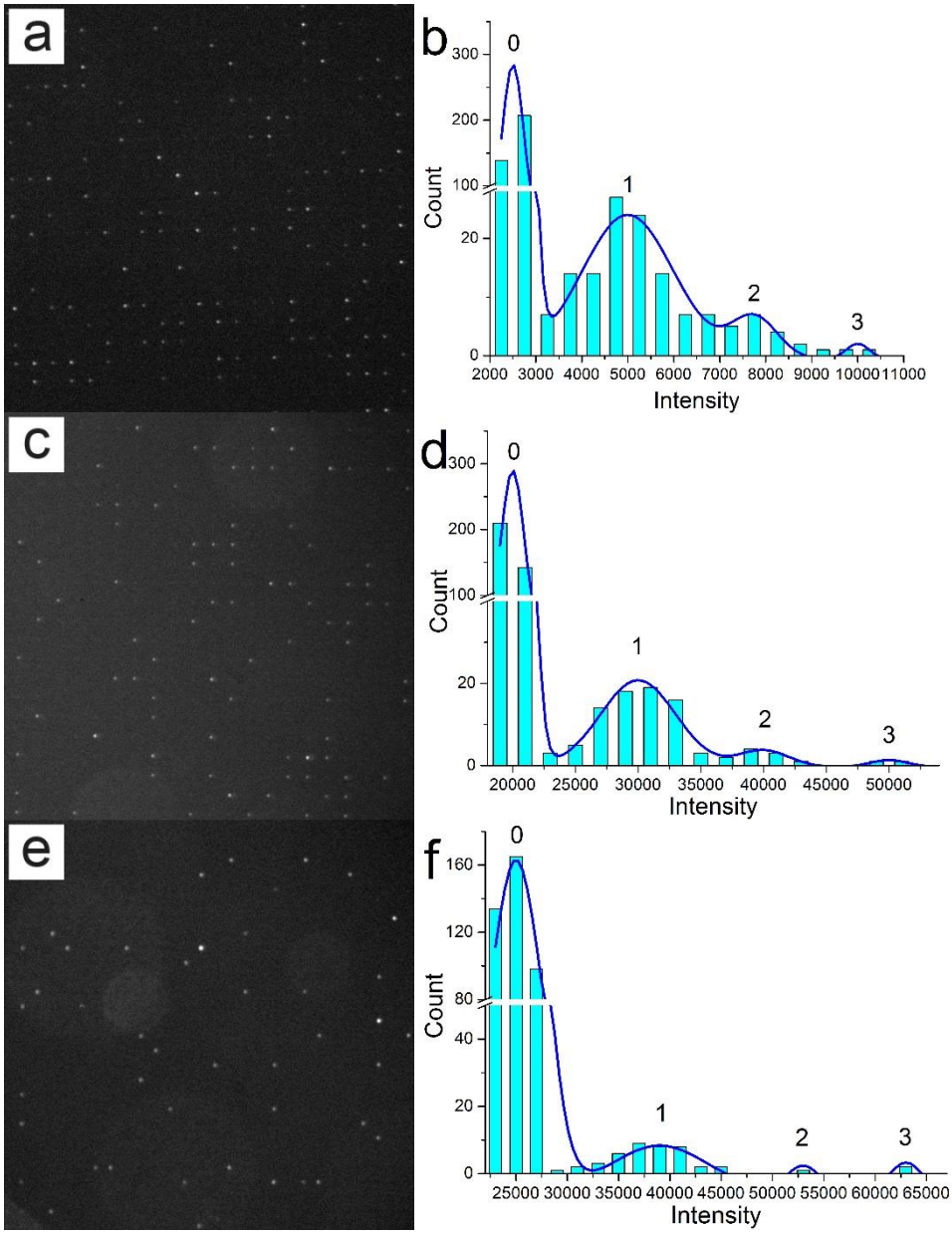

Figure 2.2. Images after 1 hour incubation of 100 μM FDG and *β*-galactosidase at enzyme to well ratio (a) 1:2, (c) 1:5 and (e) 1:10. Histograms showing the distribution of enzyme populations at enzyme to well ratio (b) 1:2, (d) 1:5 and (f) 1:10. A control was performed using only the substrate without enzyme and no fluorescent wells were observed.

The reaction kinetics of individual enzyme molecules trapped inside the microwells were also studied by taking images of the microwell array over time. The fluorescence intensity in individual microwells was recorded and analyzed. Considering the single enzyme environment in

the microwells, there is an excess of the substrates and the enzyme is always saturated. Figure 2.3 showed that the fluorescence continuously increased linearly over time in individual wells which proved a saturated enzymatic activity and the fact that the enzyme molecules were not inactivated by surface adsorption during the incubation. There were three different types of microwells with distinct reaction rates (slopes). The bottom trace showed no increase in fluorescence indicating an empty microwell without any enzymes. The three traces in the middle shared similar increasing rates in fluorescence and represented microwells with only one enzyme molecule. The top trace with the reaction rate of as twice as the middle traces were the microwells with two enzymes.

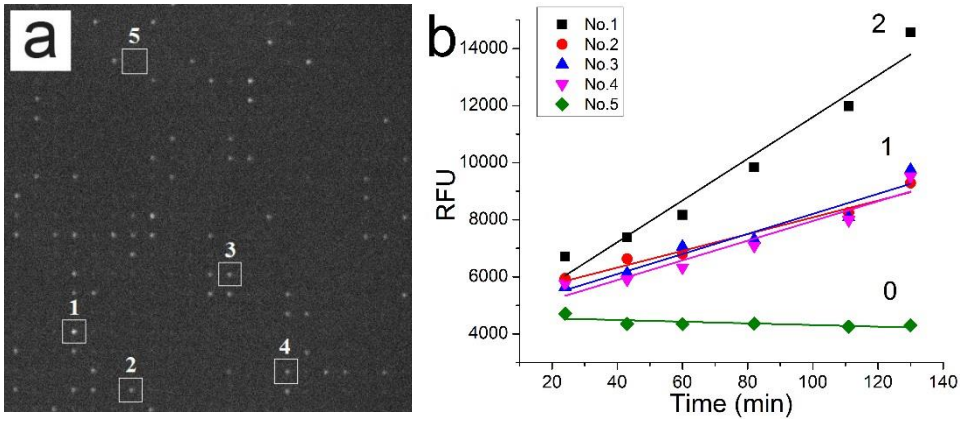

Figure 2.3. Kinetic measurement of individual enzymes. (a) Five representative microwells were selected and numbered in white squares. 100 μM FDG was incubated with 0.42 pM *β*-galactosidase (1 molecule in every 5 microwells) at room temperature. Image was taken after 82min incubation. (b) Intensity of the selected microwells was plotted for the 2 hours' incubation period. The numbers above the trajectories indicated the number of enzyme molecules in corresponding microwells: No.1 well contains two enzyme molecules; No.2, No.3, and No.4 contain one enzyme molecule; No.5 well contains no enzymes.

Catalytic nucleic acid detection

After validating the detection system using single enzyme experiments, random nucleic acid libraries were used to determine the abundance of possible ribozymes (for RNA libraries) and deoxyribozymes (for ssDNA libraries). High concentration of nucleic acid libraries (up to 500 μM or 2×10^8 molecules per well) were used to increase the number of incubated sequences and accordingly the chance of detecting catalytic sequences. Sufficient metal ions were added

into the reaction buffer to help possible foldings and catalytic activities of the nucleic acids. In previous discovery of catalytic nucleic acids, the active sequences were selected either based on binding the transition state analog[32, 33, 36, 37, 39] or as a participant in a single turnover reaction[27-31]. Therefore the sequences were not selected directly according to the definition of enzymes which should carry out multiple turnover reactions without changing themselves. This might limit the discovery of real and fast ribozymes or deoxyribozymes. However, in the method reported here, only sequences that can convert multiple fluogenic substrates into fluorescent products can be detected and quantified. And this would allow the discovery of real catalytic sequences acting on separate substrates free in solution with multiple turnovers.

Three different enzymatic reactions were studied using three different substrates. RNaseAlert substrates were used to test the ribonuclease activity. FDG was used to study *β*-galactosidase activity and AttoPhos substrates were for alkaline phosphatase activity. These enzymatic systems were chosen as most known ribozymes/deoxyribozymes catalyze reactions involving phosphodiester bonds. Unfortunately, no fluorescent microwells were detected for all three substrates and two random libraries even after two hours' incubation, indicating no catalytic sequences were present in these microwells. Figure 2.4 shows a typical image after incubating ssDNA or RNA library with one of the above fluogenic substrates. The total volume of imaged area was about 380 pL and the total number of sequences enclosed was up to 1.0×10^{11}. The PDMS device can further be moved around to take images of all the microwells on the chip so the total number of sequences can even reach as high as 1.0×10^{13}. The limit of detection for the three fluorescent products was measured to be 0.043 μM for RNaseAlert, 0.066 μM for FDG and 3.46 μM for AttoPhos. Considering the incubation time, single catalytic sequence with rate constant greater than 2.8 s^{-1}, 4.3 s^{-1} and 227 s^{-1} would have generated fluorescent products above these LODs. So we can conclude that there are no sequences with a catalytic rate at these levels among the incubated 10^{13} sequences for RNase, *β*-galactosidase and alkaline phosphatase activities and the corresponding substrates. It indicated that we would need to study much larger random libraries if we were looking for any catalytic sequences from a completely random library for comparable turnover rates for these activities or larger sequences are necessary to make the necessary structures for catalysis. This preknowledge of the abundance and catalytic efficiency of nucleic acid catalysts in a random library would also be of great importance for the design of future selection experiments.

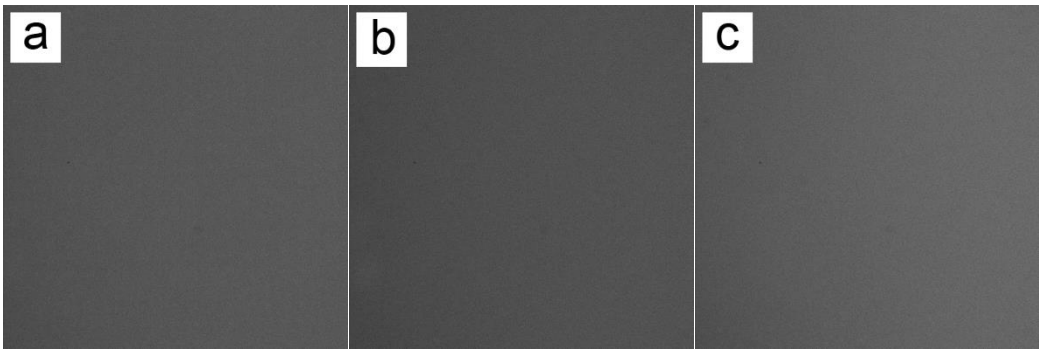

Figure 2.4. Image of microwell array after 2 hours incubation of: (a) 1 μM RNaseAlert substrate with 100 μM ssDNA library. (b) 100 μM FDG substrate with 100 μM ssDNA library. (c) 300 μM AttoPhos substrate with 100 μM ssDNA library.

2.4 Conclusions

In this work, detection of single enzyme activity has been achieved by monitoring the conversion of a non-fluorescent substrate into a highly fluorescent product using a microwell array device fabricated in PDMS. This demonstrated the feasibility of extending the strategy to any similar reactions generating multiple copies of fluorophore and catalyzed by a single molecule which works exactly like an enzyme. It is the case for the study of catalytic nucleic acids in a large random library where there may be only one copy of each sequence. However, among the three enzymatic activities studied, we didn't detect any fast catalytic sequences (k_{cat} greater than 1 s^{-1}) in 10^{13} random sequence ssDNA or RNA libraries. This indicates either less abundant active sequences or sequences with lower catalytic rates should be expected for those studied enzymatic activities in a random library. To further detect if there are any catalytic sequences with a lower turnover rate in a larger library, simultaneous monitoring of numerous ultrasmall reaction chambers and longer incubation time should be employed. Such assays have been made possible recently by advantages in microfluidics, especially droplet-based devices[201-203] and single cell/enzyme analysis research[171, 204, 205]. Future work will be focused on taking use of microdroplets as the reaction chambers to enclose larger number of sequences and provide longer incubation times and droplets containing catalytic sequences are expected to be detected and even collected for further isolation and sequencing.

Chapter 3: Capillary Electrophoresis-SELEX Selection of Catalytic DNA Aptamers for a Small-Molecule Porphyrin Target

3.1 Introduction

Aptamers are single stranded DNA (ssDNA) or RNA sequences that bind targets with high affinity and specificity. They are selected in vitro through a process referred to as systematic evolution of ligands by exponential enrichment (SELEX).[80] In the SELEX process, iterative rounds of separation of bound sequences, PCR amplification and purification are employed to evolve aptamers with high affinity. Recent technology advancement has brought in a more efficient and free-solution SELEX technique named CE-SELEX which uses capillary electrophoresis as the means of separation.[98, 99] However, CE-SELEX has been previously only used for isolating aptamers for large protein targets[99, 101, 116, 117] as it requires the aptamers to undergo a large mobility shift upon binding the targets. In a recent study, aptamers for a small peptide target neuropeptide Y (4272 Dalton) which is even smaller than the DNA itself (25 KDa) have also been successfully selected using CE-SELEX in only four rounds indicating the potential of using CE-SELEX for small molecule targets.[100] In the case of small molecule targets, the mobility of the complex is expected to be changed only minimally from the non-binding sequences, resulting in only partial separation of the bound and unbound sequences. However, due to the fact that nucleic acids can be exponentially amplified by PCR, even if only a small portion of the complex can be collected, satisfactory enrichment can be achieved. Moreover, under the case of separation with low resolution, multiple iterative rounds of enrichment can still eventually evolve a high abundant pool with high affinity aptamers.[206]

In this chapter, we describe using CE-SELEX to select DNA aptamers for a small molecule target: N-methyl mesoporphyrin Ⅸ (NMM). NMM is a small organic compound with a molecular weight of only 580 g/mol which is nearly an order of magnitude smaller than neuropeptide Y. To our knowledge, CE-SELEX has never before been used to isolate apatamers for such small targets. Figure 3.1 illustrates the chemical structure of NMM. It takes a distorted planar structure due to the presence of the methyl group. The bent aromatic ring system mimics the transition state of the porphyrin during metallation and inhibits the corresponding metal insertion reaction catalyzed by porphyrin chelatase.[207] Both RNA[36, 208] and DNA[37, 209, 210] aptamers have been selected for NMM previously using affinity columns and found to be catalytic for porphyrin metallation reactions. We are now using CE-SELEX for the selection of NMM aptamers to investigate the limit of this technique in selecting aptamers with affinity for small molecule targets.

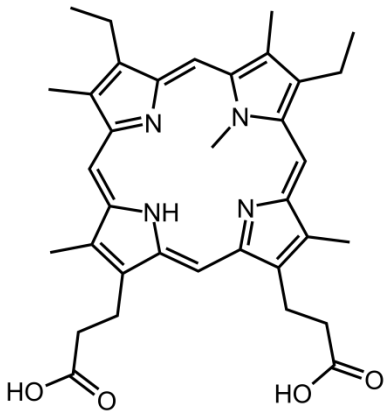

Figure 3.1.Chemical structure of the target N-methyl mesoporphyrin Ⅸ (NMM), MW=580g/mol

3.2 Experimental Section

Chemicals

N-Methyl Mesoporphyrin IX (NMM) was purchased from Frontier Scientific Inc. (Logan, Utah). The ssDNA library used for selection consisted of 40 random bases flanked by two primer regions (5'-AGC AGC ACA GAG GTC AGA TG (40 random bases) CCT ATG CGT GCT ACC GTG AA-3'). The ssDNA library, primers and selected aptamers were all synthesized by Integrated DNA Technologies, Inc. (Coralville, IA). dNTPs and 25 bp DNA ladder were obtained from Life Technologies (Grand Island, NY). Taq polymerase and ThermoPol buffer were obtained from New England Biolabs (Ipswich, CA). The gel loading dye was from Promega (Madison, WI). All other chemicals were purchased from Sigma-Aldrich (St. Louis, MO). All the samples and buffers were prepared using 0.2 μm membrane filtered water from Milli-Q water purification system (Millipore Corp., Billerica, MA).

Capillary electrophoresis selection

Before selection, ~100 μM ssDNA library was heated to 72 ℃ for 10 min in TGK buffer (25 mM Tris, 192 mM glycine, 5 mM KH_2PO_4, pH 8.3) and cooled down to room temperature. The target NMM was then added to the library to a final concentration of 1 μM for the first round and 100 nM for subsequent rounds of selection. The ssDNA library was allowed to incubate with the NMM at room temperature for at least 20 min to ensure that the binding reached equilibrium.

Capillary electrophoresis selection was performed using a 40.2 cm-long (with 30 cm to the detector), 50 μm-inner diameter, 360 μm-outer diameter uncoated fused silica capillary

(Polymicro Technologies, Phoenix, AZ) on a P/ACE MDQ capillary electrophoresis system (Beckman Coulter Inc., Fullerton, CA). The capillary was first rinsed with 0.15 M NaOH and then the TGK buffer for 4 min under 30 psi pressure before injection of the incubation mixture at 1 psi for 4 s. The mixture was separated under 30 kV voltage (normal polarity) in TGK buffer at 25 ℃ and the separation was monitored under UV absorbance detection at 254 nm. The NMM-aptamer complex migrated off the capillary before the unbound ssDNA and was collected into a vial containing 48 μL separation buffer at the capillary outlet. After collecting the bound sequences, the voltage was turned off and the unbound sequences were washed off the capillary into a waste container using high pressure.

PCR amplification and ssDNA generation

The collected sequences were then PCR amplified to generate a new pool for the next round of selection. The PCR reaction master consisted of 200 μM dNTPs, 510 nM forward primer (5'-AGC AGC ACA GAG GTC AGA TG-3'), 510 nM biotinylated reverse primer (5'/biotin/-TTC ACG GTA GCA CGC ATA GG-3'), 0.025 unit/uL Taq polymerase and 7.5 mM $MgCl_2$ in 1x ThermoPol PCR buffer (20 mM Tris-HCl, 10 mM $(NH_4)_2SO_4$, 10 mM KCl, 2 mM $MgSO_4$, 0.1% Triton X-100, pH 8.8). The high magnesium concentration helped improve the PCR efficiency of amplifying such a low concentration of the collected bound sequences. 20 cycles of denaturation (94 ℃, 30 s), annealing (53 ℃, 30 s) and extension (72 ℃, 20 s) were performed and followed by a final 5 min extension period at 72 ℃. The length and the yield of the PCR products were verified and estimated using electrophoresis on a 1.5% agarose gel stained with ethidium bromide and imaged using a UV transluminator (Spectroline, Westbury, NY).

The PCR products were purified and made single stranded using a streptavidin agarose resin (Pierce Biotechnology, Rockford, IL) and chromatography column (Bio-Rad, Hercules, CA). The PCR products were first incubated with streptavidin agarose resin in binding buffer (10 mM Tris, 50 mM NaCl and 1 mM EDTA, pH 7.5) for 30 min with periodical shaking. The column was then washed 10 times with 1 mL buffer to remove the PCR reagents while the amplified dsDNA was retained on the column through the interaction between streptavidin and the biotinylated strand. The desired forward DNA strand was eluted out of the column by incubating with 0.15 M NaOH for 10 min at 37 ℃ and desalted and concentrated by ethanol precipitation.

Dissociation constant K_d measurements

Dissociation constants K_d were measured by monitoring the increase of the fluorescence intensity of NMM after binding the aptamers[140, 211]. Aptamers of varying concentrations were

mixed with 500 nM NMM after 10 min annealing at 72 ℃ and slowly cooling down to room temperature in TGK buffer. The fluorescence intensity of 15 μL of each mixture sample was measured in a 384-well microplate (Corning Inc., Corning, NY) using a Synergy 2 Microplate Reader (BioTek, Winooski, VT). Fluorescence was excited using a tungsten lamp with a 360/40 nm filter and measured at 610 nm emission. The net increase of the fluorescence intensity was then plotted against the aptamer concentration and the dissociation constant K_d can be determined by fitting the binding curve using the following equation:

$$I - I_0 = \frac{p[aptamer]}{K_d + [aptamer]} \qquad 3.1$$

where I and I_0 are the fluorescence intensity of NMM in the presence and absence of aptamers respectively. Dissociation constant K_d and another constant p were obtained by non-linear fitting using the Origin v8.5 (OriginLab Corporation, Northampton, MA).

DNA cloning and sequencing

ssDNA sequences were cloned after 3 rounds and 6 rounds of selection using a TOPO TA Cloning kit from Invitrogen (Grand Island, NY). Aliquots of the two selected pools were PCR amplified under the same conditions described previously except using non-labeled reverse primer and 10 min final extension period. The PCR products were ligated onto pCR4-TOPO vectors and transformed into TOP10 Chemically Competent *E.coli* cells. Individual colonies were randomly picked and cultured in liquid LB broth (Invitrogen, Grand Island, NY) after growing the cells for 24 hours on a LB plate at 37 ℃. Plasmid vectors containing selected sequences were extracted from the cells after overnight growth in LB broth at 37 ℃ using the plasmid miniprep kit from Invitrogen (Grand Island, NY). The vectors were sequenced by the BioMedical Genomics Center at the University of Minnesota (St. Paul, MN) using the T7 promoter primer.

Catalytic activity measurements

The initial rate of Cu (Ⅱ) insertion into mesoporphyrin Ⅸ (MP) catalyzed by selected aptamers was measured by monitoring the absorbance at 561 nm of the reaction mixture in a clear 96-well microplate (Corning Inc., Corning, NY) using the Microplate Reader. 5 μM of the selected aptamers were initially annealed at 72 ℃ in kinetics buffer (25 mM Tris-OAc, 25 mM KCl, pH 7.5) for 10 min. After slowly cooling down to room temperature, Triton X-100, dimethyl sulfoxide (DMSO) and the MP were then added to final concentrations of 0.5% (w/v) Triton X-100, 1% (v/v) DMSO and 100 μM MP. The mixture was allowed to equilibrate for more than 20

min at room temperature before the addition of 200 μM $Cu(OAc)_2$ to initiate the reaction. The reaction rate was calculated according to the molar absorption difference (ε = 18.6 $mM^{-1}cm^{-1}$)[212] of MP and its product Cu-mesoporphyrin Ⅸ (Cu-MP). The UV absorbance spectra of MP and Cu-MP were also measured using the Microplate Reader. Cu-MP was synthesized by incubating 200 μM $Cu(OAc)_2$ with 100 μM MP in dark for 24 hours.

3.3 Results and Discussions

CE-SELEX selection

Figure 3.2 illustrates the overall selection scheme of CE-SELEX. Briefly, a random ssDNA library containing 10^{12}-10^{13} sequences is incubated with a low concentration of target in free solution followed by CE separation. The bound sequences are separated from the unbound sequences and collected for PCR amplification. The bound fraction is thus enriched and then purified and made single stranded again for next round of selection. This process repeats until there is no more affinity improvement in the selected pools. Finally the sequences can be determined by cloning and sequencing the selected pools.

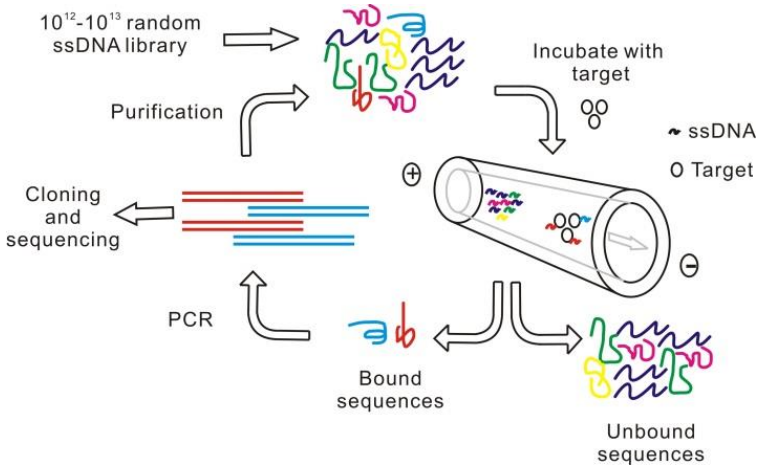

Figure 3.2. Schematic illustration of CE-SELEX process.

In the presence of electroosmotic flow (EOF), the unbound ssDNA migrates off the capillary as a single peak while the aptamer-NMM complex would be expected to migrate off the capillary earlier due to the larger size and lower electrophoretic mobility. Due to the small size of NMM, the change in the electrophoretic mobility of the ssDNA upon binding the target is

expected to be small and the complex may not be completely resolved from the unbound peak. Taking this into account a collection window was chosen immediately before the leading edge of the free ssDNA peak (see Figure 3.3). The single peak observed in the electropherogram is the large excess of unbound ssDNA. Binding sequences were collected up to the time point marked with the arrow. We anticipate CE-SELEX would be successful even if the bound and unbound ssDNA are not completely resolved since the leading edge of the unresolved peak would be biased toward the bound sequences. In this case more rounds of selection may be necessary to fully enrich the ssDNA pool with binding aptamers.

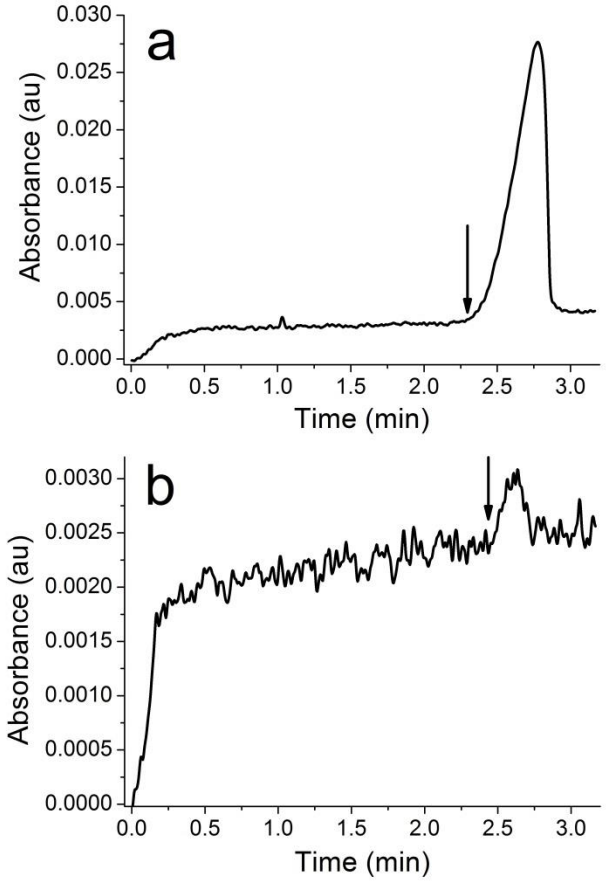

Figure 3.3. Selection electropherograms for: a) 1st round of selection and b) 2nd round of selection. The selection electropherograms for rounds 3 through 6 are similar to the 2nd round.

The affinity of the enriched pool was assessed after each round to determine if further rounds of selection were needed. Previously reported aptamers for NMM are capable of increasing the fluorescence of NMM by over 20-fold upon binding[140, 213]. Therefore a similar

fluorescence assay was chosen to assess the affinities of the selected pools for NMM. The dissociation constants of aptamers for small molecules such as NMM typically range from the high nanomolar to low micromolar range[2, 36, 208, 209]. The amount of ssDNA recovered after each selection round was limited, preventing us from obtaining a complete binding curve with the μM NMM concentrations necessary to saturate the aptamers. Instead, the fluorescence of only one sample containing 500 nM NMM and 2-fold diluted (~1 μM) ssDNA from each selected pool was used to estimate the binding affinity. Figure 3.4 shows the normalized fluorescence intensity of NMM upon binding each selected pool. From the 1st round through the 4th round, the affinity of the selected pools improves with increasing rounds of selection. After 3 rounds of selection, the fluorescence of the complex increases by over 2-fold. However, after 4 rounds of selection, instead of increasing, the overall fluorescence intensity decreases slightly for the 5th and 6th rounds. This indicates there is no more affinity improvement for 5th and 6th round of selection.

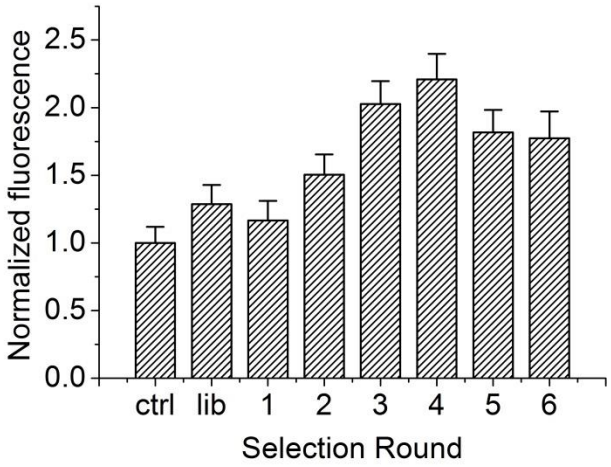

Figure 3.4. Normalized fluorescence intensity of NMM upon binding each selected pool. The first column is the fluorescence intensity of native NMM in the absence of ssDNA. All other measurements were normalized to this control. Error bars represent the standard deviation.

The ssDNA pools from the 3rd and 6th rounds were cloned and sequenced after the selection. 20 sequences from the 3rd round pool and 35 sequences from the 6th round pool were identified. The detailed sequence information is summarized in Table 3.1. 20 aptamer sequences were obtained for selection round 3. 36 clones were sequenced for round 6 but clone 6.16 failed. Therefore, only 35 sequences from round 6 are listed below. Note that sequence heterogeneity in the pools remains high throughout the selection, a characteristic common for CE-SELEX.

Although no single common sequence motif was identified, we observed that the sequences from the 3rd round pool all contain 30-40% guanines, which is statistically higher than the 25% percentage predicted in a random library. 80% of the sequences have 4 continuous guanines (-GGGG-) and 40% of sequences have 4 double guanines (-GG-) sequences. This suggests that these sequences are potentially capable of forming either inter- or intra-molecular G-quadruplex structures. This feature is in good agreement with previously selected NMM aptamers, which also adopt G-quadruplex structures[140, 209, 214]. However, the sequences from the 6th round deviate from the previous trend with only 8% -GGGG- and 17% four double guanines (-GG-) in a given sequence. The overall percentage of guanine in one sequence also drops to 25%. We attribute this deviation to the difficulty PCR amplifying sequences with high guanine percentages. It was noticed that the PCR yield for the 5th and 6th round of selection was much higher than the previous rounds probably due to the decrease in the guanine percentage.

Table 3.1. NMM aptamer sequences after 3 and 6 rounds of selection*

Clone	Sequence (5' - 3')
3.1	**AGCAGCACAGAGGTCAGATG**GTAAAGAGATTCTAATGGGGGATGGTCCTGTAGTTCCCTC**CCTATGCGTGCTACCGTGAA**
3.2	**AGCAGCACAGAGGTCAGATG**AAGGGGGGCGCCTTAGACTGGCCATAAATAGGGTAGTACT**CCTATGCGTGCTACCGTGAA**
3.3	**AGCAGCACAGAGGTCAGATG**TTGAAAGTGGGGGTCACGGTGTGCATTGGGTAAACAGATGT**CCTATGCGTGCTACCGTGAA**
3.4	**AGCAGCACAGAGGTCAGATG**TATTTCGGGGTTGATTAAACGCGAGTAAAGCACCACTGTT**CCTATGCGTGCTACCGTGAA**
3.5	**AGCAGCACAGAGGTCAGATG**AAAAGAATGCTCATCCTGGGGTAGGCATGAAGCGGGGCCG**CCTATGCGTGCTACCGTGAA**
3.6	**AGCAGCACAGAGGTCAGATG**ATTCGATGTTTTAATCTTAGAATAATTTGCTATTAAGCTT**CCTATGCGTGCTACCGTGAA**
3.7	**AGCAGCACAGAGGTCAGATG**TACGCGTTGGGTTAATATGTGGGTAGTGTGTGTAGTGGA**CCTATGCGTGCTACCGTGAA**
3.8	**AGCAGCACAGAGGTCAGATG**AGGTTATCTCATCGATTTGTCATGCATTAGAACTCGTTTC**CCTATGCGTGCTACCGTGAA**
3.9	**AGCAGCACAGAGGTCAGATG**GCTGAGAGGCCTTAGTGGGTAGGACAGTAATGGGGGTGAC**CCTATGCGTGCTACCGTGAA**
3.10	**AGCAGCACAGAGGTCAGATG**GGGGGTCTGCTGCATGACGGTTGGAGGTATGACGTTCCTA**CCTATGCGTGCTACCGTGAA**
3.11	**AGCAGCACAGAGGTCAGATG**ACCTTGAACACTCAGGTTCTTTTTCAGGGGGCCTAAACAT**CCTATGCGTGCTACCGTGAA**
3.12	**AGCAGCACAGAGGTCAGATG**ATGGTCATTGGGGGACAAACTGGCTAGAGGGCTCGGGGTT**CCTATGCGTGCTACCGTGAA**
3.13	**AGCAGCACAGAGGTCAGATG**AAGGGTTGAATATGGGAATTGGTAGAGGGGAACACAGCTG**CCTATGCGTGCTACCGTGAA**
3.14	**AGCAGCACAGAGGTCAGATG**ATTTGGGATGTCTGAAGGGGCGCCGAATTATAGTGCTTCC**CCTATGCGTGCTACCGTGAA**
3.15	**AGCAGCACAGAGGTCAGATG**CGCTCTGTAGATAGCAACACATTGGAGGGGTGTAAAGAT**CCTATGCGTGCTACCGTGAA**
3.16	**AGCAGCACAGAGGTCAGATG**ATTGGTGTTAGGGGCGATCCTGTCTGGGGGTAGTCGCTG**CCTATGCGTGCTACCGTGAA**
3.17	**AGCAGCACAGAGGTCAGATG**GGGGGTTAATAGTGTCGCCTAAGGTCACCGCCGCGGGGTA**CCTATGCGTGCTACCGTGAA**
3.18	**AGCAGCACAGAGGTCAGATG**TTCAGCGATTACTCCAGGCCAACGGGGAACCAAAGGGGT**CCTATGCGTGCTACCGTGAA**
3.19	**AGCAGCACAGAGGTCAGATG**TTGACACCGATGCGGTATCAGGGGGGCGAGTAGCGCCGCA**CCTATGCGTGCTACCGTGAA**
3.20	**AGCAGCACAGAGGTCAGATG**ACTAGCGGGAGTGCTTCGGTCTGGATGCGCATGGGGTATG**CCTATGCGTGCTACCGTGAA**

6.1	**AGCAGCACAGAGGTCAGATG**ATTAATTTTTTTGTTTGATTATAATTTTAGTACTGATTCA**CCTATGCGTGCTACCGTGAA**
6.2	**AGCAGCACAGAGGTCAGATG**ATCTACGCTGTATTCGCAAACTATAATGCCCGGTAGTACC**CCTATGCGTGCTACCGTGAA**
6.3	**AGCAGCACAGAGGTCAGATG**GACTCAGTCAGCCTGTCAAATGTACGTTAGATTTTCAATG**CCTATGCGTGCTACCGTGAA**
6.4	**AGCAGCACAGAGGTCAGATG**ATTGGAGGAAGGGAGGTACAGTTACATATCACGTTAACGG**CCTATGCGTGCTACCGTGAA**
6.5	**AGCAGCACAGAGGTCAGATG**GTCTTTTTTATCACTAGGTTAAATCCAATTCTTCGTTCTT**CCTATGCGTGCTACCGTGAA**
6.6	**AGCAGCACAGAGGTCAGATG**TAGATTATTAAGAAAGCATAGTTGGAGCTAAAATACGGTT**CCTATGCGTGCTACCGTGAA**
6.7	**AGCAGCACAGAGGTCAGATG**ATCACATCTCCAGGTTTCTGGGAAGTAGCACCCTCAAACG**CCTATGCGTGCTACCGTGAA**
6.8	**AGCAGCACAGAGGTCAGATG**TTGACTCGTTAATCGTAATTTAAAAATCAGGTATCCTTCT**CCTATGCGTGCTACCGTGAA**
6.9	**AGCAGCACAGAGGTCAGATG**GCTAGTCCAGCTGTCAGGAGTGCACACCTCCCGTCAATAG**CCTATGCGTGCTACCGTGAA**
6.10	**AGCAGCACAGAGGTCAGATG**AAGCCTATCTTGGAGCTTTGCAGACTCGATGTATAGTACG**CCTATGCGTGCTACCGTGAA**
6.11	**AGCAGCACAGAGGTCAGATG**TTTATAGCAATCTCGATAGGGTAAAGATGTGGTGGGTTGC**CCTATGCGTGCTACCGTGAA**
6.12	**AGCAGCACAGAGGTCAGATG**TTATGAAATTAAAGACTTACCTTATAAGTTGTACAAACAC**CCTATGCGTGCTACCGTGAA**
6.13	**AGCAGCACAGAGGTCAGATG**GGCGTAATAAATTCGTGGTAATAGAGGGTCTTTTGGCGCT**CCTATGCGTGCTACCGTGAA**
6.14	**AGCAGCACAGAGGTCAGATG**AGGCGCAGGTATACCAGGGCGGAGTAAAGTCCATGTAGGG**CCTATGCGTGCTACCGTGAA**
6.15	**AGCAGCACAGAGGTCAGATG**ATTATGGTGTCCGATTATGGTGGGGGAATCAC**CCTATGCGTGCTACCGTGAA**
6.17	**AGCAGCACAGAGGTCAGATG**TCGTAATCAGTGGGTGAGAACAGGCTAATCTACTAATCTG**CCTATGCGTGCTACCGTGAA**
6.18	**AGCAGCACAGAGGTCAGATG**AGTTTGCTCAATAAACGTTTTTACTGACTTGAATTCTGCC**CCTATGCGTGCTACCGTGAA**
6.19	**AGCAGCACAGAGGTCAGATG**ATCAAGCGCAGAAACCTCCTATGCGGCCACGCAGTGCCCC**CCTATGCGTGCTACCGTGAA**
6.20	**AGCAGCACAGAGGTCAGATG**TTTAGAGTGGTTTTATGTATGGGTATTTTCATAGAAAGTG**CCTATGCGTGCTACCGTGAA**
6.21	**AGCAGCACAGAGGTCAGATG**GGTCTAATCATTGACTTACGTTGATGTGTCGATCTATGCT**CCTATGCGTGCTACCGTGAA**
6.22	**AGCAGCACAGAGGTCAGATG**TTATGAAATTAAAGACTTACCTTATAAGTTGTACAAACAC**CCTATGCGTGCTACCGTGAA**
6.23	**AGCAGCACAGAGGTCAGATG**TGCTCGACTATTGAGTCAGGGGGTTGGGGCAACAATAAGC**CCTATGCGTGCTACCGTGAA**
6.24	**AGCAGCACAGAGGTCAGATG**GTTTAGTCTACGACATCGAATAAGTGTCTTTCAATTCACA**CCTATGCGTGCTACCGTGAA**
6.25	**AGCAGCACAGAGGTCAGATG**TTGGGCCTACGGGGACACCAAACGGGGAGTCTAAATGCTA**CCTATGCGTGCTACCGTGAA**
6.26	**AGCAGCACAGAGGTCAGATG**GTCACGTTATTTAACTTAGGAGAATAGAACACCCGCTGTT**CCTATGCGTGCTACCGTGAA**
6.27	**AGCAGCACAGAGGTCAGATG**TAGACGGTAACGCAACCTATATTAGGATTTTAGAGTTACC**CCTATGCGTGCTACCGTGAA**
6.28	**AGCAGCACAGAGGTCAGATG**GGTATACGTTATGATATTACTAAAAAGGGACAGTGTTCAG**CCTATGCGTGCTACCGTGAA**
6.29	**AGCAGCACAGAGGTCAGATG**CCCTTTTAAAGACTTTCACTAGGCCTTCTAACACAGTAAA**CCTATGCGTGCTACCGTGAA**
6.30	**AGCAGCACAGAGGTCAGATG**TAACGGCGAGTGATTACGACTCTCACGGGTAGTCGGTCAA**CCTATGCGTGCTACCGTGAA**
6.31	**AGCAGCACAGAGGTCAGATG**ATATACGTCTATAAGTTCTGACTTTTGAAATAGAGTGAAT**CCTATGCGTGCTACCGTGAA**
6.32	**AGCAGCACAGAGGTCAGATG**AATTCTGTTCCCTGATATTAATCTGCACCCCTCCTACACC**CCTATGCGTGCTACCGTGAA**
6.33	**AGCAGCACAGAGGTCAGATG**ATAATTGCGTATAGTATGCTCTCTGCTGTTTGGTAATAAG**CCTATGCGTGCTACCGTGAA**
6.34	**AGCAGCACAGAGGTCAGATG**TTTAGAGTGGTTTTATGTATGGGTATTTTCATAGAAAGTG**CCTATGCGTGCTACCGTGAA**
6.35	**AGCAGCACAGAGGTCAGATG**ATATGGTTTTATTTATTACATAGATTTTGCTAGGTATTTA**CCTATGCGTGCTACCGTGAA**
6.36	**AGCAGCACAGAGGTCAGATG**ATCAGTAGTAACTCTTCTATCCTACGCATAATGGTTCGGG**CCTATGCGTGCTACCGTGAA**

* Bases in bold represent the primer regions.

Dissociation constants of selected aptamers

Four sequences were randomly chosen from each of the sequenced pools for further characterization. Two sequences from 6th round pool that appeared twice in the cloning results were chosen since these sequences may be present in higher abundance. The dissociation constants for these sequences were determined by measuring the fluorescence enhancement of NMM upon binding DNA aptamers. Figure 3.5 shows a representative binding curve of one of the clones and a similar curve for the starting library. The fluorescence intensity of NMM-clone 6.23 complex (red) reaches saturation in the presence of approximately 12.5 μM aptamer while even in the presence of 100 μM library, the fluorescence intensity of NMM is less than half of the maximum and it is still continuously increasing according to the trend (blue). Clearly there is a substantial improvement in the binding affinity for the selected clones.

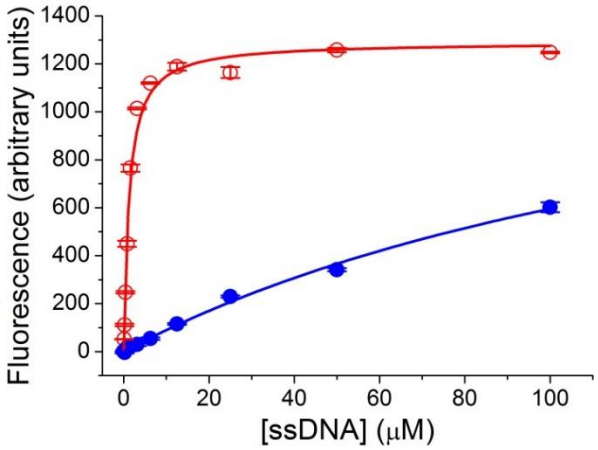

Figure 3.5. Binding curves for clone 6.23 (red open circles) and the random ssDNA library (blue solid circles). The error bar represents the standard deviation. The K_d determined for clone 6.23 is 1.2 ± 0.1 μM. The K_d for the unselected library is estimated to be > 50 μM.

The dissociation constants of all the synthesized clones are summarized in Table 3.2. All the clones from the 3rd round pool bind the NMM with K_d values ranging from hundreds of nanomolar to several micromolar. This is again in good accordance with previously reported K_d values for NMM aptamers[36, 208, 209]. It also demonstrates that DNA aptamers binding NMM can be evolved after only 3 rounds of CE-SELEX selection. However, for sequences from the 6th round, only clone 6.23 binds the NMM with a similar K_d of 1.2 μM. Clone 6.4 binds the NMM with a fairly high K_d of 43 μM and all the other clones are not fully bound even at the highest DNA concentration assessed (40 μM or 100 μM). This deterioration in the binding efficiency of the pool is probably driven by the PCR bias for sequences with lower guanine content. As the

selection goes on and the abundance of binding sequences gets higher, PCR efficiency may play a more important role, impacting the selection more than the CE separation. Another possibility is that the non-responsive clones from the 6th round pool may bind the NMM but could not be measured using the above method if binding did not induce an enhancement in fluorescence.

Table 3.2. Dissociation Constants (K_d) of Sequences Chosen at Random from Table 3.1.

Sequences	**K_d (μM)***
Clone 3.2	5.1 ± 0.9
Clone 3.5	0.88 ± 0.12
Clone 3.12	3.0 ± 0.5
Clone 3.14	6.4 ± 0.6
Clone 6.4	43 ± 32
Clone 6.6	> 50
Clone 6.8	> 50
Clone 6.12 & 6.22	> 20
Clone 6.20 & 6.34	> 20
Clone 6.23	1.2 ± 0.1
Library	> 50

* Errors represent the standard error.

Enzymatic activity

NMM is a distorted porphyrin ring that has been used as a transition state analog for the porphyrin metallation reaction[207]. Previous studies have found that NMM binding aptamers are also capable of catalyzing the corresponding metal insertion reaction by stabilizing the transition state of the reaction[36, 37, 208, 210]. In order to test whether the DNA aptamers selected by CE-SELEX are also catalytic, we studied the insertion reaction of Cu (Ⅱ) into mesoporphyrin IX (MP). Figure 3.6a illustrates the overall reaction equation. The inserted Cu (Ⅱ) coordinates the four nitrogen atoms and results in a structure with a higher degree of symmetry. This changes the electronic structure and thus the UV-Vis spectra of the porphyrin. Figure 3.6b and 6c show the UV-Vis absorption spectra of the substrate MP and the product Cu-MP. Upon metallation, the intense B band around 400 nm narrows and the intensity increases slightly. The four Q bands from 500 to 700 nm collapse into two more intense bands (λ = 525 nm and 561 nm). The overall reaction rate was measured at 561 nm due to the higher signal to noise ratio.

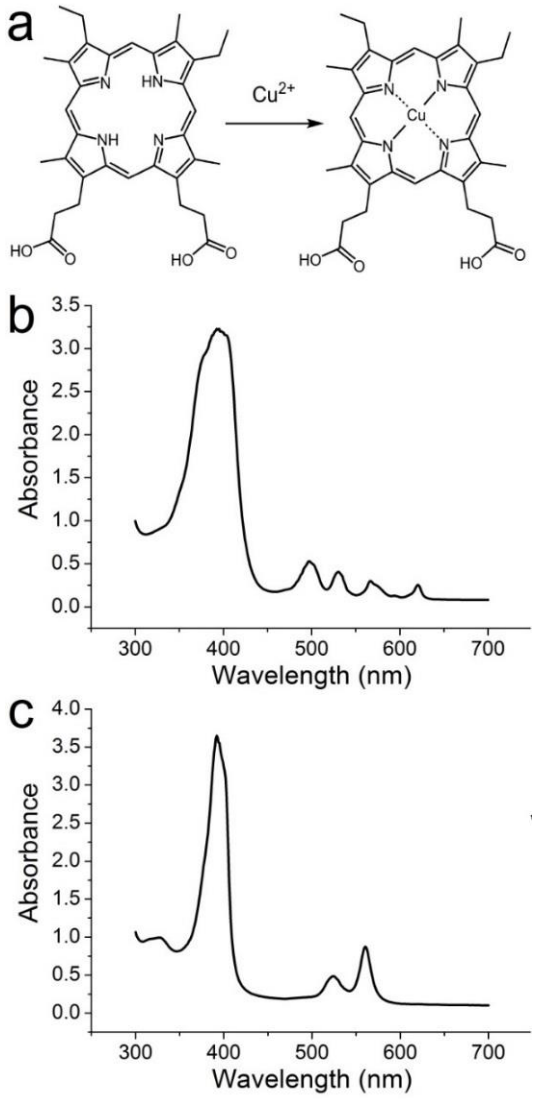

Figure 3.6. (a) Insertion reaction of Cu (Ⅱ) into mesoporphyrin Ⅸ (MP); (b, c) UV-Vis spectra of MP (b) and Cu-MP (c).

Figure 3.7 shows the increase of absorbance at 561 nm over the first 60 min of reaction. Clearly, the metalloporphyrin forms faster in the presence of clone 6.23 (red open circles) than in the absence of the DNA aptamers (blue solid circles). Among all the clones selected by CE-SELEX, clone 3.5 and clone 6.23 were found to accelerate the reaction by 1.7 and 2.0 fold, respectively (Table 3.3). All other clones listed in Table 3.2 were found to be non-catalytic. Similarly, the random library does not catalyze the reaction. It was found that the two catalytic clones are also the two with the lowest dissociation constants (0.88 μM for clone 3.5 and 1.2 μM

for clone 6.23). This suggests that the catalytic activity depends strongly on how tightly the aptamers can bind the transition state. We have also measured the reaction rate in the presence of a 18mer aptamer (5'-GTG GGT TGG GTG GGT TGG-3') that has previously been shown to bind NMM and accelerate the reaction for comparison[215]. The 18mer aptamer shows 7.1-fold rate enhancement under the same reaction conditions. The dissociation constant of the 18mer aptamer was measured to be 0.7 μM using the fluoresence method as described above. Apparently aptamers with K_d values of about 1 μM or even lower are required to catalyze this reaction. For all the other selected aptamers with K_d values significantly larger than 1.0 μM, we assume that the energy released upon binding the transition state is not sufficient to accelerate the reaction considering the low fraction of bound species under the reaction condition.

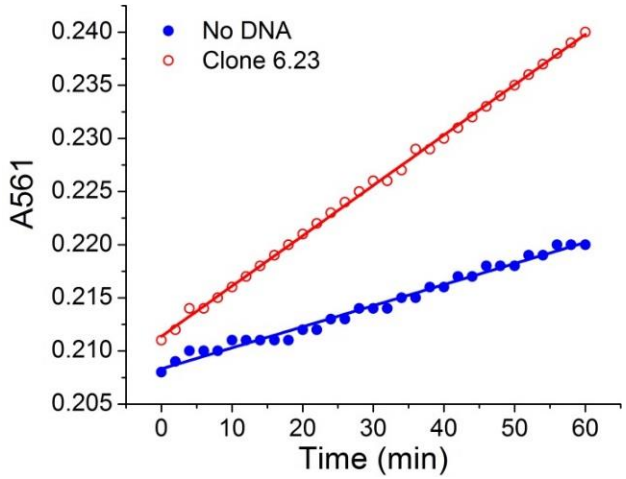

Figure 3.7. Absorbance at 561 nm in the presence (red open circles) and absence (blue solid circles) of clone 6.23.

Table 3.3. Catalytic Activity of Selected Aptamers

Sequence	V_{obs} **(μM/min)***
Clone 3.5	0.0441 ± 0.0005
Clone 6.23	0.0538 ± 0.0003
background	0.0264 ± 0.0003
library	0.0272 ± 0.0006
18mer	0.187 ± 0.001

* Errors represent the standard error.

3.4 Conclusions

We have used CE-SELEX to successfully isolate DNA aptamers for a small molecule target NMM with high nM to low μM affinity in only three rounds of selection. Among the selected aptamers, the strongest binders also exhibit catalytic activity for the porphyrin metallation reaction. Conventionally, selection of aptamers for small molecule targets like NMM requires being attached to solid phase support and subjected to affinity column separation. Compared to the affinity chromatography method, CE-SELEX greatly reduces the selection time and the number of cycles needed (3 vs 10-12 rounds). It also eliminates the necessity of solid phase attachment, reducing the potential for non-specific interactions. The free solution environment for binding and separation allows the aptamers to access the target from all directions facilitating the discovery of binders using various approaches. More importantly, this study demonstrates the feasibility of applying CE-SELEX for small molecule targets which contain a class of important compounds for cell signaling and regulation. The characteristic of nucleic acids of being able to be amplified by PCR makes even partial separation adequate for CE-SELEX to be carried out. It broadens the scope of targets for CE-SELEX and also provides a new technique for selection of aptamers towards small molecule targets. Therefore, we believe CE-SELEX is a more versatile technique than previously perceived.

Chapter 4: Selection of DNA Aptamers against a Fully Intact Membrane Protein using Capillary Electrophoresis - SELEX

4.1 Introduction

Aptamers have great applications in diagnostics and therapeutics due to their high binding affinity and specificity. They can be used for protein biomarker detection and quantification replacing antibodies. Aptamers have also been identified for a wide range of therapeutic targets and thus can be used as drugs. However, most current aptamers target extracellular proteins. Due to the high negative charge and large molecule size, it is difficult for aptamers to cross cellular membranes and target intracellular molecules. The same problem has also been encountered by many other macromolecular drugs, such as antibodies, siRNA and nanoparticles. In order to enhance the delivery of macromolecular drugs into cells for treating intracellular targets, an agent molecule that binds membrane receptors involved in receptor-mediated endocytosis would facilitate transmembrane delivery. Therefore, aptamers selected for specific membrane receptors included in endocytosis could be used as delivery agents for macromolecules into cells.

Selection of aptamers against intact membrane proteins is not an easy task for conventional SELEX which uses nitrocellulose filtration or affinity chromatography selections. This is because the lipids or detergents used to solubilize the transmembrane domains may disrupt the retention of complex on nitrocellulose filters and it is difficult to attach the whole membrane proteins onto a solid phase without denaturing. Previous selections were performed against synthetic peptide regions or truncated portions of the whole protein[216, 217]. However, the truncated portions may fold differently from the integral whole membrane protein preventing the selection of aptamers against the native conformations of the targets, and thus the selected aptamers may not even recognize the native proteins in vivo. CE-SELEX is a free-solution environment technology, fully compatible with membrane protein targets as various detergents or lipids are often used as buffer additives in capillary electrophoresis separations. Therefore, CE-SELEX is expected to be a promising approach for the selection of aptamers against fully intact membrane protein targets.

In this Chapter, we describe the selection of aptamers against a fully intact membrane protein target - transferrin receptor (TfR) using CE-SELEX. TfR is a receptor involved in receptor-mediated endocytosis and is responsible for iron delivery into cells and is ubiquitous in mammalian cells. It is a homodimer of two transmembrane subunits linked by disulfide bonds. Each subunit contains a large C-terminal extracellular domain, a hydrophobic transmembrane domain and a small N-terminal cytoplasmic domain. Two atoms of Fe^{3+} bind the soluble glycoprotein transferrin to form transferrin-Fe^{3+} which then binds the C-terminal of the receptor

to form the multimeric iron complex. The whole complex is immediately internalized into cells upon binding TfR via receptor-mediated endocytosis through clathrin-coated pits. Fe^{3+} is further released from the complex in the low pH endosome (pH 5.5) due to the conformational changes of both transferrin and the receptor. The resulting apotransferrin-receptor complex is recycled to the cell surface and dissociated later in the neutral pH environment for further iron endocytosis. TfR is expressed on all dividing cells and is particularly enriched on precursors of the erythron as these cells have the highest ion demand [218]. It has also been implicated in transcytosis across brain capillary endothelial cells, offering the potential for accessing targets across the blood-brain barrier [219, 220]. Aptamers against the truncated extracellular domain of mouse TfR has been previously selected using conventional SELEX and found to be able to deliver conjugated proteins into cells through receptor-mediated endocytosis upon binding TfR [217]. We now perform the selection against the fully intact TfR and expect the aptamers selected against the whole TfR will show higher affinity and more robust recognition for the native conformation of TfR on cellular membranes. Upon binding TfR, the aptamers can be potentially transported into cells via the receptor-mediated endocytosis process. Finally, the TfR used in this study is of human origin so that the aptamers selected can be later used to deliver macromolecular drugs for treating intracellular targets relevant to human disorders.

4.2 Experimental Section

Chemicals

Full-length human transferrin receptor (TfR) containing all domains (extracellular, intracellular and transmembrane) was purchased from OriGene (Rockville, MD). 6-FAM labeled ssDNA library containing 40 central random bases flanked by 20 primer binding regions on either end (5'-AGC AGC ACA GAG GTC AGA TG (40 random bases) CCT ATG CGT GCT ACC GTG AA-3') was purchased from IDT (Coralville, IA). 6-FAM labeled forward primer, biotin labeled reverse primer, unlabeled both primers and selected aptamers were also synthesized by IDT (Coralville, IA). dNTPs, 25 bp DNA ladder, αMEM, FBS, penicillin-streptomycin and 0.25% trypsin-EDTA were purchased from Life Technologies (Grand Island, NY). Taq polymerase and ThermoPol buffer were from New England Biolabs (Ipswich, CA). The gel loading dye was from Promega (Madison, WI). All other chemicals were purchased from Sigma-Aldrich (St. Louis, MO). All the samples and buffers were prepared using nuclease-free water (IDT, Coralville, IA).

The human pre-adipocyte cell line was kindly provided by Dr. David Bernlohr at the University of Minnesota (Minneapolis, MN) and Dr. James Kirkland from Mayo Clinic (Rochester, MN).

CE-SELEX selection

The TfR was reconstituted in 0.1% $C_{12}E_8$ micelles to solubilize the transmembrane domain and better mimic the native conformation of the protein as in cell membranes. The 6-FAM labeled ssDNA library was first heated to 72 ℃ for 5 min and then cooled down to room temperature to let sequences fold into the favorable conformations. 500 nM of the above ssDNA library was then incubated with 10 nM of the target protein TfR in MOPS buffer (20 mM MOPS, 5 mM KCl, 1 mM $MgCl_2$ and 0.1% $C_{12}E_8$, pH 7.4) at room temperature for 30 min to achieve binding equilibrium. The separation capillary (40 cm long with 30 cm to the detector, 360 μm OD and 50 μm ID, Polymicro, Phoenix, AZ) was rinsed with 0.15 M NaOH at 30 psi for 4 min and then the buffer at 30 psi for 4 min. After that, the binding mixture was loaded onto the pre-conditioned capillary at 5 psi for 32 seconds to fill 60% of the whole capillary using the P/ACE MDQ capillary electrophoresis system (Beckman Coulter, Fullerton, CA). The bound sequences were allowed to separate from the unbound sequence and migrate towards the capillary outlet vial containing 48 μL of separation buffer for collection by applying a normal polarity voltage at 30 kV. Laser-induced fluorescence detection was applied to monitor the separation.

The binding sequences collected were PCR amplified using 6-FAM labeled forward primer (5'/6-FAM/-AGC AGC ACA GAG GTC AGA TG-3') and biotinylated reverse primer (5'/biotin/-TTC ACG GTA GCA CGC ATA GG-3') for 30 cycles at the following condition: 200 μM dNTPs, 510 nM of each primers, 0.025 unit/μL Taq polymerase and 7.5 mM $MgCl_2$ in 1x ThermoPol buffer containing 20 mM Tris-HCl, 10 mM $(NH_4)_2SO_4$, 10 mM KCl, 2 mM $MgSO_4$ and 0.1% Triton X-100, pH 8.8. 30 sec of denaturation at 94 ℃, 30 sec of annealing at 53 ℃ and 20 sec of extension at 72 ℃ were carried out for each cycle and followed by a final extension period of 5 min at 72 ℃. Electrophoresis of the PCR products on 1.5% agarose gel stained with ethidium bromide was performed and the gel was imaged using a UV transluminator (Spectroline, Westbury, NY) to verify the absence of contamination bands and estimate the PCR yield.

The PCR products were then made single stranded to recover the forward strand with the binding sequence information. The PCR products were first incubated with streptavidin agarose resin (Pierce Biotechnology, Rockford, IL) in binding buffer (10 mM Tris, 50 mM NaCl and 1 mM EDTA, pH 7.5) in a chromatography column (Bio-Rad, Hercules, CA) for 30 min with periodical shaking. Then the resin was rinsed with 1 mL of binding buffer 10 times to wash off all

the PCR reagents but leaving the dsDNA products. After rinsing, the forward strand ssDNA was eluted from the column using 0.15 M NaOH. Then the sequences were desalted and precipitated by ethanol precipitation and dried in a CentriVap concentrator (LABCONCO, Kansas City, MO). The dried DNA was then dissolved in 30 μL of buffer, within which 10 μL was used for the next round of selection and the remainder could be used for binding characterization.

Binding affinity measurement

The binding affinity of each selected pool as well as the randomly chosen aptamer clones was measured using affinity capillary electrophoresis (ACE). Typically, 10 μL dilute of the selected ssDNA was heated to 72 ℃ for 5 min and cooled down to room temperature to fold into the correct structures and conformations. The DNA sample was then mixed with increasing concentrations of TfR samples ranging from 7.8 nM to 250 nM and incubated at room temperature for 30 min to allow binding to reach equilibrium. After that, the binding samples were injected onto a capillary and separated under 30 kV voltage of reverse polarity. The free unbound DNA peak was used to calculate the bound fraction f_b:

$$f_b = \frac{[A]_b}{[A]_t} = 1 - \frac{I}{I_0} = \frac{[T]}{[T] + K_d} \qquad 4.1$$

where I and I_0 are the area or height of the free DNA peak in the presence and absence of target protein [T]. The bound fraction was then fitted to the target concentration to find K_d using origin 8.5 (OriginLab Corporation, Northampton, MA).

The binding affinity of the selected pools was also estimated using fluorescence polarization. The fluorescence polarization as well as the fluorescence intensity of the binding samples at different DNA/protein molar ratios were measured using a Synergy 2 microplate reader (BioTek, Winooski, VT). It was excited using a 485/20 nm filter and the emission fluorescence was measured at 528/20 nm. The changes in the polarization of the binding mixtures relative to that of the free DNA sample was used to estimate the affinity:

$$f_b = \frac{P - P_f}{P_b - P_f} = \frac{[T]}{[T] + K_d} \qquad 4.2$$

where P, P_f and P_b are the polarization of the DNA at protein concentration [T], completely free ([T] = 0) and fully bound ([T] = ∞), respectively. Since (P_b - P_f) is constant, the relationship between (P - P_f) and [T] can be used to estimate the K_d.

Cloning and sequencing

When no further improvement in the binding affinity of the selected pools was observed, the iterative selection process was stopped and the selected pools were cloned and sequenced. Selected DNA sequences from round 2 and round 4 pools were cloned using a TOPO TA cloning kit (Invitrogen, Grand Island, NY). Briefly, the sequences from the two selected pools were PCR amplified using unlabeled primers under the same conditions as described above for only 20 cycles and a final extension period of 10 min at 72 ℃. The fresh PCR products were ligated onto the pCR4-TOPO vector, transfected into TOP10 Chemically Competent *E.coli* cells and then plated on LB agar plates. Individual colonies were randomly picked and cultured in LB broth (Invitrogen, Grand Island, NY) for 24 hours. The plasmids containing the PCR products were then extracted from *E.coli* cells using a plasmid miniprep kit from Invitrogen (Grand Island, NY). The vectors were sequenced at the BioMedical Genomics Center at the University of Minnesota (St. Paul, MN) using the M13 forward primer.

Endocytosis of selected aptamers

Human pre-adipocytes were cultured in αMEM with 10% FBS and 1% of 10000 U/mL penicillin-streptomycin (Invitrogen, Grand Island, NY) in a Nunc Lab-Tek 8-well chambered coverglass dish (Thermo Scientific, Waltham, MA) to 80% confluency. Cells were washed three times with PBS buffer and then incubated in serum-free αMEM with 10 μM of 6-FAM labeled aptamers at 37 ℃ with 5% CO_2 for 30 min. The cells were then washed three times with PBS buffer to remove any non-internalized FAM-aptamers and fixed with 4% paraformaldehyde at room temperature for 15 min. The fixed cells were further washed with PBS buffer three times and kept in PBS buffer at 4 ℃ until imaging. An inverted confocal fluorescence microscope (Olympus FluoView FV1000 IX2, Imaging Center, University of Minnesota, Minneapolis, MN) equipped with pulsed 405 and 485 nm lasers was used to image the fixed cells. Images were captured and processed using FluoView (Olympus).

4.3 Results and Discussions

Capillary electrophoresis selection

The binding buffer containing $C_{12}E_8$ surfactant was used as the CE separation buffer to solubilize the transmembrane domain of the protein and maintain its active folding structure. In the presence of the surfactant, the capillary wall was coated and the EOF was largely suppressed. When applying normal polarity separation, the free unbound sequences migrated back towards the inlet buffer vial; while the target TfR was found to migrate towards the negative cathode at the capillary outlet. Considering the large size of the target protein, especially when incorporated into micelles, the binding complex was presumed to migrate towards the outlet as well. Therefore, the collection was done at the capillary outlet under normal polarity separation at 30 kV. This strategy minimizes the contamination from collecting tailing peak of the free DNA peak.

The starting library was found to have only weak affinity for the target TfR (high nM to low μM). In order to minimize non-specific binding, the library concentration was kept low at 500 nM. The TfR concentration was kept 50-fold lower (10 nM) to create competition for binding sequences. Meanwhile, in order to maximize the number of sequences for the selection, 60% of the entire capillary was loaded with the binding mixture as opposed to the narrow plug of sample typically injected in normal CE-SELEX selection. Since the binding sequences and the free DNA migrate in opposite directions, the amount of sample injected does not affect the resolution. Under a normal polarity separation, all the binding complex migrated towards the collection buffer vial for collection while the free DNA was removed via the inlet (see Figure 4.1).

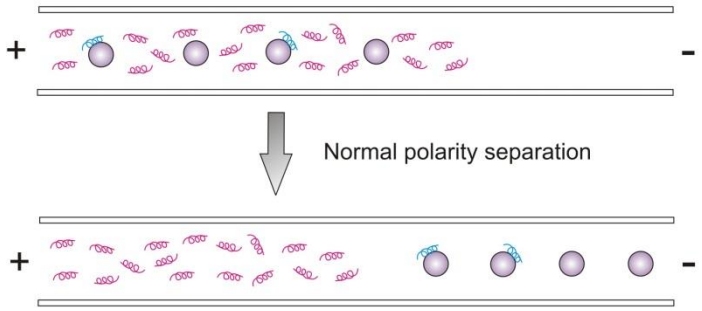

Figure 4.1. Illustration of the TfR selection scheme

Binding affinity of selected pools.

The binding affinity of the selected pools were studied using ACE to determine if further rounds of selection were needed. Figure 4.2 shows the electropherograms of the ACE analysis for the pool after three rounds of selection. As TfR increases, the intensity of the unbound DNA peak

decreases, indicating an increase in the bound fraction with increasing protein concentration. The bound fraction of the selected sequences was then fit to the equation to estimate affinity.

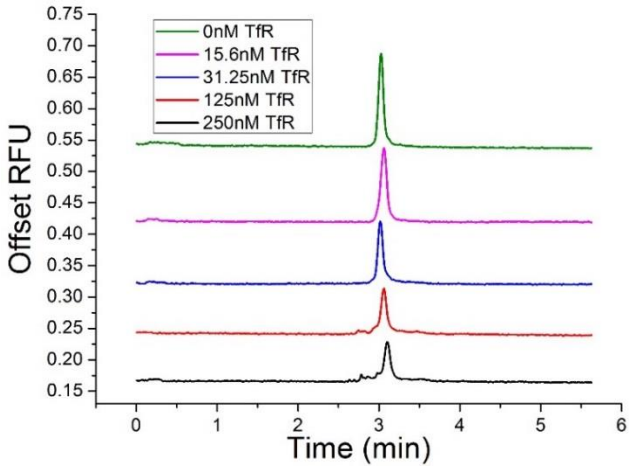

Figure 4.2. Electropherograms showing the free unbound DNA peaks in the presence of increasing concentrations of TfR for ACE measurement for selection round 3 pool.

The K_d of the selected pools as well as the starting library has been summarized in Figure 4.3. After two rounds of CE-SELEX selection, the K_d has decreased drastically from high nM to a few tens of nM. However, there is no further improvement in binding affinity for the 3rd and 4th round.

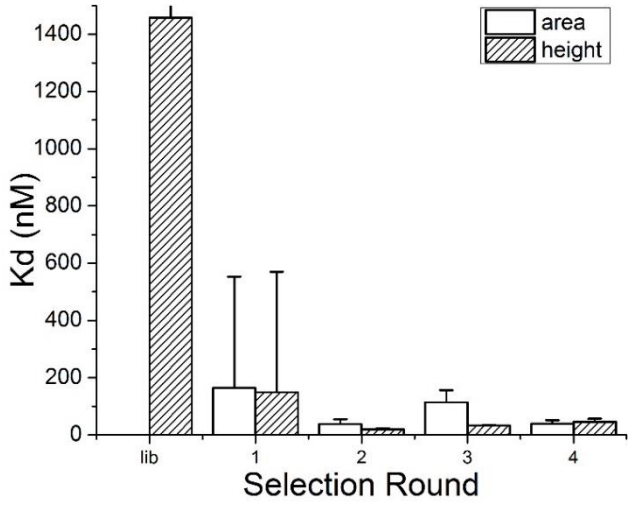

Figure 4.3. Dissociation constant K_d of starting library and selected pools measured using ACE peak area and height. The binding curve for peak area for the library did not converge. Error bars represent the standard deviation.

Figure 4.4a shows fluorescence polarization measurements for the selected pools and the starting library. At the same TfR concentration, the polarization values of the selected sequences are higher than the library, indicating a higher bound fraction at the same protein concentration and thus higher binding affinity. Excluding the data points at 250 nM TfR, the data shows trends typical of binding curves. The drop in fluorescence polarization at the highest protein concentration can be explained by the fluorescence enhancement effect with increasing protein concentrations. As shown in Figure 4.4b, the fluorescence intensity increases linearly with increasing protein concentration. The curves for the selected pools are randomly distributed. This fluorescence enhancement effect doesn't seem to have any trend in terms of selection rounds. So the fluorescence enhancement is probably due to a matrix effect (pH, glycerol level) in the protein sample rather than binding. Fluorescence enhancement is usually caused by an increase in the quantum yield and increase in fluorescence lifetime. According to the following equation, an increase in the fluorescence lifetime (τ) would result in a lower measured polarization value than in absence of that effect:

$$\frac{1}{P} - \frac{1}{3} = \left(\frac{1}{P_0} - \frac{1}{3}\right)\left(1 + \frac{RT}{\eta V}\tau\right) \qquad 4.3$$

At the early stage of the binding curves, the increase in fluorescence polarization due to binding overcomes the decrease caused by longer fluorescence lifetime. Therefore, the overall effect on the measured polarization is still increasing, resembling the binding curves. However, when the protein concentration continues to increase, the binding curves start to reach a plateau and the decrease in polarization due to the longer fluorescence lifetime becomes dominant leading to a drop in the measured polarization values.

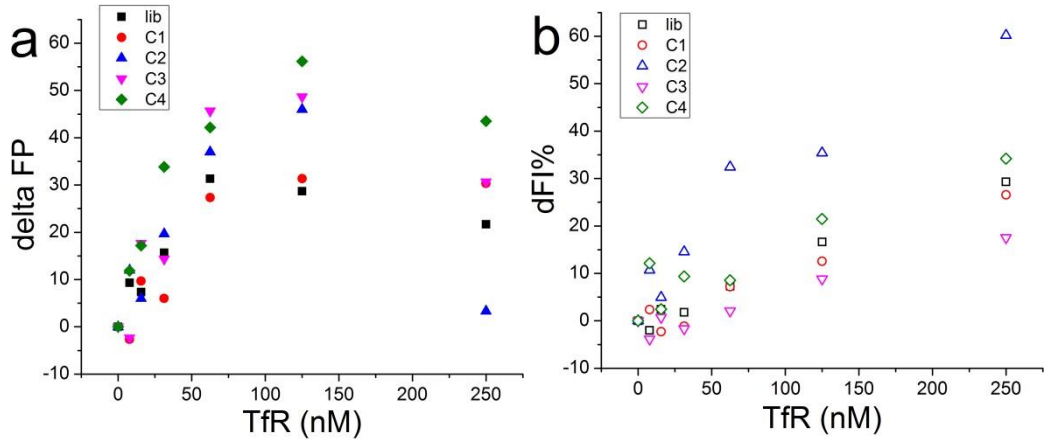

Figure 4.4. Change in fluorescence polarization (a) and fluorescence intensity (b) with increasing concentrations of TfR for library and selected pools.

Given the limitation of top TfR concentration, it would be difficult to obtain a quantitative measurement for K_d from the fluorescence polarization data. However, from the early trend at lower protein concentrations, the polarization data still provides evidence supporting an increased bound fraction of DNA and increased affinity for TfR after CE-SELEX selections.

Sequencing the selected pools

Cloning and sequencing was performed for the selection round 2 and 4 pools. The sequences of aptamer clones randomly picked from the two pools are listed in Table 4.1. 24 sequences were identified for each round. No sequence motif was identified and the sequence heterogeneity was high throughout the selection which are in agreement with previous CE-SELEX studies. It also indicates that there are quite a few sequences in the library that could bind TfR.

Table 4.1 TfR aptamer sequences identified from round 2 and round 4 pools*.

Clone	Sequence (5’ - 3’)
2_1:	**AGCAGCACAGAGGTCAGATG**ACAAGGGAGATAGTCTTGCTATTTGATATTTACTTTGCA**CCTATGCGTGCTACCGTGAA**
2_2:	**AGCAGCACAGAGGTCAGATG**GTACGGTATACTGTTTCTTATTTTTAGGTTAGATCTGGAC**CCTATGCGTGCTACCGTGAA**
2_3:	**AGCAGCACAGAGGTCAGATG**GCAGGTTTCGACGTACAATGCTATGGAGACTTTATGATCG**CCTATGCGTGCTACCGTGAA**

2_4: **AGCAGCACAGAGGTCAGATG**CATTTATGTATCCTCTGTGAATGGCAGTTTATTGGACTAA**CCTATGCGTGCTACCGTGAA**

2_5: **AGCAGCACAGAGGTCAGATG**GTCTGTAGTGCTAATATTTAATTTAGTTATGTAACTGTTT**CCTATGCGTGCTACCGTGAA**

2_6: **AGCAGCACAGAGGTCAGATG**GTCTCTGATACGATTATCGATCTAATTCCGATCGTAAGCT**CCTATGCGTGCTACCGTGAA**

2_7: **AGCAGCACAGAGGTCAGATG**TAAAGTAAGTGTCGAATTCAATTTATGATTGTAGTTATGC**CCTATGCGTGCTACCGTGAA**

2_8: **AGCAGCACAGAGGTCAGATG**CCAGGGGTATGACAATCGGTAGTTTGGAATGTATTCTAAC**CCTATGCGTGCTACCGTGAA**

2_9: **AGCAGCACAGAGGTCAGATG**AGTTTTTGTTGGGTTGTCTTGGATTTGTTGATTTAGTATG**CCTATGCGTGCTACCGTGAA**

2_10: **AGCAGCACAGAGGTCAGATG**TGTGTTTATAGAAATGGTTTGACTTTGGTTAAGTAAATTA**CCTATGCGTGCTACCGTGAA**

2_12: **AGCAGCACAGAGGTCAGATG**AAGTTGTATTTGGTTATATGGCCTCGTGCTACTCGTTATT**CCTATGCGTGCTACCGTGAA**

2_13: **AGCAGCACAGAGGTCAGATG**TACGCCATTCAGACATGGGCTTGGCAGCTGCAGAACTTTC**CCTATGCGTGCTACCGTGAA**

2_14: **AGCAGCACAGAGGTCAGATG**CTTATAATAAGTTGATCTTATGCGGACAGGTCGCCCTCGT**CCTATGCGTGCTACCGTGAA**

2_15: **AGCAGCACAGAGGTCAGATG**ACTGTTATTTAGTTTTTCATCCTTGTTTTGCCCTTGTAAT**CCTATGCGTGCTACCGTGAA**

2_16: **AGCAGCACAGAGGTCAGATG**AGCCTTGCCATGTTGATTTAGAATTTAGCAGTATCCTTCT**CCTATGCGTGCTACCGTGAA**

2_17: **AGCAGCACAGAGGTCAGATG**TCCTCTTTTCTTGTTAGCTACTGTACCTTATAGAATCTAA**CCTATGCGTGCTACCGTGAA**

2_18: **AGCAGCACAGAGGTCAGATG**TTGGTACGAGGCTGTGTTCTTATTAGTGGTGACTTTCCTA**CCTATGCGTGCTACCGTGAA**

2_19: **AGCAGCACAGAGGTCAGATG**CTTTGTCTTCATTCATTCATACTCCTGTCTGAACGGCTAC**CCTATGCGTGCTACCGTGAA**

2_20: **AGCAGCACAGAGGTCAGATG**TGACAGTTTTTAGTTACTGAACGATCTCAGCTAACATAT**CCTATGCGTGCTACCGTGAA**

2_21: **AGCAGCACAGAGGTCAGATG**TATGGTCATCACCACCCACGTTCGTGTGAAGAGTTGTGTT**CCTATGCGTGCTACCGTGAA**

2_22: **AGCAGCACAGAGGTCAGATG**AGTTTTTGTTGGGTTGTCTTGGATTTGTTGATTTAGTATG**CCTATGCGTGCTACCGTGAA**

2_23: **AGCAGCACAGAGGTCAGATG**TGACAGTTTTTAGTTACTGAACGATCTCAGCTAACATAT**CCTATGCGTGCTACCGTGAA**

4_1: **AGCAGCACAGAGGTCAGATG**TCCTGAAATATATAAGTAGTTTTGCTCTGCATCTCTCCGG**CCTATGCGTGCTACCGTGAA**

4_2: **AGCAGCACAGAGGTCAGATG**GTATGTT**CCTATGCGTGCTACCGTGAA**

4_4: **AGCAGCACAGAGGTCAGATG**GTTTGTTGTTCCGAATTCTGGTGTTGGTTCTTCTCGGAT**CCTATGCGTGCTACCGTGAA**

4_5: **AGCAGCACAGAGGTCAGATG**CCGAAGGTTCCTGTACAGTTGCAATCTATTTTAAGTTAGG**CCTATGCGTGCTACCGTGAA**

4_6: **AGCAGCACAGAGGTCAGATG**TGGTAGTTAGTAGGCTTGAGGAACTTGTAGCTCAAACGCG**CCTATGCGTGCTACCGTGAA**

4_7: **AGCAGCACAGAGGTCAGATG**ACATTGTATCAGATCTCGCCGATCTTCTTGGTATCTGGAA**CCTATGCGTGCTACCGTGAA**

4_8: **AGCAGCACAGAGGTCAGATG**TTACTCTTTTTTTGGCTGTGACTTTCTATTCTGTTTGGTT**CCTATGCGTGCTACCGTGAA**

4_9: **AGCAGCACAGAGGTCAGATG**TAATTGGGCGGGCCATCCTGTGTGGGGGGGTGCGTTTGTG**CCTATGCGTGCTACCGTGAA**

4_10: **AGCAGCACAGAGGTCAGATG**TTGTATTTCGAATTTAAGCTCGTTGTACGGTCTATTTGGT**CCTATGCGTGCTACCGTGAA**

4_12: **AGCAGCACAGAGGTCAGATG**TATTTGTTGTCTAGCGGGGATAGTGGTCAGTAAATCGTCA**CCTATGCGTGCTACCGTGAA**

4_13: **AGCAGCACAGAGGTCAGATG**TATTGTGTCCATAAACTTATCTGAGGATTGTTCCTACAGT**CCTATGCGTGCTACCGTGAA**

4_14: **AGCAGCACAGAGGTCAGATG**TGCATAAGATGGTTCGGATTTCCTACTTTTTACCGAGGAA**CCCATGCGTGCTACCGTGAA**

4_15: **AGCAGCACAGAGGTCAGATG**CCATCTATATTAGTGGGTAGTGAATACTTGTCTGGGGTT**CCTATGCGTGCTACCGTGAA**

4_16: **AGCAGCACAGAGGTCAGATG**TTTCTGTTCGGTGGATTACTTCTCACTGGATTGACTATT**CCTATGCGTGCTACCGTGAA**

4_17: **AGCAGCACAGAGGTCAGATG**TTAAAAAACTAGGGTTTTCATCACAGGTGTGGTGAATTAA**CCTATGCGTGCTACCGTGAA**

4_18: **AGCAGCACAGAGGTCAGATG**ATAATTCTGGTGGTCGTGGAGGCTGAGAGTCTTATGGCAA**CCTATGCGTGCTACCGTGAA**

4_19: **AGCAGCACAGAGGTCAGATG**CTGTAGTTCTATTTCCGTCGATATGATCGAGTACAGGTTT**CCTATGCGTGCTACCGTGAA**

4_20: **AGCAGCACAGAGGTCAGATG**TCACTCGGGTAGGTGTTATGGAGCGATCAGTGTTCTCGGT**CCTATGCGTGCTACCGTGAA**

4_21: **AGCAGCACAGAGGTCAGATG**CATGGGTGTGGGGGCCAGGGGTGCGAAGTTGTGTGAGTTC**CCTATGCGTGCTACCGTGAA**

4_22: **AGCAGCACAGAGGTCAGATG**GGCCCTGTTGATTCTTTCTCCTGGCGTCGTTTGTGCAGCT**CCTATGCGTGCTACCGTGAA**

4_23: **AGCAGCACAGAGGTCAGATG**TTCCAAATGCGGGGATTGTTTAGATTAGTTAGTGTTTGTC**CCTATGCGTGCTACCGTGAA**

4_24: **AGCAGCACAGAGGTCAGATG**TAGTGTTACCTGAATGATAATAAGTAAGCGGTGTTCAGAT**CCTATGCGTGCTACCGTGAA**

* Bases in bold represent the primer regions.

Binding affinity of selected aptamers

Four sequences were randomly chosen from each of the sequenced pools for further K_d characterization using ACE. Figure 4.5 shows typical binding curves for the selected aptamers. The curves plateau at approximately 50 - 60% bound fraction, indicating only a fraction of the aptamers could fold into a binding conformation with affinity for TfR.

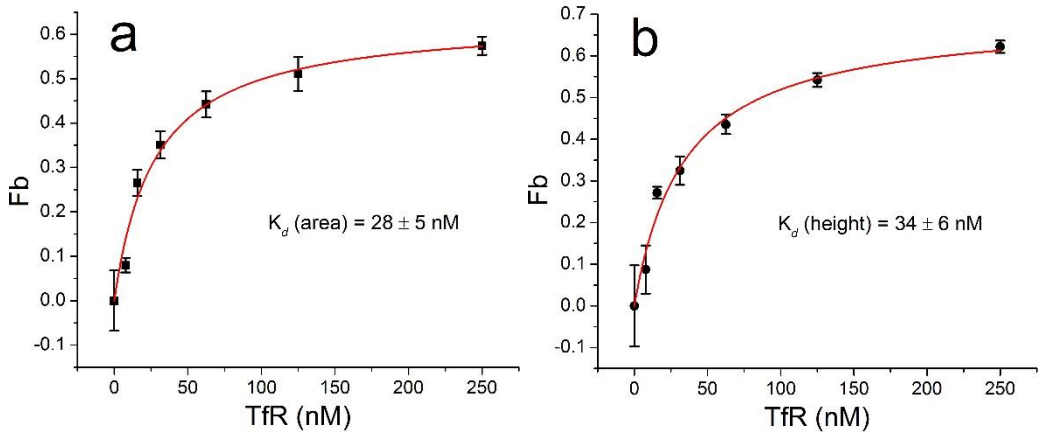

Figure 4.5. Binding curves of selected aptamer Clone 2_22 fitted by ACE peak area (a) and height (b). Error bars represent the standard deviation.

The dissociation constants K_d of all the aptamers chosen at random from Table 4.1 measured by ACE and fitted by peak area and height are summarized Table 4.2. All the sequences bind TfR with low nM K_d values, which is in good agreement with the bulk K_d measured for the selected pools (see Figure 4.3).

Table 4.2. Dissociation constants (K_d) of selected TfR aptamers

Clone	ACE area K_d (nM)*	ACE height K_d (nM)*
2_8	37 ± 9	44 ± 7
2_10	50 ± 10	59 ± 5
2_12	38 ± 5	100 ± 10
2_22	28 ± 5	34 ± 6
4_6	48 ± 7	90 ± 30
4_12	130 ± 30	100 ± 30
4_17	70 ± 20	60 ± 20
4_20	24 ± 4	41 ± 4
Library**	N/A	1500 ± 2000

* Errors represent the standard deviation

** Library K_d fitted by peak area does not converge

Endocytosis of TfR aptamers

The selected aptamers were synthesized with 6-FAM label at the 5' position to facilitate both binding measurements and the microscopy imaging for endocytosis assessment. Since the TfR used in the selection is of human origin, a human cell line was used for the endocytosis. A human pre-adipocyte cell line was chosen. It was assumed that the aptamers could bind TfR on cell membrane and be internalized into the cells similarly to diferric transferrin. As shown in Figure 4.6 a, the cells themselves exhibit minimal green autofluorescence background. Upon treating with selected aptamers for 30 min, green fluorescence starts to develop both inside and outside the cells (Figure 4.6 c & d). The DNA aptamers seem to stick to the surface of the coverglass causing fluorescence outside of the cells. In order to combat that, the glass surface needs to be coated and passivated to minimize non-specific binding. Moreover, in order to determine whether the fluorescence inside the cells is internalized FAM-aptamers or non-specific binding of the aptamers to the bottom of the glass surface or the membrane surface, a z-stack scan along the depth or thickness of the cells is needed. Random sequence DNA library also gave rise to green fluorescence inside the cells (Figure 4.6 b). Considering the relative high affinity for the starting library, the DNA concentration (10 μM) used for treating the cells might be high enough to bind TfR and be internalized. Another possible explanation is that the synthesized aptamers

contain some free dyes and the observed fluorescence is the internalized free dye instead of the large aptamer complex.

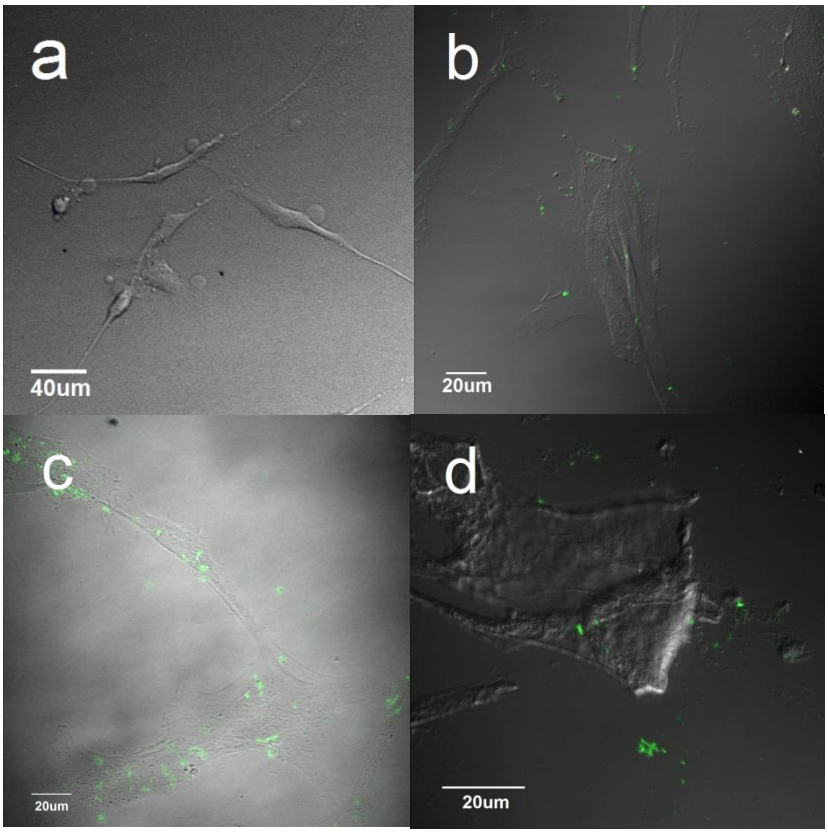

Figure 4.6. Endocytosis of TfR aptamers by cultured human pre-adipocytes. The aptamers are labeled with FAM (show in green) and the cells are imaged using confocal microscopy after 30 min incubation at 37 ℃ with (a) PBS buffer; (b) 10 μM FAM-library; (c) 10 μM FAM-clone 2_8; (d) 10 μM FAM-clone 4_6. Both transmitted light and green fluorescence channels are shown in the images.

Therefore in order to clarify the endocytosis of the TfR aptamers, further experiments such as using a different human cell line that has better adherent property, or surface coating for the coverglass, or using HPLC purification to remove any free dye in the aptamers are needed.

4.4 Conclusions

In this study, DNA aptamers with nM K_d have been selected against a fully intact membrane protein TfR using CE-SELEX. As opposed to conventional SELEX using only the extracellular domain of the membrane protein target, full-length protein has been reconstituted in micelles and used in this CE-SELEX study to mimic its native conformation as it is in cellular membranes. This prevents the selection against a misfolded or changed conformation of truncated extracellular domain of the whole membrane protein and is expected to provide better recognition against the native protein in cellular membranes. In order to confirm and obtain more accurate quantification of binding affinity of the selected aptamers, an orthogonal technique other than affinity CE needs to be applied for K_d measurement, such as isothermal titration calorimetry (ITC).

It remains unclear whether the TfR aptamers can be endocytosed into cells upon binding the receptors. More experiments under different conditions need to be performed to achieve a conclusive answer. If the aptamers can transport across the cell membranes, further cellular pathways inside the cells, such as the eventual destination of the aptamer-TfR complex, dissociation of the complex, time course of the distribution of the internalized aptamers and the recylcling pathway of dissociated TfR, need to be assessed to fully understand the mechanisms and help the design of such delivery agents. To further test the ability of the aptamers as delivery agents, macromolecule cargoes can be conjugated onto the aptamers and the resulting cell function can be monitored to determine the delivery efficacy.

Chapter 5: Characterization of DNA/RNA Analogs' Affinity against Cardiac Muscle Proteins

5.1 Introduction

The heart beat is regulated by the Ca^{2+} concentration in cardiomyocytes with concentration reaching 1-10 μM for the systolic phase and 0.1 μM for the diastolic phase. Sarcoplasmic Reticulum (SR) and extracellular space are two calcium sources for Ca^{2+} cycling with Ca^{2+} concentration at 500 μM and 2-3 mM, respectively. Cardiac contraction is then triggered by elevated Ca^{2+} released from the lumen of the SR or extracellular space into the cytosol of cardiac cells. Later the Ca^{2+} is removed from the cytosol into the lumen by the Ca^{2+} pump Sarco(endo)plasmic Reticulum Ca^{2+}-ATPase (SERCA) and the extracellular space by plasma-membrane Ca^{2+}-ATPases (PMCAs) and Na^{+}/Ca^{2+} exchangers (NCXs), in which SERCA accounts for over 70% of the Ca^{2+} removal [221]. Therefore, SERCA determines the muscle relaxation rate and size of stored Ca^{2+} in the lumen which consequently affects the contractility in the subsequent beat.

Phospholamban (PLN) is a small and reversibly phosphorylated transmembrane protein located in the cardiac sarcoplasmic reticulum (SR). When it is unphosphorylated, PLN binds to the SERCA and inhibits the activity of this Ca^{2+} pump. Adrenaline and other β-agonists released by the nervous system can bind the cell membrane β-adrenaline receptors and activate a signal cascade to generate cyclic AMP by adenylate cyclase. Elevated cAMP concentration activates the cAMP dependent protein kinase A (PKA) which in turn phosphorylates PLN. Once phosphorylated, the inhibition effect of PLN on SERCA is relieved. This phosphorylation can be then be reversed by a protein phosphatase (PP1).

Ca^{2+} activates the muscle contraction by binding to the troponin in the thin filament. Troponin complex is a heterotrimer consisting of troponin C (TnC), troponin T (TnT) and troponin I (TnI). TnC is a Ca^{2+} binding subunit; TnT is used to anchor the complex to tropomyosin and TnI is an inhibition subunit that binds actin and blocks its binding site for myosin. When Ca^{2+} binds the TnC, it results in a conformational change to remove the steric block and allow the actin in the thin filament to bind myosin in the thick filament for muscle contraction [222]. Upon removal of the Ca^{2+} or lowering of the concentration, Ca^{2+} dissociates from TnC and the TnI blocks the actin-myosin interaction again for relaxation. Like PLN, myofibrillar proteins such as troponin I and C proteins can also be phosphorylated by PKA, which regulates the tension-generating ability at a given submaximal [Ca^{2+}] and the myofilament Ca^{2+} sensitivity [223, 224].

As discussed above, these contractile proteins or Ca^{2+} channels in cardiomyocytes are important in regulating the Ca^{2+} level and maintaining heart function. Dysfunction of Ca^{2+} cycling in cardiac myocytes is relevant in the development of heart failure. For example, super-inhibition or loss of inhibition effect of PLN on SERCA activities can cause the development of dilated cardiomyopathies [225, 226]. ssDNA was found to bind PLN with high affinity and reverse its inhibition effect on SERCA. It acts in a tunable and length dependent way with 80mer completely relieving the inhibition effect and 5mer with almost no effect. Therefore, ssDNA can be potentially used for treating heart diseases caused by super-inhibition of PLN on SERCA. However, ssDNA is not stable in vivo and can be quickly degraded by DNases. Better drug candidates would be molecules with similar binding affinity for PLN but have higher biostability. Various nucleic acid analogs that are modified against enzymatic degradation are suitable for this task. Moreover, the effect of these analogs on other contractile proteins need to be evaluated and the mechanism of the high affinity binding needs to be investigated. In this Chapter, the binding affinity of DNA/RNA analogs with several important cardiac muscle proteins have been studied and more experiments are needed to elucidate the DNA/protein interaction profiles in cardiac myocytes.

5.2 Experimental Section

Chemicals

5mer, 10mer, 20mer, 35mer and 50mer random RNA libraries and 50mer 2'-O-methyl modified random RNA were purchased from IDT (Coralville, IA). 50mer random sequences of L-DNA was purchased from ChemGenes (Wilmington, MA). All the above sequences are labeled by 6-FAM for fluorescence detection. Phospholamban (PLN) reconstituted in 0.1% $C_{12}E_8$ was kindly given by Professor Veglia lab. Troponin complex, its subunit C, T and I, and Myosin S1 subunit were kindly provided by Professor Metzger lab. All the other chemicals for buffers are obtained from Sigma-Aldrich (St. Louis, MO) and the buffers are all prepared using nuclease-free water from IDT (Coralville, IA).

Binding affinity measurement

The dissociation constants of various DNA/RNA analogs binding different cardiac muscle proteins are measured using both affinity capillary electrophoresis (ACE) and fluorescence polarization (FP) methods. The concentration of the DNA/RNA analog was kept

constant and titrated with increasing concentration of proteins. Typically, 5 nM of the DNA/RNA analog was heated to 72 ℃ and cooled down to room temperature to allow sequences to fold into the most stable conformations. They were then mixed with proteins of concentrations ranging from low nM to μM and incubated at room temperature for 30 min to reach binding equilibrium before measurement.

For ACE measurement, equilibrium mixtures at different binding ratios are separated in a 40 cm long (with 30 cm to detector), 360 μm OD and 50 μm ID fused silica capillary (Polymicro, Phoenix, AZ) on P/ACE MDQ capillary electrophoresis system (Beckman Coulter, Fullerton, CA). The free unbound DNA/RNA peak was used to calculate the bound fraction and fitted to the binding curve to obtain K_d values:

$$f_b = \frac{[A]_b}{[A]_t} = 1 - \frac{I}{I_0} = \frac{[T]}{[T] + K_d} \qquad 5.1$$

where I and I_0 are the area or height of the free DNA peak in the presence and absence of target protein $[T]$.

For FP measurement, the polarization of the binding samples are measured using a Synergy 2 microplate reader (BioTek, Winooski, VT). The excitation light at 485/20 nm was polarized and emission fluorescence was measured at 528/20 nm. The bound fraction of DNA/RNA analogs was determined by the following equations:

$$f_b = \frac{P - P_f}{P_b - P_f} = \frac{[T]}{[T] + K_d} \qquad 5.2$$

where the difference of polarization of sequences at fully bound and completely unbound (P_b - P_f) is treated as a constant. Then the increase in polarization (P - P_f) can be fitted with respect to the target protein concentration $[T]$ to obtain K_d.

5.3 Results and Discussions

Binding affinity of DNA/RNA analogs for PLN

All the DNA/RNA analogs showed binding affinity in low nM range except for the shortest RNA 5mer (Figure 5.1). The 2'-O-methyl modification and the chirality does not affect

the binding affinity either. Since all the sequences are completely random, it reveals that the binding is independent of sequence and is probably through pure electrostatic interaction between the highly negatively charged nucleic acids and the relatively high PI protein PLN. The difference between the K_d measured by ACE and FP is due to the fact that FP measures equilibrium mixture while ACE requires high voltage separation and is also under nonequilibrium conditions. The equilibrium mixture may dissociate under high electric field and in the nonequilibrium buffers. This phenomenon is especially significant when the binding is weak or the dissociation rate of the complex is high, such as in the case of 5mer RNA. For the natural RNA sequences of different lengths, the binding affinity decrease as the length decreases, with the drastic drop in binding affinity for sequences less than 10 bases long. The length dependent binding property reveals that the binding site has a certain amount of positive charges that need to be saturated with enough long sequences to achieve high affinity binding or a certain amount of flexibility is needed.

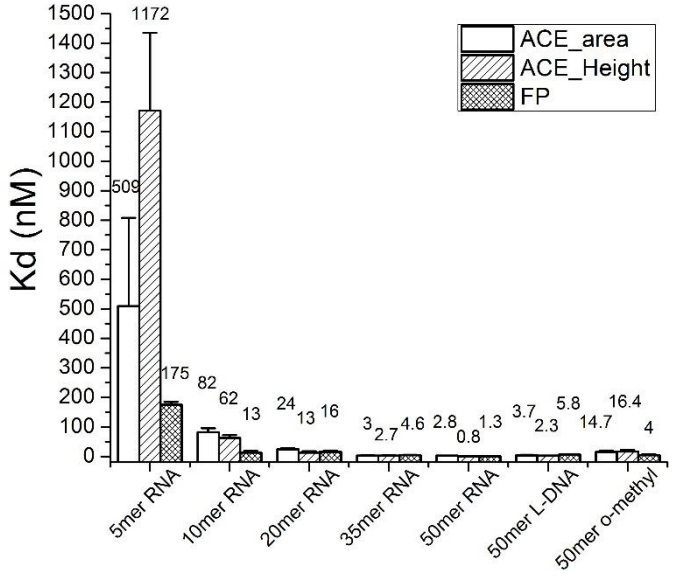

Figure 5.1. Dissociation constants (K_d) of the DNA/RNA analogs measured by ACE peak area, height and FP. The numbers above the columns are the corresponding K_d values in nM. Error bars represent the standard deviation.

Binding affinity of ssDNA for troponin complex and its subunits

Figure 5.2 shows the separation electropherograms for 80mer ssDNA and troponin complex (Tn3). As the concentration of troponin complex increases, the free unbound ssDNA peak decreases rapidly. The ssDNA shows high binding affinity (13 nM) against the troponin

complex, which is in the similar range as the PLN. It shows that there might be multiple protein targets in cardiac myocytes that can interact with ssDNA.

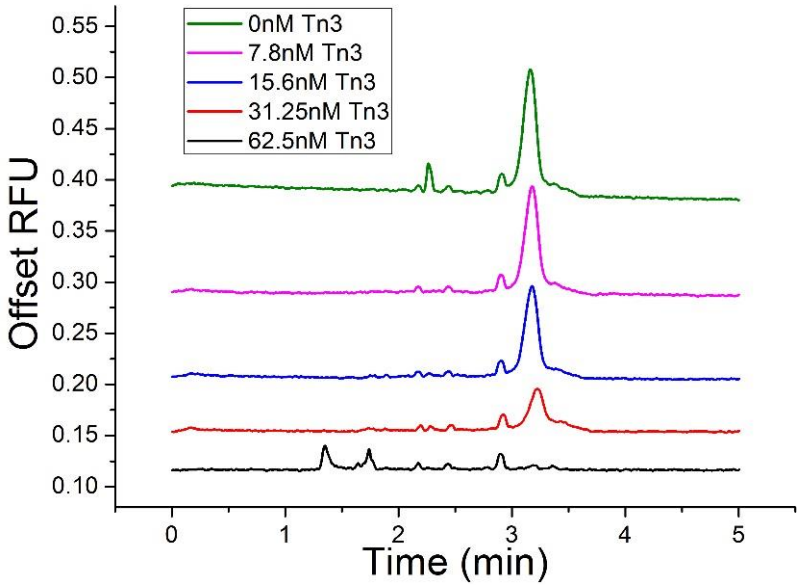

Figure 5.2. Stacked electropherograms showing the change of the free unbound ssDNA peaks in response to increasing concentrations of troponin complex.

Different troponin subunits show different binding affinity for the 80mer ssDNA (Figure 5.3). The subunit I (TnI) binds the 80mer ssDNA with a lower affinity of a few hundred nM K_d. The subunit T (TnT) shows even higher K_d values. The subunit C (TnC) does not show any binding affinity towards ssDNA (> 12.5 μM). This suggests that the formation or the proper folding of troponin complex is required for high affinity binding (low nM K_d) with ssDNA given that the subunits themselves are not very much structured.

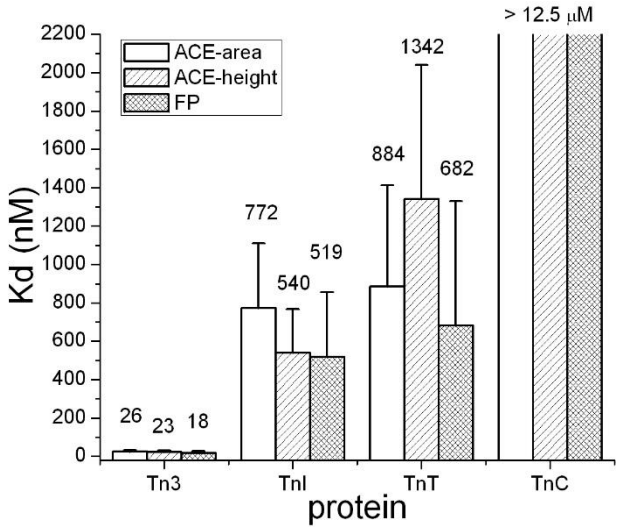

Figure 5.3. Dissociation constants (K_d) of 80mer ssDNA binding different subunits of troponin fitted by ACE peak area, height and FP data. The numbers above the column indicates the actual K_d values in nM. Error bars represent the standard deviation.

Binding affinity of ssDNA for myosin S1

Considering the fact that ssDNA binds the contractile protein troponin, we further studied if there are other proteins that are in high abundance in cardiomyocytes that could also bind the ssDNA. Myosin is a high abundant protein (40-50% of total muscle protein) consisting of two heavy chains and four light chains. The two heavy chains are wound around each other to form the backbone of the thick filament and at one end they form two globular heads with the light chains that are responsible for cross-bridging with the thin filament. The S1 fragment of myosin is a proteolytic portion from the heavy chain. It is water-soluble and can hydrolyze ATP and bind actin to form actomyosin complex, which is essential for the muscle to produce forces [227]. In our experiment, myosin S1 fragment was found to bind ssDNA as well but to a lesser extent. As shown in Figure 5.4, the 80mer ssDNA also binds the soluble myosin S1 subfragment with a few hundred of nM K_d, which indicates a lower affinity than the PLN and troponin complex.

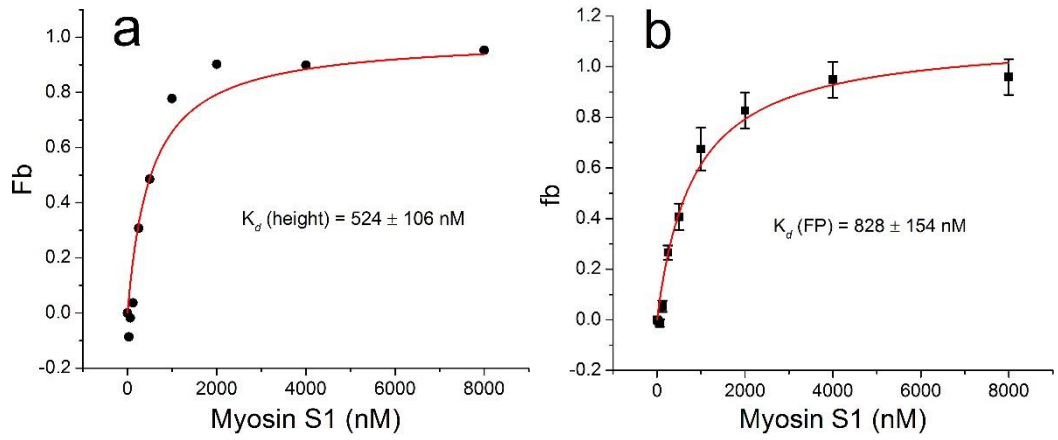

Figure 5.4. Binding curves fitted by (a) ACE peak height and (b) FP for 80mer ssDNA binding myosin S1 subunit. The K_d obtained are 524 ± 106 nM for ACE and 828 ± 154 nM for the FP respectively. The error bars represent the standard deviation.

5.4 Conclusions

In conclusion, PLN binds ssDNA, L-DNA, RNA and O-methyl RNA with low nM dissociation constants for sequences at least 10 nucleotides long. If the sequence is even shorter (*e.g.* 5 nt), the affinity drops drastically. This binding affinity is also independent of sequence, which implies a pure electrostatic binding mechanism. To further test this hypothesis, DNA/RNA analogs with non-charged backbone, such as Peptide Nucleic Acid (PNA) or less charged backbone such as phosphorothioate nucleic acids are needed to investigate the binding mechanism. ssDNA is not the naturally occurring format in vivo, however, single strand RNA is abundant in cells, such as miRNA and mRNA. Since RNA binds PLN equally well as or even tighter than ssDNA of the same length, it might play an important role in regulating heart functions. This is further supported by the fact that not only PLN binds with high affinity but also many other contractile proteins such as troponin and myosin bind. And it would be significant if nucleic acids can directly regulate protein activities. Last but not least, more studies need to be done before we can apply DNA/RNA analogs as treatment for PLN related heart failures.

Chapter 6: Conclusions and Future Directions

6.1 Summary of Research

In summary, this dissertation is focused on the attempt to detect nucleic acid catalyst using a self-fabricated microfluidic device and CE-SELEX selection against difficult target molecules. In Chapter 2, we have demonstrated the use of a PDMS microwell array device for the detection of single enzyme molecules. The number of single enzyme molecules in the microwells followed Poisson distribution and different enzyme molecules showed heterogeneous activities over a wide range. The same strategy were then applied for the detection of catalytic sequences in a random nucleic acid library and allowed for the detection of sequences catalyzing separate substrates with multiple turnovers. However, initial effort on nucleic acid library failed to detect any catalytic sequences, indicating a lower abundance or lower activity should be expected.

Chapter 3 described the application of CE-SELEX against a small molecule target - NMM. Aptamers have been selected after only three rounds of CE-SELEX selection. Two out of eight randomly chosen aptamers also showed catalytic activity for the corresponding metal insertion reaction of mesoporphyrin. This study has greatly lowered the low size limitation for CE-SELEX.

Chapter 4 described the CE-SELEX selection against an intact membrane protein target - TfR. Aptamers have been isolated for full-length recombinant TfR after four rounds of selection, indicating that CE-SELEX is a preferred method than conventional SELEX as it allows the use of various membrane models to solubilize the transmembrane domains. Since TfR has important implication in receptor-mediated endocytosis, aptamers against TfR can be potentially engineered to deliver cargoes across membrane to intracellular spaces. Preliminary experiments were designed to study the endocytosis of aptamers upon binding TfR using confocal fluorescence microscope. Further studies are necessary to understand the efficacy of aptamer facilitated transmembrane delivery.

Capillary electrophoresis also serves as an important analytical tool for binding affinity measurement. Chapter 5 discussed binding measurement for various DNA/RNA analogs with important cardiac muscle proteins using ACE and FP. All the analogs tested had high binding affinity for PLN, showing the potential as therapeutics for treating PLN-superinhibition related cardiomyopathy. These oligos also exhibited high affinity against contractile protein - trophonin and modest affinity for myosin, indicating possibly more sophisticated roles in regulating protein functions in cardiac myocytes.

6.2 Future Directions

Researches on aptamers and nucleic acid catalysts have gained great success and are continuing to advance. One essential research area is the development of more efficient selection strategies for both aptamers and nucleic acid catalysts. It allows more convenient and effective discovery of valuable aptamer tools. On the more application side that is also prospering, aptamers can be selected against targets involved in more complicated systems with the promise of becoming regulation or therapeutic tools for more sophisticated functions.

6.2.1 μFFE-SELEX vs CE-SELEX

Although successfully solving difficulties in conventional SELEX, CE-SELEX still suffers from a few aspects. The small sample consumption is an advantage for CE when it comes to analytical purpose, however, it can be a limitation for SELEX as it limits the number of sequences (~10^{12}) that can be analyzed. Sample overloading can cause serious loss of resolution and result in poor separation of bound and unbound sequences. Secondly, the separation is defined by the migration time and thus the collection is made along the separation direction, which requires the determination of the fraction collection window while performing the separation. Accurate collection time window is important in order not to lose resolution. Dilution factor is also an important factor to be considered. In CE-SELEX, the binding complex is typically electrophoretically migrated into the collection vial that is also used as buffer reservoir for electrophoresis. Considering the small loading capacity and the minimal amount of buffer required for electrophoresis, the dilution of the binding sequences after separation is fairly high (~10^{4}). Therefore, small amount of contaminated sequences can contribute largely to the final composition of collected pools, causing deviation from the right track during selection. High voltage in CE separation for improving column efficiency and resolution can also be problematic as it might disrupt the binding and cause serious complex dissociation in cases involving weak binding.

Similar to CE separation, micro-free flow electrophoresis (μFFE) is also a free solution based electrophoresis separation technique. Therefore, it possesses the advantages of CE-SELEX such as the high separation resolution and the minimal non-specific interaction. In addition, it overcomes many challenges that CE-SELEX encounters. μFFE separates continuous flowing sample stream laterally by applying electric field perpendicular to the flow direction of the sample stream. The sample introduce and separation are performed along two different

dimensions, which allows continuous separation to be carried out and thus greatly expands the sample size or the sequence library size that can be analyzed. Bound and unbound fractions are collected perpendicular to the deflection direction, allowing the collection window determined within predefined area. Since the sample stream is introduced at the center, the bound fraction can be collected at either end of the separation chamber. This minimizes the contamination introduced in cases where bound sequences are eluted later than free unbound sequences. μFFE-SELEX has recently been performed successfully and demonstrated to be a more robust technique than CE-SELEX [105]. We expect more applications of aptamer selection on various targets coming forward. Owing to its continuous property, μFFE-SELEX holds great promise in automated SELEX platforms.

6.2.2 Aptamers Targeting Endocytosis

It is straightforward to target the membrane surface receptors involved in the receptor-mediated endocytosis (RME) for transporting therapeutics into cells. The large extracellular domains of the receptors provide perfect binding sites for aptamers to bind and transport. Aptamers binding the transmembrane receptor TfR have been selected using CE-SELEX. However, the transport potential across plasma membrane of these aptamers remains unclear. Future experiments will be focused on whether the aptamers can be endocytosed or they just stay bound on the cell membranes. The transportation of the aptamers into the cells can be monitored with a confocal fluorescence microscope using dye-labeled aptamers.

Effective treatment for intracellular targets requires not only the uptake of the therapeutics, but also the correct delivery to the destinations where the targets are located. Following the ligand binding TfR, the complex is then packaged with the help of adaptor proteins into clathrin coated vesicles (CCV), matured to acidified endosomes and then fused with lysosomes for digestion and degradation. However, this is not ideal since cargoes are expected to enter desired subcellular organelles or be released before fusion with lysosomes. In order to avoid lysosomal degradation, other membrane receptors or endocytosis mechanisms should be targeted and used for aptamer selection.

One limitation of the above mentioned clathrin-mediated endocytosis (CME) is the inevitable trafficking through acidified endosome to eventually degradative lysosome [228]. Fortunately alternative endocytosis pathways exist. A clathrin-independent pathway that is named caveolin-mediated endocytosis (CvME) involves caveolin internalizing proteins that interact with

glycosphingolipid (GSL) in the lipid raft as caveosome and transporting to endoplasmic reticulum and then nucleus [229]. The protein caveolin does not contain any extracellular portions itself but the GSL with exposed carbohydrate groups can be targeted as binding sites for aptamers. Similarly, glycosyl phosphatidylinositol (GPI) linked proteins (*e.g.* folate receptor) can take a clathrin-independent and caveolin-independent pathway that directs the cargoes to Golgi apparatus [230]. These alternative endocytosis pathways can also be targeted, which will greatly increase the chance of success in finding appropriate targets or aptamers and a variety of organelles can be targeted using different receptors and pathways.

6.2.3 Collection and Selection of Catalytic Nucleic Acids

The microwell array device can only be used for detection purpose. In order to eventually identify the catalytic sequences, these sequences need to be collected, amplified and selected iteratively to evolve a high abundant pool just like SELEX for aptamers. However, the attempt to recover the content of the microwells using micromanipulation is challenging since a large portion of the solution transfers to the sealing glass after the PDMS slab is peeled off the glass. Water-in-oil emulsion droplets represent better compartments for the purpose of collection and recovery of catalytic sequences than the microwells with physical barriers. Various types of techniques have been used in microfluidics for droplet sorting and later the collection of droplets with desired properties, such as electric force [174, 205, 231, 232], magnetic force [233], hydrodynamic force [234, 235], acoustic wave [236] and optical trap [237].

Droplets containing enzyme molecules have been extensively studied and individual droplets have been sorted according to their fluorescence generated by the enzymatic activities. Resembling the enzyme molecules, sorting and collection of droplets containing catalytic nucleic acids can fit perfectly into the same techniques. A directly accessible planar droplet array on a solid surface was invented by Noji group [171]. Droplets were discriminated from each other based on their fluorescence intensity and further collection was achieved by using a pressure-controlled micropipette. Another potential technique is the fluorescence-activated droplet sorting (FADS) [174]. Water-in-oil droplets were generated by microfluidic flow-focusing of an aqueous stream with twin streams of oil phase. The droplets were then incubated in a reservoir for extended period and sorted at an asymmetric Y-shaped junction by dielectrophoresis according to fluorescence generated by enclosed cells expressing β-galactosidase. The whole process including incubation, detection, sorting and collection can be performed within one integrated piece of PDMS device,

and holds promise for automation. However, in this type of techniques, one problem that needs to be taken into account is the potential leak of generated fluorescent molecules into the oil phase causing cross-talking between droplets, especially when the incubation period is long [171].

Bibliography:

1. Weigand, B. S.; Zerressen, A.; Schlatterer, J. C.; Helm, M.; Jaschke, A., *The Aptamer Handbook*. WILEY-VCH Verlag GmbH & Co. KGaA: Weinheim, 2006.
2. Wilson, D. S.; Szostak, J. W., In vitro Selection of Functional Nucleic Acids. *Annual Review of Biochemistry* 1999, 68, 611-647.
3. Doudna, J. A.; Cech, T. R., The Chemical Repertoire of Natural Ribozymes. *Nature* 2002, 418, 222-228.
4. Bock, L. C.; Griffin, L. C.; Latham, J. A.; Vermaas, E. H.; Toole, J. J., Selection of single-stranded DNA molecules that bind and inhibit human thrombin. *Nature* 1992, 355, 564-566.
5. Wiegand, T. W.; Williams, P. B.; Dreskin, S. C.; Jouvin, M. H.; Kinet, J. P.; Tasset, D., High-affinity oligonucleotide ligands to human IgE inhibit binding to Fc epsilon receptor I. *Journal of Immunology* 1996, 157, 221-230.
6. Ruckman, J.; Green, L. S.; Beeson, J.; Waugh, S.; Gillette, W. L.; Henninger, D. D.; Claesson-Welsh, L.; Janjic, N., 2 '-fluoropyrimidine RNA-based aptamers to the 165-amino acid form of vascular endothelial growth factor (VEGF(165)) - Inhibition of receptor binding and VEGF-induced vascular permeability through interactions requiring the exon 7-encoded domain. *Journal of Biological Chemistry* 1998, 273, 20556-20567.
7. Nieuwlandt, D.; Wecker, M.; Gold, L., In-vitro selection of RNA ligands to substance-P. *Biochemistry* 1995, 34, 5651-5659.
8. Faulhammer, D.; Eschgfaller, B.; Stark, S.; Burgstaller, P.; Englberger, W.; Erfurth, J.; Kleinjung, F.; Rupp, J.; Vulcu, S. D.; Schroder, W.; Vonhoff, S.; Nawrath, H.; Gillen, C.; Klussmann, S., Biostable aptamers with antagonistic properties to the neuropeptide nociceptin/orphanin FQ. *RNA* 2004, 10, 516-527.
9. Famulok, M., Oligonucleotide aptamers that recognize small molecules. *Curr. Opin. Struct. Biol.* 1999, 9, 324-329.
10. Ciesiolka, J.; Yarus, M., Small RNA-divalent domains. *RNA* 1996, 2, 785-793.
11. Hofmann, H. P.; Limmer, S.; Hornung, V.; Sprinzl, M., Ni^{2+}-binding RNA motifs with an asymmetric purine-rich internal loop and a G-A base pair. *RNA* 1997, 3, 1289-1300.
12. Ringquist, S.; Jones, T.; Snyder, E. E.; Gibson, T.; Boni, I.; Gold, L., High-Affinity RNA Ligands to *Escherichia Coli* Ribosomes and Ribosomal Protein S1: Comparison of Natural and Unnatural Binding Sites. *Biochemistry* 1995, 34, 3640-3648.
13. Shangguan, D.; Li, Y.; Tang, Z.; Cao, Z.; Chen, H.; Mallikaratchy, P.; Sefah, K.; Yang, C.; Tan, W., Aptamers evolved from live cells as effective molecular probes for cancer study. *Proc. Natl. Acad. Sci. U.S.A.* 2006, 103, 11838-11843.
14. Pieken, W. A.; Olsen, D. B.; Benseler, F.; Aurup, H.; Eckstein, F., Kinetic characterization of ribonuclease-resistant 2'-modified hammerhead ribozymes. *Science* 1991, 253, 314-317.
15. Green, L. S.; Jellinek, D.; Bell, C.; Beebe, L. A.; Feistner, B. D.; Gill, S. C.; Jucker, F. M.; Janjic, N., Nuclease-resistant nucleic acid ligands to vascular permeability factor/vascular endothelial growth factor. *Chemistry & Biology* 1995, 2, 683-695.
16. Jellinek, D.; Green, L. S.; Bell, C.; Lynott, C. K.; Gill, N.; Vargeese, C.; Kirschenheuter, G.; McGee, D. P. C.; Abesinghe, P.; Pieken, W. A.; Shapiro, R.; Rifkin, D. B.; Moscatelli, D.; Janjic, N., Potent 2'-amino-2'-deoxypyrimidine RNA inhibitors of basic fibroblast growth factor. *Biochemistry* 1995, 34, 11363-11372.
17. Kim, S. J.; Kim, M. Y.; Lee, J. H.; You, J. C.; Jeong, S., Selection and stabilization of the RNA aptamers against the human immunodeficiency virus type-1 nucleocapsid protein. *Biochemical and Biophysical Research Communications* 2002, 291, 925-931.

18. Beigelman, L.; McSwiggen, J. A.; Draper, K. G.; Gonzalez, C.; Jensen, K.; Karpeisky, A. M.; Modak, A. S.; Matulicadamic, J.; Direnzo, A. B.; Haeberli, P.; Sweedler, D.; Tracz, D.; Grimm, S.; Wincott, F. E.; Thackray, V. G.; Usman, N., Chemical modification of hammerhead ribozymes-catalytic activity and nuclease resistance. *Journal of Biological Chemistry* 1995, 270, 25702-25708.
19. Schmidt, K. S.; Borkowski, S.; Kurreck, J.; Stephens, A. W.; Bald, R.; Hecht, M.; Friebe, M.; Dinkelborg, L.; Erdmann, V. A., Application of locked nucleic acids to improve aptamer in vivo stability and targeting function. *Nucleic Acids Research* 2004, 32, 5757-5765.
20. Williams, K. P.; Liu, X. H.; Schumacher, T. N. M.; Lin, H. Y.; Ausiello, D. A.; Kim, P. S.; Bartel, D. P., Bioactive and nuclease-resistant L-DNA ligand of vasopressin. *Proceedings of the National Academy of Sciences of the United States of America* 1997, 94, 11285-11290.
21. Eulberg, D.; Klussmann, S., Spiegelmers: Biostable aptamers. *Chembiochem* 2003, 4, 979-983.
22. Ng, E. W. M.; Adamis, A. P.; Tuschl, T.; Rossi, J., Anti-VEGF aptamer (pegaptanib) therapy for ocular vascular diseases. *Oligonucleotide Therapeutics* 2006, 1082, 151-171.
23. Ng, E. W. M.; Shima, D. T.; Calias, P.; Cunningham, E. T.; Guyer, D. R.; Adamis, A. P., Pegaptanib, a targeted anti-VEGF aptamer for ocular vascular disease. *Nature Reviews Drug Discovery* 2006, 5, 123-132.
24. Jayasena, S. D., Aptamers: An emerging class of molecules that rival antibodies in diagnostics. *Clin. Chem.* 1999, 45, 1628-1650.
25. Kruger, K.; Grabowski, P. J.; Zaug, A. J.; Sands, J.; Gottschling, D. E.; Cech, T. R., Self-splicing RNA - Auto-excision and Auto-cyclization of the Ribosomal-RNA Intervening Sequence of Tetrahymena. *Cell* 1982, 31, 147-157.
26. Gilbert, W., Origin of life - the RNA world. *Nature* 1986, 319, 618-618.
27. Landweber, L. F.; Pokrovskaya, I. D., Emergence of a dual-catalytic RNA with metal-specific cleavage and ligase activities: The spandrels of RNA evolution. *Proceedings of the National Academy of Sciences of the United States of America* 1999, 96, 173-178.
28. Santoro, S. W.; Joyce, G. F., A general purpose RNA-cleaving DNA enzyme. *Proceedings of the National Academy of Sciences of the United States of America* 1997, 94, 4262-4266.
29. Carmi, N.; Balkhi, S. R.; Breaker, R. R., Cleaving DNA with DNA. *Proceedings of the National Academy of Sciences of the United States of America* 1998, 95, 2233-2237.
30. Bartel, D. P.; Szostak, J. W., Isolation of new ribozymes from a large pool of random sequences. *Science* 1993, 261, 1411-1418.
31. Cuenoud, B.; Szostak, J. W., A DNA metalloenzyme with DNA ligase activity. *Nature* 1995, 375, 611-614.
32. Prudent, J. R.; Uno, T.; Schultz, P. G., Expanding the scope of RNA catalysis. *Science* 1994, 264, 1924-1927.
33. Prudent, J. R.; Staunton, J.; Schultz, P. G., Probing the structural determinants of a catalytic RNA with isomerase activity. *Journal of the American Chemical Society* 1995, 117, 10145-10146.
34. Seelig, B.; Jaschke, A., A small catalytic RNA motif with Diels-Alderase activity. *Chemistry & Biology* 1999, 6, 167-176.
35. Seelig, B.; Keiper, S.; Stuhlmann, F.; Jaschke, A., Enantioselective ribozyme catalysis of a bimolecular cycloaddition reaction. *Angewandte Chemie-International Edition* 2000, 39, 4576-4579.
36. Conn, M. M.; Prudent, J. R.; Schultz, P. G., Porphyrin metalation catalyzed by a small RNA molecule. *Journal of the American Chemical Society* 1996, 118, 7012-7013.
37. Li, Y. F.; Sen, D., A catalytic DNA for porphyrin metallation. *Nature Structural Biology* 1996, 3, 743-747.

38. Yang, J.; Bowser, M. T., Capillary Electrophoresis-SELEX Selection of Catalytic DNA Aptamers for a Small-Molecule Porphyrin Target. *Analytical Chemistry* 2013, 85, 1525-1530.
39. Chun, S. M.; Jeong, S. J.; Kim, J. M.; Chong, B. O.; Park, Y. K.; Park, H.; Yu, J., Cholesterol esterase activity by in vitro selection of RNA against a phosphate transition-state analogue. *Journal of the American Chemical Society* 1999, 121, 10844-10845.
40. Illangasekare, M.; Sanchez, G.; Nickles, T.; Yarus, M., Aminoacyl-RNA synthesis catalyzed by an RNA. *Science* 1995, 267, 643-647.
41. Lohse, P. A.; Szostak, J. W., Ribozyme-catalysed amino-acid transfer reactions. *Nature* 1996, 381, 442-444.
42. Jenne, A.; Famulok, M., A novel ribozyme with ester transferase activity. *Chemistry & Biology* 1998, 5, 23-34.
43. Wiegand, T. W.; Janssen, R. C.; Eaton, B. E., Selection of RNA amide syntheses. *Chemistry & Biology* 1997, 4, 675-683.
44. Zhang, B. L.; Cech, T. R., Peptide bond formation by in vitro selected ribozymes. *Nature* 1997, 390, 96-100.
45. Sun, L. L.; Cui, Z. Y.; Gottlieb, R. L.; Zhang, B. L., A selected ribozyme catalyzing diverse dipeptide synthesis. *Chemistry & Biology* 2002, 9, 619-628.
46. Unrau, P. J.; Bartel, D. P., RNA-catalysed nucleotide synthesis. *Nature* 1998, 395, 260-263.
47. Sheppard, T. L.; Ordoukhanian, P.; Joyce, G. F., A DNA enzyme with N-glycosylase activity. *Proceedings of the National Academy of Sciences of the United States of America* 2000, 97, 7802-7807.
48. Wilson, C.; Szostak, J. W., In-vitro evolution of a self-alkylating ribozyme. *Nature* 1995, 374, 777-782.
49. Wecker, M.; Smith, D.; Gold, L., In vitro selection of a novel catalytic RNA: Characterization of a sulfur alkylation reaction and interaction with a small peptide. *RNA* 1996, 2, 982-994.
50. Sengle, G.; Eisenfuhr, A.; Arora, P. S.; Nowick, J. S.; Famulok, M., Novel RNA catalysts for the Michael reaction. *Chemistry & Biology* 2001, 8, 459-473.
51. Fusz, S.; Eisenfuhr, A.; Srivatsan, S. G.; Heckel, A.; Famulok, M., A ribozyme for the aldol reaction. *Chemistry & Biology* 2005, 12, 941-950.
52. Ryu, Y.; Kim, K. J.; Roessner, C. A.; Scott, A. I., Decarboxylative Claisen condensation catalyzed by in vitro selected ribozymes. *Chemical Communications* 2006, 1439-1441.
53. Roth, A.; Breaker, R. R., An amino acid as a cofactor for a catalytic polynucleotide. *Proceedings of the National Academy of Sciences of the United States of America* 1998, 95, 6027-6031.
54. Joyce, G. F., Nucleic acid enzymes: playing with a fuller deck. *Proceedings of the National Academy of Sciences of the United States of America* 1998, 95, 5845-5847.
55. German, I.; Buchanan, D. D.; Kennedy, R. T., Aptamers as ligands in affinity probe capillary electrophoresis. *Analytical Chemistry* 1998, 70, 4540-4545.
56. Pavski, V.; Le, X. C., Detection of human immunodeficiency virus type 1 reverse transcriptase using aptamers as probes in affinity capillary electrophoresis. *Analytical Chemistry* 2001, 73, 6070-6076.
57. Haes, A. J.; Giordano, B. C.; Collins, G. E., Aptamer-based detection and quantitative analysis of ricin using affinity probe capillary electrophoresis. *Analytical Chemistry* 2006, 78, 3758-3764.
58. Deng, Q. P.; Tie, C.; Zhou, Y. L.; Zhang, X. X., Cocaine detection by structure-switch aptamer-based capillary zone electrophoresis. *Electrophoresis* 2012, 33, 1465-1470.
59. Ruta, J.; Ravelet, C.; Baussanne, I.; Decout, J. L.; Peyrin, E., Aptamer-based enantioselective competitive binding assay for the trace enantiomer detection. *Analytical Chemistry* 2007, 79, 4716-4719.

60. Zhang, H. Q.; Wang, Z. W.; Li, X. F.; Le, X. C., Ultrasensitive detection of proteins by amplification of affinity aptamers. *Angewandte Chemie-International Edition* 2006, 45, 1576-1580.
61. Deng, Q.; German, I.; Buchanan, D.; Kennedy, R. T., Retention and separation of adenosine and analogues by affinity chromatography with an aptamer stationary phase. *Analytical Chemistry* 2001, 73, 5415-5421.
62. Charles, J. A. M.; McGown, L. B., Separation of Trp-Arg and Arg-Trp using G-quartet-forming DNA oligonucleotides in open-tubular capillary electrochromatography. *Electrophoresis* 2002, 23, 1599-1604.
63. Rehder-Silinski, M. A.; McGown, L. B., Capillary electrochromatographic separation of bovine milk proteins using a G-quartet DNA stationary phase. *Journal of Chromatography a* 2003, 1008, 233-245.
64. Romig, T. S.; Bell, C.; Drolet, D. W., Aptamer affinity chromatography: combinatorial chemistry applied to protein purification. *Journal of Chromatography B* 1999, 731, 275-284.
65. Deng, Q.; Watson, C. J.; Kennedy, R. T., Aptamer affinity chromatography for rapid assay of adenosine in microdialysis samples collected in vivo. *Journal of Chromatography a* 2003, 1005, 123-130.
66. Michaud, M.; Jourdan, E.; Ravelet, C.; Villet, A.; Ravel, A.; Grosset, C.; Peyrin, E., Immobilized DNA aptamers as target-specific chiral stationary phases for resolution of nucleoside and amino acid derivative enantiomers. *Analytical Chemistry* 2004, 76, 1015-1020.
67. Brumbt, A.; Ravelet, C.; Grosset, C.; Ravel, A.; Villet, A.; Peyrin, E., Chiral stationary phase based on a biostable L-RNA aptamer. *Analytical Chemistry* 2005, 77, 1993-1998.
68. Dick, L. W.; McGown, L. B., Aptamer-enhanced laser desorption/ionization for affinity mass spectrometry. *Analytical Chemistry* 2004, 76, 3037-3041.
69. Connor, A. C.; Frederick, K. A.; Morgan, E. J.; McGown, L. B., Insulin capture by an insulin-linked polymorphic region G-quadruplex DNA oligonucleotide. *Journal of the American Chemical Society* 2006, 128, 4986-4991.
70. Cho, E. J.; Collett, J. R.; Szafranska, A. E.; Ellington, A. D., Optimization of aptamer microarray technology for multiple protein targets. *Analytica Chimica Acta* 2006, 564, 82-90.
71. Petach, H.; Gold, L., Dimensionality is the issue: use of photoaptamers in protein microarrays. *Current Opinion in Biotechnology* 2002, 13, 309-314.
72. Siddiqui, M. A. A.; Keating, G. M., Pegaptanib - In exudative age-related macular degeneration. *Drugs* 2005, 65, 1571-1577.
73. Lee, J. F.; Stovall, G. M.; Ellington, A. D., Aptamer therapeutics advance. *Current Opinion in Chemical Biology* 2006, 10, 282-289.
74. Liu, J. W.; Cao, Z. H.; Lu, Y., Functional Nucleic Acid Sensors. *Chemical Reviews* 2009, 109, 1948-1998.
75. Rossi, J. J., Ribozymes, genomics and therapeutics. *Chemistry & Biology* 1999, 6, R33-R37.
76. Sun, L. Q.; Cairns, M. J.; Saravolac, E. G.; Baker, A.; Gerlach, W. L., Catalytic nucleic acids: From lab to applications. *Pharmacological Reviews* 2000, 52, 325-347.
77. Kashani-Sabet, M., Ribozyme therapeutics. *Journal of Investigative Dermatology Symposium Proceedings* 2002, 7, 76-78.
78. Frauendorf, C.; Jaschke, A., Catalysis of organic reactions by RNA. *Angewandte Chemie-International Edition* 1998, 37, 1378-1381.
79. Silverman, S. K., Catalytic DNA (deoxyribozymes) for synthetic applications - current abilities and future prospects. *Chemical Communications* 2008, 3467-3485.
80. Tuerk, C.; Gold, L., Systematic Evolution of Ligands by Exponential Enrichment - RNA Ligands to Bacteriophage-T4 DNA Polymerase. *Science* 1990, 249, 505-510.
81. Ellington, A. D.; Szostak, J. W., In vitro Selection of RNA Molecules That Bind Specific Ligands. *Nature* 1990, 346, 818-822.

82. Rhie, A.; Kirby, L.; Sayer, N.; Wellesley, R.; Disterer, P.; Sylvester, I.; Gill, A.; Hope, J.; James, W.; Tahiri-Alaoui, A., Characterization of 2 '-fluoro-RNA aptamers that bind preferentially to disease-associated conformations of prion protein and inhibit conversion. *Journal of Biological Chemistry* 2003, 278, 39697-39705.
83. Zhang, F.; Anderson, D., In vitro selection of bacteriophage phi 29 prohead RNA aptamers for prohead binding. *Journal of Biological Chemistry* 1998, 273, 2947-2953.
84. Homann, M.; Goringer, H. U., Combinatorial selection of high affinity RNA ligands to live African trypanosomes. *Nucleic Acids Research* 1999, 27, 2006-2014.
85. Stoltenburg, R.; Reinemann, C.; Strehlitz, B., FluMag-SELEX as an advantageous method for DNA aptamer selection. *Analytical and Bioanalytical Chemistry* 2005, 383, 83-91.
86. Mann, D.; Reinemann, C.; Stoltenburg, R.; Strehlitz, B., In vitro selection of DNA aptamers binding ethanolamine. *Biochemical and Biophysical Research Communications* 2005, 338, 1928-1934.
87. Wochner, A.; Cech, B.; Menger, M.; Erdmann, V. A.; Glokler, J., Semi-automated selection of DNA aptamers using magnetic particle handling. *Biotechniques* 2007, 43, 344-353.
88. Cox, J. C.; Rudolph, P.; Ellington, A. D., Automated RNA selection. *Biotechnology Progress* 1998, 14, 845-850.
89. Haruki, M.; Noguchi, E.; Kanaya, S.; Crouch, R. J., Kinetic and stoichiometric analysis for the binding of Escherichia coli ribonuclease HI to RNA-DNA hybrids using surface plasmon resonances. *Journal of Biological Chemistry* 1997, 272, 22015-22022.
90. Wang, J. L.; Lv, R. J.; Xu, J. J.; Xu, D. K.; Chen, H. Y., Characterizing the interaction between aptamers and human IgE by use of surface plasmon resonance. *Analytical and Bioanalytical Chemistry* 2008, 390, 1059-1065.
91. Liang, X. W.; Nazarenus, T. J.; Stone, J. M., Identification of a consensus DNA-binding site for the Arabidopsis thaliana SBP domain transcription factor, AtSPL14, and binding kinetics by surface plasmon resonance. *Biochemistry* 2008, 47, 3645-3653.
92. Misono, T. S.; Kumar, P. K. R., Selection of RNA aptamers against human influenza virus hemagglutinin using surface plasmon resonance. *Analytical Biochemistry* 2005, 342, 312-317.
93. Khati, M.; Schuman, M.; Ibrahim, J.; Sattentau, Q.; Gordon, S.; James, W., Neutralization of infectivity of diverse R5 clinical isolates of human immunodeficiency virus type 1 by gp120-binding 2 ' F-RNA aptamers. *Journal of Virology* 2003, 77, 12692-12698.
94. Yang, X. B.; Li, X.; Prow, T. W.; Reece, L. M.; Bassett, S. E.; Luxon, B. A.; Herzog, N. K.; Aronson, J.; Shope, R. E.; Leary, J. F.; Gorenstein, D. G., Immunofluorescence assay and flow-cytometry selection of bead-bound aptamers. *Nucleic Acids Research* 2003, 31.
95. Blank, M.; Weinschenk, T.; Priemer, M.; Schluesener, H., Systematic evolution of a DNA aptamer binding to rat brain tumor microvessels - Selective targeting of endothelial regulatory protein pigpen. *Journal of Biological Chemistry* 2001, 276, 16464-16468.
96. Yao, W. S.; Adelman, K.; Bruenn, J. A., In vitro selection of packaging sites in a double-stranded RNA virus. *Journal of Virology* 1997, 71, 2157-2162.
97. Goodman, S. D.; Velten, N. J.; Gao, Q. A.; Robinson, S.; Segall, A. M., In vitro selection of integration host factor binding sites. *Journal of Bacteriology* 1999, 181, 3246-3255.
98. Mendonsa, S. D.; Bowser, M. T., In vitro evolution of functional DNA using capillary electrophoresis. *Journal of the American Chemical Society* 2004, 126, 20-21.
99. Mendonsa, S. D.; Bowser, M. T., In vitro selection of high-affinity DNA ligands for human IgE using capillary electrophoresis. *Analytical Chemistry* 2004, 76, 5387-5392.
100. Mendonsa, S. D.; Bowser, M. T., In vitro selection of aptamers with affinity for neuropeptide Y using capillary electrophoresis. *Journal of the American Chemical Society* 2005, 127, 9382-9383.

101. Mosing, R. K.; Mendonsa, S. D.; Bowser, M. T., Capillary electrophoresis-SELEX selection of aptamers with affinity for HIV-1 reverse transcriptase. *Analytical Chemistry* 2005, 77, 6107-6112.
102. Lou, X. H.; Qian, J. R.; Xiao, Y.; Viel, L.; Gerdon, A. E.; Lagally, E. T.; Atzberger, P.; Tarasow, T. M.; Heeger, A. J.; Soh, H. T., Micromagnetic selection of aptamers in microfluidic channels. *Proceedings of the National Academy of Sciences of the United States of America* 2009, 106, 2989-2994.
103. Qian, J. R.; Lou, X. H.; Zhang, Y. T.; Xiao, Y.; Soh, H. T., Generation of Highly Specific Aptamers via Micromagnetic Selection. *Analytical Chemistry* 2009, 81, 5490-5495.
104. Cho, M.; Xiao, Y.; Nie, J.; Stewart, R.; Csordas, A. T.; Oh, S. S.; Thomson, J. A.; Soh, H. T., Quantitative selection of DNA aptamers through microfluidic selection and high-throughput sequencing. *Proceedings of the National Academy of Sciences of the United States of America* 2010, 107, 15373-15378.
105. Jing, M.; Bowser, M. T., Isolation of DNA aptamers using micro free flow electrophoresis. *Lab on a Chip* 2011, 11, 3703-3709.
106. Hybarger, G.; Bynum, J.; Williams, R. F.; Valdes, J. J.; Chambers, J. P., A microfluidic SELEX prototype. *Analytical and Bioanalytical Chemistry* 2006, 384, 191-198.
107. Huang, C. J.; Lin, H. I.; Shiesh, S. C.; Lee, G. B., Integrated microfluidic system for rapid screening of CRP aptamers utilizing systematic evolution of ligands by exponential enrichment (SELEX). *Biosensors & Bioelectronics* 2010, 25, 1761-1766.
108. Jensen, K. B.; Atkinson, B. L.; Willis, M. C.; Koch, T. H.; Gold, L., Using in vitro selection to direct the covalent attachment of human immunodeficiency virus type 1 Rev protein to high-affinity RNA ligands. *Proceedings of the National Academy of Sciences of the United States of America* 1995, 92, 12220-12224.
109. Golden, M. C.; Collins, B. D.; Willis, M. C.; Koch, T. H., Diagnostic potential of PhotoSELEX-evolved ssDNA aptamers. *Journal of Biotechnology* 2000, 81, 167-178.
110. Schultz, P. G.; Lerner, R. A., From molecular diversity to catalysis: lessons from the immune system. *Science* 1995, 269, 1835-1842.
111. Breaker, R. R.; Joyce, G. F., A DNA enzyme that cleaves RNA. *Chemistry & Biology* 1994, 1, 223-229.
112. Skoog, D. A.; West, D. M., *Principles of instrumental analysis*. Saunders College: Philadelphia, 1980.
113. Landers, J. P., *Handbook of capillary electrophoresis*. Boca Raton : CRC Press: 1994.
114. Rizvi, S. A. A.; Zheng, J.; Apkarian, R. P.; Dublin, S. N.; Shamsi, S. A., Polymeric sulfated amino acid surfactants: A class of versatile chiral selectors for micellar electrokinetic chromatography (MEKC) and MEKC-MS. *Analytical Chemistry* 2007, 79, 879-898.
115. Cao, J.; Li, B.; Chang, Y. X.; Li, P., Direct on-line analysis of neutral analytes by dual sweeping via complexation and organic solvent field enhancement in nonionic MEKC. *Electrophoresis* 2009, 30, 1372-1379.
116. Berezovski, M.; Drabovich, A.; Krylova, S. M.; Musheev, M.; Okhonin, V.; Petrov, A.; Krylov, S. N., Nonequilibrium capillary electrophoresis of equilibrium mixtures: A universal tool for development of aptamers. *Journal of the American Chemical Society* 2005, 127, 3165-3171.
117. Drabovich, A.; Berezovski, M.; Krylov, S. N., Selection of smart aptamers by equilibrium capillary electrophoresis of equilibrium mixtures (ECEEM). *Journal of the American Chemical Society* 2005, 127, 11224-11225.
118. Tang, J. J.; Xie, J. W.; Shao, N. S.; Yan, Y., The DNA aptamers that specifically recognize ricin toxin are selected by two in vitro selection methods. *Electrophoresis* 2006, 27, 1303-1311.
119. Berezovski, M.; Krylov, S. N., Nonequilibrium capillary electrophoresis of equilibrium mixtures - A single experiment reveals equilibrium and kinetic parameters of protein-DNA interactions. *Journal of the American Chemical Society* 2002, 124, 13674-13675.

120. Berezovski, M.; Nutiu, R.; Li, Y. F.; Krylov, S. N., Affinity analysis of a protein-aptamer complex using nonequilibrium capillary electrophoresis of equilibrium mixtures. *Analytical Chemistry* 2003, 75, 1382-1386.
121. Okhonin, V.; Krylova, S. M.; Krylov, S. N., Nonequilibrium capillary electrophoresis of equilibrium mixtures, mathematical model. *Analytical Chemistry* 2004, 76, 1507-1512.
122. Okhonin, V.; Berezovski, M.; Krylov, S. N., Sweeping capillary electrophoresis: A non-stopped-flow method for measuring bimolecular rate constant of complex formation between protein and DNA. *Journal of the American Chemical Society* 2004, 126, 7166-7167.
123. Okhonin, V.; Petrov, A. P.; Berezovski, M.; Krylov, S. N., Plug-plug kinetic capillary electrophoresis: Method for direct determination of rate constants of complex formation and dissociation. *Analytical Chemistry* 2006, 78, 4803-4810.
124. Bao, J. Y.; Krylova, S. M.; Reinstein, O.; Johnson, P. E.; Krylov, S. N., Label-Free Solution-Based Kinetic Study of Aptamer-Small Molecule Interactions by Kinetic Capillary Electrophoresis with UV Detection Revealing How Kinetics Control Equilibrium. *Analytical Chemistry* 2011, 83, 8387-8390.
125. Bao, J. Y.; Krylov, S. N., Volatile Kinetic Capillary Electrophoresis for Studies of Protein-Small Molecule Interactions. *Analytical Chemistry* 2012, 84, 6944-6947.
126. Berezovski, M.; Krylov, S. N., Thermochemistry of protein-DNA interaction studied with temperature-controlled nonequilibrium capillary electrophoresis of equilibrium mixtures. *Analytical Chemistry* 2005, 77, 1526-1529.
127. Cruz-Aguado, J. A.; Penner, G., Determination of Ochratoxin A with a DNA Aptamer. *Journal of Agricultural and Food Chemistry* 2008, 56, 10456-10461.
128. Wong, I.; Lohman, T. M., A double-filter method for nitrocellulose-filter binding: application to protein-nucleic acid interactions. *Proceedings of the National Academy of Sciences of the United States of America* 1993, 90, 5428-5432.
129. Hage, D. S.; Tweed, S. A., Recent advances in chromatographic and electrophoretic methods for the study of drug-protein interactions. *Journal of Chromatography B* 1997, 699, 499-525.
130. Tahiri-Alaoui, A.; Frigotto, L.; Manville, N.; Ibrahim, J.; Romby, P.; James, W., High affinity nucleic acid aptamers for streptavidin incorporated into bi-specific capture ligands. *Nucleic Acids Research* 2002, 30.
131. Juskowiak, B., Analytical potential of the quadruplex DNA-based FRET probes. *Analytica Chimica Acta* 2006, 568, 171-180.
132. Li, J. W. J.; Fang, X. H.; Tan, W. H., Molecular aptamer beacons for real-time protein recognition. *Biochemical and Biophysical Research Communications* 2002, 292, 31-40.
133. Hamaguchi, N.; Ellington, A.; Stanton, M., Aptamer beacons for the direct detection of proteins. *Analytical Biochemistry* 2001, 294, 126-131.
134. McAfee, J. G.; Edmondson, S. P.; Zegar, I.; Shriver, J. W., Equilibrium DNA binding of Sac7d protein from the hyperthermophile Sulfolobus acidocaldarius: Fluorescence and circular dichroism studies. *Biochemistry* 1996, 35, 4034-4045.
135. Endoh, T.; Funabashi, H.; Mie, M.; Kobatake, E., Method for detection of specific nucleic acids by recombinant protein with fluorescent resonance energy transfer. *Analytical Chemistry* 2005, 77, 4308-4314.
136. Jing, M.; Bowser, M. T., Methods for measuring aptamer-protein equilibria: A review. *Analytica Chimica Acta* 2011, 686, 9-18.
137. Fang, X. H.; Cao, Z. H.; Beck, T.; Tan, W. H., Molecular aptamer for real-time oncoprotein platelet-derived growth factor monitoring by fluorescence anisotropy. *Analytical Chemistry* 2001, 73, 5752-5757.
138. Li, W.; Wang, K. M.; Tan, W. H.; Ma, C. B.; Yang, X. H., Aptamer-based analysis of angiogenin by fluorescence anisotropy. *Analyst* 2007, 132, 107-113.

139. Wei, A. P.; Herron, J. N., Use of synthetic peptides as tracer antigens in fluorescence polarization immunoassays of high molecular weight analytes. *Analytical Chemistry* 1993, 65, 3372-3377.
140. Arthanari, H.; Basu, S.; Kawano, T. L.; Bolton, P. H., Fluorescent dyes specific for quadruplex DNA. *Nucleic Acids Research* 1998, 26, 3724-3728.
141. del Toro, M.; Gargallo, R.; Eritja, R.; Jaumot, J., Study of the interaction between the G-quadruplex-forming thrombin-binding aptamer and the porphyrin 5,10,15,20-tetrakis-(N-methyl-4-pyridyl)-21, 23H-porphyrin tetratosylate. *Analytical Biochemistry* 2008, 379, 8-15.
142. Joyce, M. V.; McGown, L. B., Detection of G-quartet structure in a DNA aptamer stationary phase using a fluorescent dye. *Applied Spectroscopy* 2004, 58, 831-835.
143. Lin, P. H.; Chen, R. H.; Lee, C. H.; Chang, Y.; Chen, C. S.; Chen, W. Y., Studies of the binding mechanism between aptamers and thrombin by circular dichroism, surface plasmon resonance and isothermal titration calorimetry. *Colloids and Surfaces B-Biointerfaces* 2011, 88, 552-558.
144. Pagano, B.; Mattia, C. A.; Giancola, C., Applications of Isothermal Titration Calorimetry in Biophysical Studies of G-quadruplexes. *International Journal of Molecular Sciences* 2009, 10, 2935-2957.
145. Burnouf, D.; Ennifar, E.; Guedich, S.; Puffer, B.; Hoffmann, G.; Bec, G.; Disdier, F.; Baltzinger, M.; Dumas, P., kinITC: A New Method for Obtaining Joint Thermodynamic and Kinetic Data by Isothermal Titration Calorimetry. *Journal of the American Chemical Society* 2012, 134, 559-565.
146. Wiseman, T.; Williston, S.; Brandts, J. F.; Lin, L. N., Rapid measurement of binding constants and heats of binding using a new titration calorimeter. *Analytical Biochemistry* 1989, 179, 131-137.
147. Deamer, D. W.; Branton, D., Characterization of nucleic acids by nanopore analysis. *Accounts of Chemical Research* 2002, 35, 817-825.
148. Moerner, W. E., High-resolution optical spectroscopy of single molecules in solids. *Accounts of Chemical Research* 1996, 29, 563-571.
149. Wu, A. H. B.; Fukushima, N.; Puskas, R.; Todd, J.; Goix, P., Development and preliminary clinical validation of a high sensitivity assay for cardiac troponin using a capillary flow (Single molecule) fluorescence detector. *Clinical Chemistry* 2006, 52, 2157-2159.
150. Rissin, D. M.; Walt, D. R., Digital Concentration Readout of Single Enzyme Molecules Using Femtoliter Arrays and Poisson Statistics. *Nano Letters* 2006, 6, 520-523.
151. Li, H. L.; Xue, G.; Yeung, E. S., Selective Detection of Individual DNA Molecules by Capillary Polymerase Chain Reaction. *Analytical Chemistry* 2001, 73, 1537-1543.
152. Xue, Q. F.; Yeung, E. S., Differences in the Chemical-reactivity of Individual Molecules of an Enzyme. *Nature* 1995, 373, 681-683.
153. Craig, D. B.; Arriaga, E. A.; Wong, J. C. Y.; Lu, H.; Dovichi, N. J., Studies on Single Alkaline Phosphatase Molecules: Reaction Rate and Activation Energy of a Reaction Catalyzed by a Single Molecule and the Effect of Thermal Denaturation - The Death of an Enzyme. *Journal of the American Chemical Society* 1996, 118, 5245-5253.
154. Polakowski, R.; Craig, D. B.; Skelley, A.; Dovichi, N. J., Single Molecules of Highly Purified Bacterial Alkaline Phosphatase Have Identical Activity. *Journal of the American Chemical Society* 2000, 122, 4853-4855.
155. Craig, D. B.; Dovichi, N. J., Escherichia coli beta-galactosidase is heterogeneous with respect to the activity of individual molecules. *Canadian Journal of Chemistry-Revue Canadienne De Chimie* 1998, 76, 623-626.
156. Tan, W. H.; Yeung, E. S., Monitoring the Reactions of Single Enzyme Molecules and Single Metal Ions. *Analytical Chemistry* 1997, 69, 4242-4248.

157. Rondelez, Y.; Tresset, G.; Tabata, K. V.; Arata, H.; Fujita, H.; Takeuchi, S.; Noji, H., Microfabricated arrays of femtoliter chambers allow single molecule enzymology. *Nature Biotechnology* 2005, 23, 361-365.
158. Zhang, H. B.; Nie, S.; Etson, C. M.; Wang, R. M.; Walt, D. R., Oil-sealed femtoliter fiber-optic arrays for single molecule analysis. *Lab on a Chip* 2012, 12, 2229-2239.
159. Gorris, H. H.; Walt, D. R., Mechanistic Aspects of Horseradish Peroxidase Elucidated through Single-Molecule Studies. *Journal of the American Chemical Society* 2009, 131, 6277-6282.
160. Rissin, D. M.; Gorris, H. H.; Walt, D. R., Distinct and Long-lived Activity States of Single Enzyme Molecules. *Journal of the American Chemical Society* 2008, 130, 5349-5353.
161. Gorris, H. H.; Rissin, D. M.; Walt, D. R., Stochastic inhibitor release and binding from single-enzyme molecules. *Proceedings of the National Academy of Sciences of the United States of America* 2007, 104, 17680-17685.
162. Rissin, D. M.; Kan, C. W.; Campbell, T. G.; Howes, S. C.; Fournier, D. R.; Song, L.; Piech, T.; Patel, P. P.; Chang, L.; Rivnak, A. J.; Ferrell, E. P.; Randall, J. D.; Provuncher, G. K.; Walt, D. R.; Duffy, D. C., Single-molecule enzyme-linked immunosorbent assay detects serum proteins at subfemtomolar concentrations. *Nature Biotechnology* 2010, 28, 595-599.
163. Rissin, D. M.; Kan, C. W.; Song, L. N.; Rivnak, A. J.; Fishburn, M. W.; Shao, Q. C.; Piech, T.; Ferrell, E. P.; Meyer, R. E.; Campbell, T. G.; Fournier, D. R.; Duffy, D. C., Multiplexed single molecule immunoassays. *Lab on a Chip* 2013, 13, 2902-2911.
164. Nie, S.; Benito-Pena, E.; Zhang, H.; Wu, Y.; Walt, D. R., Multiplexed Salivary Protein Profiling for Patients with Respiratory Diseases Using Fiber-Optic Bundles and Fluorescent Antibody-Based Microarrays. *Analytical Chemistry* 2013, 85, 9272-9280.
165. Deiss, F.; LaFratta, C. N.; Symer, M.; Blicharz, T. M.; Sojic, N.; Walt, D. R., Multiplexed Sandwich Immunoassays Using Electrochemiluminescence Imaging Resolved at the Single Bead Level. *Journal of the American Chemical Society* 2009, 131, 6088-+.
166. Li, Z. H.; Hayman, R. B.; Walt, D. R., Detection of single-molecule DNA hybridization using enzymatic amplification in an array of femtoliter-sized reaction vessels. *Journal of the American Chemical Society* 2008, 130, 12622-12623.
167. Song, L. A.; Shan, D. D.; Zhao, M. W.; Pink, B. A.; Minnehan, K. A.; York, L.; Gardel, M.; Sullivan, S.; Phillips, A. F.; Hayman, R. B.; Walt, D. R.; Duffy, D. C., Direct Detection of Bacterial Genomic DNA at Sub-Femtomolar Concentrations Using Single Molecule Arrays. *Analytical Chemistry* 2013, 85, 1932-1939.
168. Rotman, B., Measurement of activity of single molecules of β-D-galactosidase. *Proceedings of the National Academy of Sciences of the United States of America* 1961, 47, 1981-1991.
169. Hirono-Hara, Y.; Ishuzuka, K.; Kinosita, K.; Yoshida, M.; Noji, H., Activation of pausing F-1 motor by external force. *Proceedings of the National Academy of Sciences of the United States of America* 2005, 102, 4288-4293.
170. Jung, S. Y.; Liu, Y.; Collier, C. P., Fast mixing and reaction initiation control of single-enzyme kinetics in confined volumes. *Langmuir* 2008, 24, 4439-4442.
171. Sakakihara, S.; Araki, S.; Iino, R.; Noji, H., A single-molecule enzymatic assay in a directly accessible femtoliter droplet array. *Lab on a Chip* 2010, 10, 3355-3362.
172. Song, H.; Chen, D. L.; Ismagilov, R. F., Reactions in droplets in microflulidic channels. *Angewandte Chemie-International Edition* 2006, 45, 7336-7356.
173. Garstecki, P.; Fuerstman, M. J.; Stone, H. A.; Whitesides, G. M., Formation of droplets and bubbles in a microfluidic T-junction - scaling and mechanism of break-up. *Lab on a Chip* 2006, 6, 437-446.
174. Baret, J. C.; Miller, O. J.; Taly, V.; Ryckelynck, M.; El-Harrak, A.; Frenz, L.; Rick, C.; Samuels, M. L.; Hutchison, J. B.; Agresti, J. J.; Link, D. R.; Weitz, D. A.; Griffiths, A. D.,

Fluorescence-activated droplet sorting (FADS): efficient microfluidic cell sorting based on enzymatic activity. *Lab on a Chip* 2009, 9, 1850-1858.
175. Becker, H.; Gartner, C., Polymer Microfabrication Methods for Microfluidic Analytical Applications. *Electrophoresis* 2000, 21, 12-26.
176. Weck, M.; Fischer, S.; Vos, M., Fabrication of Microcomponents Using Ultraprecision Machine Tools. *Nanotechnology* 1997, 8, 145-148.
177. McCormick, R. M.; Nelson, R. J.; AlonsoAmigo, M. G.; Benvegnu, J.; Hooper, H. H., Microchannel Electrophoretic Separations of DNA in Injection-molded Plastic Substrates. *Analytical Chemistry* 1997, 69, 2626-2630.
178. McDonald, J. C.; Chabinyc, M. L.; Metallo, S. J.; Anderson, J. R.; Stroock, A. D.; Whitesides, G. M., Prototyping of Microfluidic Devices in Poly(dimethylsiloxane) Using Solid-object Printing. *Analytical Chemistry* 2002, 74, 1537-1545.
179. Duffy, D. C.; McDonald, J. C.; Schueller, O. J. A.; Whitesides, G. M., Rapid Prototyping of Microfluidic Systems in Poly(dimethylsiloxane). *Analytical Chemistry* 1998, 70, 4974-4984.
180. Heckele, M.; Bacher, W.; Muller, K. D. In *Hot Embossing - The Molding Technique for Plastic Microstructures*, 1998; pp 122-124.
181. Effenhauser, C. S.; Bruin, G. J. M.; Paulus, A.; Ehrat, M., Integrated Capillary Electrophoresis on Flexible Silicone Microdevices: Analysis of DNA Restriction Fragments and Detection of Single DNA Molecules on Microchips. *Analytical Chemistry* 1997, 69, 3451-3457.
182. Kim, E.; Xia, Y. N.; Whitesides, G. M., Polymer Microstructures Formed by Molding in Capillaries. *Nature* 1995, 376, 581-584.
183. Beebe, D. J.; Mensing, G. A.; Walker, G. M., Physics and Applications of Microfluidics in Biology. *Annual Review of Biomedical Engineering* 2002, 4, 261-286.
184. Whitesides, G. M.; Ostuni, E.; Takayama, S.; Jiang, X. Y.; Ingber, D. E., Soft Lithography in Biology and Biochemistry. *Annual Review of Biomedical Engineering* 2001, 3, 335-373.
185. McDonald, J. C.; Whitesides, G. M., Poly(dimethylsiloxane) as a Material for Fabricating Microfluidic Devices. *Accounts of Chemical Research* 2002, 35, 491-499.
186. McDonald, J. C.; Duffy, D. C.; Anderson, J. R.; Chiu, D. T.; Wu, H. K.; Schueller, O. J. A.; Whitesides, G. M., Fabrication of Microfluidic Systems in Poly(dimethylsiloxane). *Electrophoresis* 2000, 21, 27-40.
187. Chaudhury, M. K.; Whitesides, G. M., Direct Measurement of Interfacial Interactions Between Semispherical Lenses and Flat Sheets of Poly(dimethylsiloxane) and Their Chemical Derivatives. *Langmuir* 1991, 7, 1013-1025.
188. Chaudhury, M. K.; Whitesides, G. M., Correlation Between Surface Free-energy and Surface Constitution. *Science* 1992, 255, 1230-1232.
189. Fritz, J. L.; Owen, M. J., Hydrophobic Recovery of Plasma-treated Polydimethylsiloxane. *Journal of Adhesion* 1995, 54, 33-45.
190. Ocvirk, G.; Munroe, M.; Tang, T.; Oleschuk, R.; Westra, K.; Harrison, D. J., Electrokinetic Control of Fluid Flow in Native Poly(dimethylsiloxane) Capillary Electrophoresis Devices. *Electrophoresis* 2000, 21, 107-115.
191. Hu, S. W.; Ren, X. Q.; Bachman, M.; Sims, C. E.; Li, G. P.; Allbritton, N., Surface Modification of Poly(dimethylsiloxane) Microfluidic Devices by Ultraviolet Polymer Grafting. *Analytical Chemistry* 2002, 74, 4117-4123.
192. Yang, T. L.; Jung, S. Y.; Mao, H. B.; Cremer, P. S., Fabrication of Phospholipid Bilayer-coated Microchannels for on-chip Immunoassays. *Analytical Chemistry* 2001, 73, 165-169.
193. Linder, V.; Verpoorte, E.; Thormann, W.; de Rooij, N. F.; Sigrist, M., Surface Biopassivation of Replicated Poly(dimethylsiloxane) Microfluidic Channels and Application to Heterogeneous Immunoreaction with on-chip Fluorescence Detection. *Analytical Chemistry* 2001, 73, 4181-4189.

194. Ismagilov, R. F.; Ng, J. M. K.; Kenis, P. J. A.; Whitesides, G. M., Microfluidic Arrays of Fluid-fluid Diffusional Contacts as Detection Elements and Combinatorial Tools. *Analytical Chemistry* 2001, 73, 5207-5213.
195. Chou, H. P.; Spence, C.; Scherer, A.; Quake, S., A Microfabricated Device for Sizing and Sorting DNA Molecules. *Proceedings of the National Academy of Sciences of the United States of America* 1999, 96, 11-13.
196. Eteshola, E.; Leckband, D., Development and Characterization of an ELISA Assay in PDMS Microfluidic Channels. *Sensors and Actuators B-Chemical* 2001, 72, 129-133.
197. Makamba, H.; Kim, J. H.; Lim, K.; Park, N.; Hahn, J. H., Surface modification of poly(dimethylsiloxane) microchannels. *Electrophoresis* 2003, 24, 3607-3619.
198. Xiao, D. Q.; Van Le, T.; Wirth, M. J., Surface modification of the channels of poly(dimethylsiloxane) microfluidic chips with polyacrylamide for fast electrophoretic separations of proteins. *Analytical Chemistry* 2004, 76, 2055-2061.
199. Wu, D. P.; Zhao, B. X.; Dai, Z. P.; Qin, J. H.; Lin, B. C., Grafting epoxy-modified hydrophilic polymers onto poly(dimethylsiloxane) microfluidic chip to resist nonspecific protein adsorption. *Lab on a Chip* 2006, 6, 942-947.
200. Zhou, J. H.; Yan, H.; Ren, K. N.; Dai, W.; Wu, H. K., Convenient Method for Modifying Poly(dimethylsiloxane) with Poly(ethylene glycol) in Microfluidics. *Analytical Chemistry* 2009, 81, 6627-6632.
201. Song, H.; Ismagilov, R. F., Millisecond Kinetics on a Microfluidic Chip Using Nanoliters of Reagents. *Journal of the American Chemical Society* 2003, 125, 14613-14619.
202. Zheng, B.; Tice, J. D.; Ismagilov, R. F., Formation of arrayed droplets of soft lithography and two-phase fluid flow, and application in protein crystallization. *Advanced Materials* 2004, 16, 1365-1368.
203. Chiu, D. T.; Lorenz, R. M.; Jeffries, G. D. M., Droplets for Ultrasmall-Volume Analysis. *Analytical Chemistry* 2009, 81, 5111-5118.
204. Shim, J. U.; Olguin, L. F.; Whyte, G.; Scott, D.; Babtie, A.; Abell, C.; Huck, W. T. S.; Hollfelder, F., Simultaneous Determination of Gene Expression and Enzymatic Activity in Individual Bacterial Cells in Microdroplet Compartments. *Journal of the American Chemical Society* 2009, 131, 15251-15256.
205. Granieri, L.; Baret, J. C.; Griffiths, A. D.; Merten, C. A., High-Throughput Screening of Enzymes by Retroviral Display Using Droplet-Based Microfluidics. *Chemistry & Biology* 2010, 17, 229-235.
206. Bowser, M. T., SELEX: Just another separation? *Analyst* 2005, 130, 128-130.
207. Cochran, A. G.; Schultz, P. G., Antibody-catalyzed porphyrin metallation. *Science* 1990, 249, 781-783.
208. Kawazoe, N.; Teramoto, N.; Ichinari, H.; Imanishi, Y.; Ito, Y., In vitro selection of nonnatural ribozyme-catalyzing porphyrin metalation. *Biomacromolecules* 2001, 2, 681-686.
209. Li, Y. F.; Geyer, C. R.; Sen, D., Recognition of anionic porphyrins by DNA aptamers. *Biochemistry* 1996, 35, 6911-6922.
210. Li, Y. F.; Sen, D., Toward an efficient DNAzyme. *Biochemistry* 1997, 36, 5589-5599.
211. Oh, S. S.; Plakos, K.; Lou, X. H.; Xiao, Y.; Soh, H. T., In vitro selection of structure-switching, self-reporting aptamers. *Proceedings of the National Academy of Sciences of the United States of America* 2010, 107, 14053-14058.
212. Falk, J. E., *Porphyrins and metalloporphyrins: their general, physical and coordination chemistry, and laboratory methods*. Elsevier: New York, 1964.
213. Hu, D.; Huang, Z. Z.; Pu, F.; Ren, J. S.; Qu, X. G., A Label-Free, Quadruplex-Based Functional Molecular Beacon (LFG4-MB) for Fluorescence Turn-On Detection of DNA and Nuclease. *Chemistry-a European Journal* 2011, 17, 1635-1641.
214. Ren, J. S.; Chaires, J. B., Sequence and structural selectivity of nucleic acid binding ligands. *Biochemistry* 1999, 38, 16067-16075.

215. Sugimoto, N.; Toda, T.; Ohmichi, T., Reaction field for efficient porphyrin metallation catalysis produced by self-assembly of a short DNA oligonucleotide. *Chemical Communications* 1998, 1533-1534.
216. Lupold, S. E.; Hicke, B. J.; Lin, Y.; Coffey, D. S., Identification and characterization of nuclease-stabilized RNA molecules that bind human prostate cancer cells via the prostate-specific membrane antigen. *Cancer Research* 2002, 62, 4029-4033.
217. Chen, C. H. B.; Dellamaggiore, K. R.; Ouellette, C. P.; Seclano, C. D.; Lizadjohry, M.; Chernis, G. A.; Gonzales, M.; Baltasar, F. E.; Fan, A. L.; Myerowitz, R.; Neufeld, E. F., Aptamer-based endocytosis of a lysosomal enzyme. *Proceedings of the National Academy of Sciences of the United States of America* 2008, 105, 15908-15913.
218. De Domenico, I.; Ward, D. M.; Kaplan, J., Regulation of iron acquisition and storage: consequences for iron-linked disorders. *Nature Reviews Molecular Cell Biology* 2008, 9, 72-81.
219. Jefferies, W. A.; Brandon, M. R.; Hunt, S. V.; Williams, A. F.; Gatter, K. C.; Mason, D. Y., Transferrin receptor on endothelium of brain capillaries. *Nature* 1984, 312, 162-163.
220. Lee, H. J.; Engelhardt, B.; Lesley, J.; Bickel, U.; Pardridge, W. M., Targeting rat anti-mouse transferrin receptor monoclonal antibodies through blood-brain barrier in mouse. *Journal of Pharmacology and Experimental Therapeutics* 2000, 292, 1048-1052.
221. MacLennan, D. H.; Kranias, E. G., Phospholamban: A crucial regulator of cardiac contractility. *Nature Reviews Molecular Cell Biology* 2003, 4, 566-577.
222. Zot, A. S.; Potter, J. D., Structural aspects of troponin-tropomyosin regulation of skeletal muscle contraction. *Annual Review of Biophysics and Biophysical Chemistry* 1987, 16, 535-559.
223. Hofmann, P. A.; Lange, J. H., Effects of phosphorylation of troponin-I and C protein on isometric tension and velocity of unloaded shortening in skinned single cardiac myocytes from rats. *Circulation Research* 1994, 74, 718-726.
224. Colson, B. A.; Locher, M. R.; Bekyarova, T.; Patel, J. R.; Fitzsimons, D. P.; Irving, T. C.; Moss, R. L., Differential roles of regulatory light chain and myosin binding protein-C phosphorylations in the modulation of cardiac force development. *Journal of Physiology-London* 2010, 588, 981-993.
225. Zhai, J.; Schmidt, A. G.; Hoit, B. D.; Kimura, Y.; MacLennan, D. H.; Kranias, E. G., Cardiac-specific overexpression of a superinhibitory pentameric phospholamban mutant enhances inhibition of cardiac function in vivo. *Journal of Biological Chemistry* 2000, 275, 10538-10544.
226. Asahi, M.; Kurzydlowski, K.; Tada, M.; MacLennan, D. H., Sarcolipin inhibits polymerization of phospholamban to induce superinhibition of sarco(endo)plasmic reticulum Ca2+-ATPases (SERCAs). *Journal of Biological Chemistry* 2002, 277, 26725-26728.
227. Toyoshima, Y. Y.; Kron, S. J.; Mcnally, E. M.; Niebling, K. R.; Toyoshima, C.; Spudich, J. A., Myosin subfragment-1 is sufficient to move actin-filaments in vitro. *Nature* 1987, 328, 536-539.
228. Doherty, G. J.; McMahon, H. T., Mechanisms of Endocytosis. *Annual Review of Biochemistry* 2009, 78, 857-902.
229. Pelkmans, L.; Kartenbeck, J.; Helenius, A., Caveolar endocytosis of simian virus 40 reveals a new two-step vesicular-transport pathway to the ER. *Nature Cell Biology* 2001, 3, 473-483.
230. Nichols, B. J.; Kenworthy, A. K.; Polishchuk, R. S.; Lodge, R.; Roberts, T. H.; Hirschberg, K.; Phair, R. D.; Lippincott-Schwartz, J., Rapid cycling of lipid raft markers between the cell surface and Golgi complex. *Journal of Cell Biology* 2001, 153, 529-541.
231. Link, D. R.; Grasland-Mongrain, E.; Duri, A.; Sarrazin, F.; Cheng, Z. D.; Cristobal, G.; Marquez, M.; Weitz, D. A., Electric control of droplets in microfluidic devices. *Angewandte Chemie-International Edition* 2006, 45, 2556-2560.
232. Fidalgo, L. M.; Whyte, G.; Bratton, D.; Kaminski, C. F.; Abell, C.; Huck, W. T. S., From microdroplets to microfluidics: Selective emulsion separation in microfluidic devices. *Angewandte Chemie-International Edition* 2008, 47, 2042-2045.

233. Zhang, K.; Liang, Q. L.; Ma, S.; Mu, X. A.; Hu, P.; Wang, Y. M.; Luo, G. A., On-chip manipulation of continuous picoliter-volume superparamagnetic droplets using a magnetic force. *Lab on a Chip* 2009, 9, 2992-2999.
234. Abate, A. R.; Agresti, J. J.; Weitz, D. A., Microfluidic sorting with high-speed single-layer membrane valves. *Applied Physics Letters* 2010, 96.
235. Chabert, M.; Viovy, J. L., Microfluidic high-throughput encapsulation and hydrodynamic self-sorting of single cells. *Proceedings of the National Academy of Sciences of the United States of America* 2008, 105, 3191-3196.
236. Franke, T.; Abate, A. R.; Weitz, D. A.; Wixforth, A., Surface acoustic wave (SAW) directed droplet flow in microfluidics for PDMS devices. *Lab on a Chip* 2009, 9, 2625-2627.
237. Lorenz, R. M.; Edgar, J. S.; Jeffries, G. D. M.; Chiu, D. T., Microfluidic and optical systems for the on-demand generation and manipulation of single femtoliter-volume aqueous droplets. *Analytical Chemistry* 2006, 78, 6433-6439.